Modeling of Diffusion in Zeolites

Frerich J. Keil
Technical University of Hamburg-Harburg, Chair of Chemical Reaction Engineering,
Eissendorfer Str. 38, D-21071 Hamburg, Germany
E-mail: keil@tu-harburg.de

Rajamani Krishna
University of Amsterdam, Department of Chemical Engineering,
Nieuwe Achtergracht 166, NL-1018 WV Amsterdam, The Netherlands

Marc-Olivier Coppens
Delft University of Technology, Department of Chemical Technology,
Julianalaan 136, NL-2628 BL Delft, The Netherlands

Abstract

Diffusion of adsorbed molecules in zeolites plays an important role in the use of zeolites as adsorbents in separation processes and in shape-selective catalysis. Computational chemistry is in a stage where diffusion phenomena, even for multicomponent diffusion, can be treated at a level of high accuracy. The present review presents most of the results on diffusion in zeolites obtained by classical Molecular Dynamics, dynamic Monte-Carlo approaches, Transition-State Theory, and the Maxwell-Stefan approach. Reactive and non-reactive conditions are considered.

Keywords: Diffusion in Zeolites, Modeling, Molecular Dynamics, Monte-Carlo, Transition-State Theory, Maxwell-Stefan.

1. INTRODUCTION

Zeolites consist of crystalline three-dimensionally connected SiO_4 and AlO_4^- tetrahedra, which enclose cavities containing exchangeable cations and water molecules. The cations compensate the negative charges of the AlO_4^- units. The water molecules can be reversibly removed without a change of the framework structure. Zeolites occur in nature as minerals. Already in 1925 Weigel and Steinhoff /1/ discovered that not only water but also small molecules can be sorbed into the cavities of these crystals, while larger ones are excluded. This selective sorption behavior ("molecular sieving") could be explained as the crystal structures became known. The openings of zeolites revealed free diameters between 3 and 10 Å, which is of the same order of magnitude as the gas collision cross-section of small molecules. Barrer /2, 3/ synthesized many zeolites and employed them as selective sorbents. In the years up to about 1960 many synthetic zeolites were discovered, and in 1950 Weisz and Frilette /4, 5/ reported that zeolites are active catalysts in the cracking of hydrocarbons. They can be selective with respect to the shape of the reactant molecules in reactions. This discovery introduces the field of shape-selective catalysis which is a combination of catalysis with the molecular sieve effect. Shape selectivity effects can occur, if the sizes and shapes of reactants,

of products, of transition states or of reaction intermediates are similar to the dimensions of the pores and cavities of the zeolite. The selectivity of a heterogeneously catalyzed reaction depends, therefore, on the pore width and pore architecture. As maximizing the selectivities of the desired products is one of the most important tasks in catalysis, zeolites offer a unique opportunity of controlling reaction selectivities via the pore structure. Many zeolites have been synthesized and characterized so far /6-9/. Owing to their crystalline structure, zeolites possess discrete pore sizes, in contrast to amorphous porous solids like silica gel and activated charcoal. The well-defined pore dimensions of zeolites are determined by the number of SiO_4 or AlO_4 tetrahedra in the ring which circumscribes the pore. If the tetrahedra are arranged in an ideally circular and planar manner, the maximum possible free diameter results. In most cases, the shapes of the pore openings deviate from the ideal geometry. One should keep in mind that neither the crystal structure nor the molecules are really rigid. The pore sizes enlarge with increasing temperature due to larger molecular vibrations. The "pore diameter" is a dynamic and not a static value.

As the atoms and molecules within the zeolite pores are always in close contact with the force field of the adsorbent, a new type of diffusion mechanism, the so-called "configurational diffusion" occurs /10/. The close contact with walls around the diffusing molecules leads to a diffusing process which is comparable to surface diffusion, whereby the surface surrounds the molecules. This particular diffusion mechanism has attracted researchers since the sixties. A variety of experimental methods, like uptake measurements, Wicke-Kallenbach cells, pulsed field gradient NMR (PFG NMR), quasielastic neutron scattering (QUENS), Fourier Transform Infrared Spectroscopy (FTIR) and positron emission profiling (PEP) were employed for the investigation of diffusion and reaction in zeolites. Reviews on these experimental methods are e.g. given by Kärger and Ruthven /11/, Rees /12/, Post /13/, Chen et al. /14/, Keil /15/, Stallmach and Kärger /49/. A very comprehensive review of recent experimental methods for the characterization of zeolites was presented by Karge et al. /16/. Parallel to experimental investigations modeling of diffusion processes in zeolites was carried out. At the beginning the conventional concepts of diffusion processes in catalyst pellets were extended to zeolites. In the eighties Molecular Dynamics (MD) and Monte Carlo (MC) approaches were introduced into zeolite modeling. Additionally, transition-state theory (TST), energy function minimization and quantum chemical calculations were employed. The first calculations were quite simple but over time they became more and more sophisticated. In the beginning only atoms like argon or xenon in zeolites were considered. The lattices were treated as being rigid. Later on diffusivities of aromatics, n-alkanes and water in flexible lattices were calculated. Diffusion coefficients play a key role in the design of catalytic reactions and separation processes. Under equilibrium conditions, self-diffusivity is defined by Einstein's relation:

$$D_{self} = \frac{1}{d}\lim_{t\to\infty}\frac{\left|\left\langle|\mathbf{r}(t)-\mathbf{r}(0)|^2\right\rangle\right|}{t} \tag{1.1}$$

whereby d represents the dimensionality of the movement, $\mathbf{r}(t)$ and $\mathbf{r}(0)$ the position of a particle at time t and $t = 0$, respectiveley. Experimental methods, including sorption, gravimetric measurements and Zero-Length Chromatography (ZLC), lead to transport diffusivities, D_T, which are determined in the presence of a concentration gradient under transient conditions. For a mixture, the diffusivities obtained are Maxwell-Stefan diffusivities. For a single component, the sorbate flux $\mathbf{N}$ is proportional to the concentration gradient ∇C, i.e., Fick's

first law holds:

$$\mathbf{N} = -D_T \nabla C \tag{1.2}$$

While the transport and self-diffusivities are the same at zero coverage, if the diffusion mechanism is the same (exceptions see Brandani et al. /17/), at higher occupancies or loadings θ transport and self-diffusivity are in general different. A phenomenological expression, known as the "Darken equation", but actually a result from the theories of Maxwell and Stefan, was proposed to relate both diffusivities (Darken /18/, Barrer and Jost /19/):

$$D_T = D_c \left(\partial \ln f / \partial \ln C\right)_T \tag{1.3}$$

where f is the sorbate fugacity, which can be replaced by the pressure for an ideal gas, C is the intra-crystalline concentration, and T is the temperature. A difficulty arises from the fact that the corrected diffusivity, D_c, but not the self-diffusivity appears in this equation. Like the self-diffusivity, it is related to the mobility of the molecules. In the limit of infinite dilution, $D_c = D_T$, so that the self-diffusivity and the transport diffusivity can be calculated from each other. This is useful both for experiments and for computational techniques. In situations where the corrected diffusivity is independent of occupancy, the equation can also be used at higher occupancies.

The discrepancy between diffusivities obtained using different experimental methods explains in part the large effort put in numerical studies of diffusion in zeolites. Even so, diffusion in zeolites remains only partially understood. Therefore, another reason for the increasing use of numerical methods is to obtain a better understanding of diffusion in zeolites, and how the diffusion of single components and mixtures depends on various parameters, in particular the structure of the zeolite, the geometric structure of molecules and the operating conditions.

With the advent of ever faster computers, microscopic methods, in particular molecular dynamics (MD), have become more and more popular. In MD, successive configurations of the system are generated by integrating Newton's laws of motion. The result is a trajectory that specifies how the positions and velocities of the particles in the system vary with time. Molecular dynamics is now successfully applied to obtain quantitative results for the diffusion of single components and recently also mixtures in certain zeolites. However, such methods are not yet suitable for more complex materials and large diffusing molecules. Diffusion in zeolites is indeed in most cases an activated process, i.e. of the "hopping" type. Molecules with sizes close the the size of the micropores spend a long time close to certain sites corresponding to a potential well. A molecule adsorbed on a site vibrates and its energy fluctuates until it reaches a high enough value to surmount the energy barrier needed to move out of the energy well to another site. In the many cases where this scenario occurs, the motion of the molecules is close to a discontinuous site-to-site hopping, rather than a continuous movement. Such a hopping picture of diffusion in zeolites, similar to that for defect diffusion in solids, was already introduced by Barrer in 1941 /20/. The integration of Newton's second equation of motion has to be performed in small time steps, typically of the order of a few femtoseconds. As a result, only short simulation times are feasible, typically of the the order of a few nanoseconds. This may be enough to obtain important quantitative information for the situations where the zeolite is purely siliceous. Sorbate molecules must traverse about one unit

cell for a reliable calculation of the self-diffusivity. As soon as the zeolite contains not only Si but also Al and associated counter-ions to compensate for the negative charge, or other strong adsorption sites, MD becomes prohibitively slow. Molecules cannot probe a representative part of the pore space within times accessible to even the largest supercomputers. This can be illustrated by a simple calculation given by Theodorou et al. /21/. On a Cray Y-MP supercomputer the computational requirement of MD for simulating 1 ps of real motion of a simple sorbate molecule (e.g., benzene) in a rigid model of a zeolite lattice (e.g., silicalite), using pretabulated potential energy fields for the sites and partial charges, is around 30 CPU seconds. Assume that the self-diffusivity is around 10^{-12} m^2/s. In order to obtain a reliable estimate of D_{self} from MD, one should let the sorbate molecules move for sufficient time to sample all local regions of the zeolite framework. For this to happen, the translational displacement of molecules must be commensurate with the zeolite unit cell parameters, that is, around 2 nm. This will lead for an equilibrium MD simulation to a computing time of at least:

$$t = \langle r^2 \rangle / (6 D_{self}) = (2\mathbf{nm})^2 / \left(6 \cdot \left(10^{-12}\mathbf{m^2 s^{-1}}\right)\right) \approx 670\mathbf{ns}$$

This figure corresponds to 5600 h of Cray Y-MP computing time.

Using integration time steps needed to simulate the movement associated to weak adsorption sites, molecules would spend a very large number of time steps around the aluminium or other strong adsorption sites, which are usually randomly distributed over the zeolite. Molecules should move along a representative number of weak and strong adsorption sites to simulate diffusion, and sufficient realizations need to be simulated. In any case, the simulations need to be long enough to observe a cross-over from a necessarily deterministic trajectory at short distances to an apparently diffusive motion over longer distances /22, 23/. The equations are very stiff, with large differences in characteristic time steps.

Techniques to simulate diffusion and reaction in zeolites not accessible to MD yet employ a mechanism that is intrinsically discontinuous to filter vibrations and separately treat fast and slow movements to simulate the hopping. These methods are dynamic Monte-Carlo (DMC) simulations and Transition-State Theory (TST). Both DMC and TST can be related to a Markovian master equation, which describes the evolution over time of the system, through jumps between "states" or configurations in phase space:

$$dP_j / dt = \sum_i \left(W_{ji} P_i - W_{ij} P_j\right) \tag{1.4}$$

where P_j is the probability for a system to be in a certain configuration j, and W_{ij} is the transition probability per unit time to move from a state or configuration j to i. These states can be associated to sites in a diffusion problem. The detailed derivation of this equation from first principles is given by Binder /24, 25/. It is similar to the derivation of rate equations in the framework of TST for gas phase reactions /26, 29/. For the mathematical derivation with the explicit equations see e.g. Gelten et al. /27/ and van Kampen /28/. The transition probabilities W_{ij} correspond to reaction rate constants that transform configuration j into i and vice versa. In the master equation, the first term (see Eq. 1.4) in the right hand side expresses how P_j increases, because reactions or hops can bring the system from some configuration j into configuration i. The second term expresses how P_j decreases because reactions or hops can change the system from j to another configuration i. One has to sum over all possible configurations j. The transition probabilities can be obtained from quantum chemical

calculations and/or from transition-state theory. A limitation of the DMC approach arises when the reaction types in a model can be partitioned into two classes with vastly different reaction rates, e.g. when diffusion is simulated together with chemical reactions. Diffusion is often much faster than the chemical reactions, so that most of the computing time is consumed for simulating diffusion. Extremely large amounts of computer time are required to simulate a reasonable number of chemical reactions. This is a similar problem as was mentioned for molecular dynamics simulations. Ways out are to allow a fixed number of diffusion steps after each reaction /30/, or to relax the configuration to equilibrium after each reaction /31, 32/. Hybrid models in which the treatment of diffusion is separated from the MC method /33, 34/ are also in use. Only a number of highly mobile particles is stored, but not their positions. The probability that an immobile particle finds a mobile species at relevant sites is calculated. These probabilities are then accounted for in the pattern matching for the source patterns of the reactions. These approaches are less expensive than treating diffusion correctly. There are, of course, drawbacks like assuming uniform distribution of adsorbates, even if sites are topologically disconnected /34/.

Besides the molecular approaches, the Maxwell-Stefan equations, although developed for highly diluted gases, could be extended to model surface diffusion and diffusion in zeolites for multicomponent systems. This is a macroscopic approach, which can be used in conjunction with the previous micro- and mesoscopic techniques.

The present review focusses on the modeling of diffusion and reaction in zeolites by

- Molecular Dynamics (MD)
- Dynamic Monte-Carlo (MC)
- Transition-State Theory (TST)
- Maxwell-Stefan approach.

Some remarks on adsorption will also be made, although we have chosen to limit ourselves mostly to diffusion in this review.

A few reviews on these subjects have been published previously /11, 14, 15, 21, 35-38/.

2. MOLECULAR DYNAMICS SIMULATIONS

In this section a short introduction into the molecular dynamics (MD) approach will be given followed by a survey of calculation results obtained for the diffusivities of some atoms and molecules in various zeolites.

2.1 Molecular Dynamics

Molecular dynamics starts with the selection of a model system consisting of atoms and/or molecules. Successive configurations of the system are generated by integrating Newton's laws of motion. The result is a trajectory that specifies how the positions and velocities of the particles vary with time. The standard MD approach is a classical and not a quantum mechanical method to study the dynamics of the system. The molecular dynamics technique solves the classical equations of motion of N molecules interacting through a potential V. The classical Hamiltonian, which is equivalent to the system's total energy, kinetic plus potential energy,

can be written as:

$$H(\mathbf{p}_i, \mathbf{r}_i) = \sum_{i=1}^{N} \frac{1}{2m_i} \mathbf{p}_i^2 + V(\mathbf{r}_i) \tag{2.1}$$

where $\mathbf{p}_i$ is the momentum of particle i and V is the effective potential. The Hamiltonian is a function of $6N$ variables, $3N$ particle momenta and $3N$ particle positions. By means of Hamilton's equations one obtains from eq. 2.1 the equations of motion:

$$\dot{\mathbf{p}}_i = -\frac{\partial H}{\partial \mathbf{r}_i} = -\frac{\partial V}{\partial \mathbf{r}_i} = \mathbf{f}_i \tag{2.2}$$

$$\dot{\mathbf{r}}_i = \frac{\partial H}{\partial \mathbf{p}_i} = \frac{\mathbf{p}_i}{m_i} \tag{2.3}$$

Substituting the second derivative of $\mathbf{r}_i$ into eq. 2.2 gives Newton's second law:

$$m_i \ddot{\mathbf{r}}_i = \mathbf{f}_i \tag{2.4}$$

The dynamics of a system is obtained by integrating either eqs. 2.2 and 2.3 or eq. 2.4. For high-accuracy solutions predictor-corrector algorithms can be employed to solve eqs. 2.2 and 2.3. Alternatively, the second-order differential equation 2.4 can be solved directly. For this problem Verlet methods are preferably used. The starting point for the Verlet algorithm is a Taylor series expansion about $\mathbf{r}(t)$:

$$\mathbf{r}(t + \Delta t) = \mathbf{r}(t) + \frac{d\mathbf{r}}{dt}\Delta t + \frac{1}{2!}\frac{d^2\mathbf{r}}{dt^2}\Delta t^2 - O(\Delta t^3) \tag{2.5}$$

$$\mathbf{r}(t - \Delta t) = \mathbf{r}(t) - \frac{d\mathbf{r}}{dt}\Delta t + \frac{1}{2!}\frac{d^2\mathbf{r}}{dt^2}\Delta t^2 + O(\Delta t^3) \tag{2.6}$$

Adding eqs. 2.5 and 2.6 results in:

$$\mathbf{r}(t + \Delta t) = 2\mathbf{r}(t) - \mathbf{r}(t - \Delta t) + \frac{d^2\mathbf{r}}{dt^2}\Delta t^2 \tag{2.7}$$

The eq. 2.7 is known as Verlet's algorithm. It enables us to advance the position of the molecules without calculating their velocities. One can derive the velocity from knowledge of the trajectory, using

$$\mathbf{r}(t + \Delta t) - \mathbf{r}(t - \Delta t) = 2\mathbf{v}(t)\Delta t + O(\Delta t^3) \tag{2.8}$$

$$\mathbf{v}(t) = \frac{\mathbf{r}(t + \Delta t) - \mathbf{r}(t - \Delta t)}{2\Delta t} + O(\Delta t^2) \tag{2.9}$$

The velocities are used to compute the kinetic energies and, thereby, the instantaneous temperature. Before the Verlet algorithm can be implemented, the forces must be calculated. The forces are used subsequently to calculate the accelerations:

$$\mathbf{a}(t) = \frac{d^2\mathbf{r}}{dt^2} = \frac{\mathbf{f}}{m} \tag{2.10}$$

There exist efficient techniques to speed up the evaluation of both short-range and long-range forces, such that the computing time scales as N. There are various improvements of the

standard Verlet algorithm. Details may be found in the books mentioned below. Calculating the forces requires interaction potentials. The potential energy can be split up into terms which depend on the coordinates of individual interaction sites, pairs of interactions sites, triplets etc. If $\mathbf{r}_1$, $\mathbf{r}_2$, ... $\mathbf{r}_N$ represent the coordinates of all interaction sites in the system and neglecting any external fields, the potential energy can be written as:

$$V(\mathbf{r}_1,....,\mathbf{r}_N) = \sum_{i=1}^{N}\sum_{j>1}^{N} V_2(\mathbf{r}_i,\mathbf{r}_j) + \sum_{i=1}^{N}\sum_{j>1}^{N}\sum_{k>j>i}^{N} V_3(\mathbf{r}_i,\mathbf{r}_j,\mathbf{r}_k) + ... \tag{2.11}$$

V_2 accounts for two-body interactions and V_3 for three-body interactions. Higher terms are not given here. In most cases it is assumed that only two-body interactions are important. Two-body interactions make indeed the most significant contribution to particle interactions. There are a broad variety of pairwise potentials for atoms and simple molecules. A commonly used potential energy expression that represents systems with dispersive interactions quite well is the Lennard-Jones 12-6 potential:

$$V_2 = \sum_{i=1}^{N}\sum_{j>1}^{N} 4\varepsilon_{ij}\left[\left(\frac{\sigma_{ij}}{r_{ij}}\right)^{12} - \left(\frac{\sigma_{ij}}{r_{ij}}\right)^{6}\right] \tag{2.12}$$

where σ is the collision diameter (separation for which the energy is zero) and the well depth ε. The Lennard-Jones potential is characterized by an attractive part that varies as r^{-6} and a repulsive part that varies as r^{-12}. There are no sound theoretical reasons in favour of the repulsive r^{-12}. Therefore, instead of this term often an exponential term (Buckingham potential) is employed. There are various modifications of this exponential term. The parameters σ and ε are for self-interactions. Cross-interaction parameters are found by e.g. the Lorentz-Berthelot mixing rules:

$$\sigma_{ab} = (\sigma_{aa} + \sigma_{bb})/2 \tag{2.13}$$

$$\varepsilon_{ab} = (\varepsilon_{aa}\varepsilon_{bb})^{1/2} \tag{2.14}$$

In order to reduce the computing time, a potential cutoff (about 10-15Å) is employed to limit the number of interaction sites that must be summed over. Molecular species require additional potential expressions for the intramolecular bond potentials, angle bending potentials, out-of-plane bending potentials and torsional potentials. There are also effective pairwise potentials for molecules available. Molecular mechanic potentials like AMBER, CHARMM, MM3, CFF93 and KFF can be employed. Computing the energy from these potentials requires an extraodinary increase in computational time compared with using a simple intermolecular potential. Of course, one can get quite accurate results with these potentials. Long-range contributions to the potential energy in a system with boundary conditions are calculated by the so-called Ewald summation or alternative approaches like the reaction field or the particle-particle and particle-mesh (PPPM) methods.

A commonly used simplification of the calculation of intramolecular potentials is to consider groups of atoms as single interaction sites. For example the CH_3 or CH_2 units of an alkane chain can be "lumped" into one interaction group described by one single pair of effective Lennard-Jones parameters. This approach is called "united atom approximation". The advantage is that the number of interaction sites to sum over is considerably reduced. The

atoms comprising the zeolite framework are generally represented as Lennard-Jones spheres.

The MD algorithm can be summarized as follows:

- Define the system: number and type of atoms and molecules, their masses and their intramolecular and/or interaction potentials
- Define the initial ($t = 0$) positions and velocities; the velocities can be found for a desired temperature T by means of an instantaneous temperature at time t, $T(t)$:

$$kT(t) = \sum_{i=1}^{N} \frac{m_i V_i^2(t)}{N_f} \tag{2.15}$$

where N_f is the number of degrees of freedom ($3N$). The desired temperature T is adjusted to $T(t)$ by scaling with $\sqrt{T/T(t)}$.

- Define a time step, Δt, for the integration and choose a maximum simulation time. Too small time steps lead to a trajectory that covers only a small portion of the phase space; too large time steps lead to instabilities in the integration algorithm owing to high overlaps between atoms. In general the time step is set to a few femtoseconds, in some cases even less.
- Calculate the forces between the species at $t = 0$ and start the integration by means of the Verlet algorithm. This step is repeated until the end of simulation time is reached.
- Compute the averages of measured quantities, e.g., the self-diffusivity by the Einstein relation (eq. 1.1).

For reasons of computing time, the number of particles is limited to at most a few thousand, and. In order to avoid surface effects when simulating bulk systems, periodic boundary conditions are commonly used, which mimic the presence of an infinite bulk surrounding the N-particle model system. The volume containing the N particles is treated as the primitive cell of an infinite periodic lattice of identical cells. A given particle interacts with all other particles in this infinite periodic system. The statistical mechanical ensemble generated by the usual MD simulations is the microcanonical or NVE ensemble, where the number of particles, volume, and total energy are constant, but it is possible to simulate a canonical or NVT ensemble, where a thermal reservoir is added to the system, or the isobaric-isothermal ensemble (NPT), where pressure and temperature are held constant.

Molecular dynamics can also be applied to non-equilibrium systems. Non-equilibrium molecular dynamics algorithms (NEMD) were already developed in the seventies, and improved later on. NEMD involves simulating a system at steady state away from equilibrium, where the steady state is attained through the application of an external field. The ratio of the field-induced current to the field itself yields the transport coefficient of interest. The theoretical basis of many NEMD algorithms is underpinned by linear and non-linear response theory /39/.

There are some introductory books on MD. An overview of many molecular simulation methods is given by Leach /40/, Allen and Tildesley /41/, Frenkel and Smit /42/, Sadus and Rowley /44/ and Field /45/. Molecular dynamics methods are described in the books by Haile /46/, Rapaport /47/ and Haberlandt et al. /48/.

2.2 Molecular dynamics simulations of atoms and spherical molecules

The first molecular dynamics (MD) calculations were on noble gases (mainly Ar, Kr, Xe) and spherical molecules like CH_4, CF_4 and less frequently SF_6. They were modeled as soft spheres interacting between them and with the zeolite framework via Lennard-Jones 6-12 potential functions (see eq. 2.12). If polarization interactions are accounted for, eq. 2.12 is written as:

$$V_2 = \sum_{i=1}^{N}\sum_{j>1}^{N}\left[\frac{A_{ij}}{r_{ij}^{12}} - \frac{B_{ij}}{r_{ij}^{6}}\right], \tag{2.16}$$

where $A_{ij} = 4\varepsilon_{ij}\sigma_{ij}^{12}$; $B_{ij} = 4\varepsilon_{ij}\sigma_{ij}^{6}$ and r_{ij} is the distance between interacting centers i and j. Parameter sets were derived from various sources /50-59/. If cations were present in the framework, quite often a shifted-force potential was employed /41/. Schrimpf et al. /59/ also included induced dipole-dipole interactions. Recently, Jaramillo and Auerbach /60/ developed and validated a new force field for cations in zeolites, which explicitly distinguishes Si and Al atoms, as well as different types of oxygens in the framework. The new force field gives excellent agreement with experimental data on cation positions, site occupancies and vibrational frequencies. Henson et al. /61/ derived a new force field for the modeling of interactions between aromatics and siliceous zeolites by fitting to calorimetric data on the sorption of benzene in siliceous faujasite. Nicholson et al. /62/ reviewed the construction of a potential function for the interaction of non-polar probes with silicalite and with $AlPO_4$-5, and analyzed the contributions arising from the different terms. The study revealed that carefully tuned 12-6 potentials can be used as input to adsorption simulations in the type of zeolites considered here. However, in some cases it appears advisable to include all atoms, rather than oxygen only, and not to place any reliance on transferability of the parameters obtained. June et al. /63/ derived potential parameters from thermodynamical investigations on alkanes in silicalite. The coefficients B_{ij} in eq. 2.16 were calculated via the Slater-Kirkwood formula /76/

$$B_{ij} = \frac{3e^2 a_o^{1/2}\alpha_i\alpha_j}{(\alpha/n_e)_i^{1/2} + (\alpha/n_e)_j^{1/2}}. \tag{2.17}$$

The short-range repulsion coefficient, A_{ij}, is obtained as:

$$A_{ij} = {}^{1}/_{2}\, B_{ij}\left(r_i^o + r_j^o\right), \tag{2.18}$$

where α_i is the atomic polarizability of atomic species i, e the charge of an electron, a_o the Bohr radius (0.52918 Å), r_i^o represents the van der Waals radius of atom i, and n_e is an effective number of electrons in an atom (approximately equivalent to the number of electrons in the outer shell). The sum of the van der Waals radii of a pair (i, j) is equivalent to the minimum distance of the Lennard Jones potential:

$$r_{min} = r_i^o + r_j^o = \sigma_{ij}\sqrt[6]{2} = 1.12246\sigma_{ij}. \tag{2.19}$$

The atomic parameters were taken from the literature except the van der Waals radius of the zeolite oxygen atoms, which was adjusted to yield the experimental Henry's constant for methane in silicalite at one temperature.

Many MD simulations were carried out for xenon /59, 64-74/. Jost et al. /75/ investigated the diffusion of xenon-methane mixtures. Pickett et al. /65/ used a constant temperature algorithm (rather than NVE) and with different Lennard-Jones potential parameters, they obained results for the diffusivities that are in good agreement with the simulations of June et al. /64/ and with the PFG NMR measurements of Heink et al. /77/. Pickett et al. /65/ calculated the diffusivities for Xe in silicalite. Silicalite is the aluminum-free and therefore cation-free variant of ZSM-5. The symmetry group of silicalite is Pnma with cell parameters $a = 20.07$ Å, $b = 19.92$ Å, and $c = 13.42$ Å. The three-dimensional channel network consists of two types of channels: straight channels parallel to the y-direction and zigzag (sinusoidal) channels with main component along the x-direction plus an oscillating component parallel to the z-direction. These two kinds of channels are connected to each other at intersections which enable displacements in z-direction. The channels have a slightly elliptical cross section of 5.3 x 5.6 $Å^2$ (straight channels) or 5.1 x 5.5 $Å^2$ (zigzag channels). The intersections are elongated cavities up to 9 Å in diameter. One crystallographic cell contains 288 atoms, in fact 96 Si and 192 O atoms. Silicalite shows a reversible phase transition at about 340 K to monoclinic symmetry ($P2_1/n11$ space group). The space group symbolism is, e.g., explained in the book by Hall /79/. Picket et al. /65/ assumed a rigid zeolite framework, and a Lennard-Jones 6-12 potential was used to describe interactions between Xe and zeolite oxygen atoms. As the bulky and rather polarizable oxygen atoms cover the Si atoms, and in other cases also the Al atoms, only Xe-oxygen interactions were taken into account in the potential. A number of 32 Xe atoms were distributed randomly over 8 unit cells of silicalite at the beginning of the simulations which were run over 300 ps with time steps of 10-12 fs at temperatures from 77 K to 450 K. At 77 K the Xe atoms were mostly trapped at the adsorption sites. From an Arrhenius plot, the activation barrier to diffusion was found to be 5.5 kJ/mol. The xenon loadings were gradually increased up to 16 atoms per unit cell. Infinite dilution was simulated by eliminating the guest-guest interactions without reducing the number of particles in the box. At 298 K, the diffusion coefficient was found to be $1.86 \cdot 10^{-9}$ m^2/s (77 K: $3 \cdot 10^{-11}$ m^2/s; 450 K: $3.25 \cdot 10^{-9}$ m^2/s). The experimental value obtained by PFG NMR /77/ for 298 K was $4 \cdot 10^{-9}$ m^2/s. An increase of the loading leads to increased Xe-Xe interactions and collisions. Therefore, the diffusivity decreases with increasing loading. Separate diffusion coefficients for the x, y, and z directions are of particular interest in zeolite systems. The calculated diffusion coefficients at 298 K and 4 atoms per unit cell, $D_x = 1.26 \cdot 10^{-9}\,m^2/s$, $D_y = 4.03 \cdot 10^{-9}\,m^2/s$ (straight channel), $D_z = 0.28 \cdot 10^{-9}\,m^2/s$, suggest that diffusion is fastest along the straight channel and slower along the sinusoidal channels. Diffusion along the z-direction requires the alternating motion of atoms between straight and sinusoidal channels. The small value of D_z shows that only occasional transitions of atoms from one channel system to the other occur.

June et al. /64/ investigated the dynamics of Xe in silicalite as well. Xenon was represented as a Lennard-Jones sphere. The zeolite lattice was assumed rigid. All of the potential parameters were taken from the literature. The polarizability (see eq. 2.17) of the oxygen atoms was taken from Kiselev /66/. The effective number of electrons ($n_e = 7(O), 5(C), 0.9(H)$) and an optimal van der Waals radius of oxygen (1.575 Å) were taken from a previous paper by June et al. /63/. MD runs were executed for 200, 300 and 400 K. Each total simulation time was over 1 ns. The diffusion coefficients decreased with increasing Xe loading (see Fig. 1). At the highest temperature this effect was very pronounced, but weaker at 300 K, and at 200 K a weak maximum was observed in the predicted self-diffusivity. The authors explain this effect

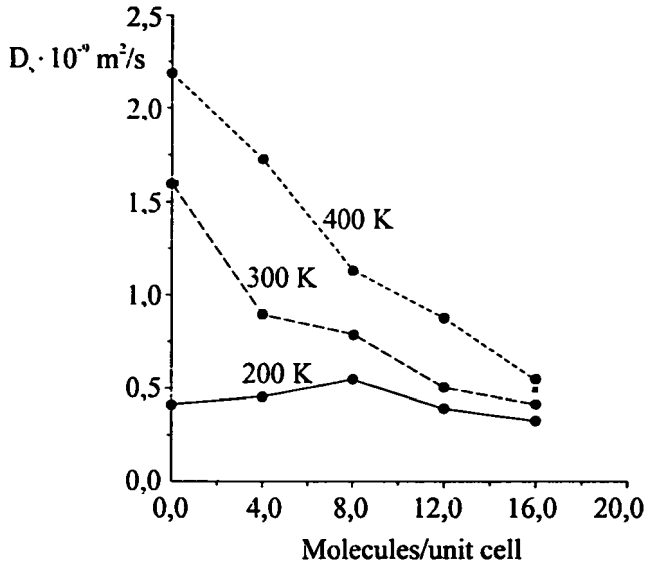

Fig. 1 Computed self-diffusivites of xenon in silicalite at 200 K, 300 K, 400 K as a function of loading /64/

in some detail. At low temperature and low occupancy, a significant portion of the sorbate molecules will be "trapped" in individual channel segments, and, consequently, only those atoms or molecules possessing translational energies in excess of the potential barriers will be able to move freely between channel segments. As the concentration of sorbate molecules increases, intermolecular collisions act to push a sorbate molecule from a channel interior past the intersection and into an adjacent channel segment. Collisions between sorbate molecules occupying the same channel segment have two effects: the first is an exchange of energy during a collision, and the second is a reduction of the mean free path for motion along the axis of the channel. The first of these effects leads to an increase in the rate of barrier crossings between channel segments, whereas the second effect leads to a decrease. The degree to which the first or the second effect dominates depends, at constant temperature, on sorbate occupancy. Increasing the occupancy of sorbate molecules also makes the density distribution less diffuse. As temperature was lowered, sorbate molecules were found to preferentially populate the sinusoidal channels over the straight channels, because the former are energetically more favorable. Xenon did not frequent the channel intersections at any of the temperatures investigated. In the paper several three-dimensional contour plots of particle density distribution are presented.

Yashonath and Banyopadhyay /81/ calculated the diffusivities of simple Lennard-Jones particles in silicalite as a function of the adsorbate diameter. The diffusion coefficient exhibited a peak when the diameter of the adsorbate approached the channel diameter. This "ring effect" was also observed for many other cases. MD calculations were performed in a microcanonical ensemble (NVE) on 32 unit cells (4 x 4 x 2) of silicalite for the rigid

framework model, whereas 8 unit cells (2 x 2 x 2) were used for the flexible framework model. The number of adsorbate molecules were 26 and 16 for rigid and flexible frameworks respectively. All calculations were carried out at a temperature of about 300 K for a concentration of one adsorbate per channel. A MD time step of 10 fs and 1 fs for fixed and flexible framework simulations respectively yielded excellent energy conservation. Equilibration was performed for about 100 ps. This was followed by runs of 400 ps duration during which period the diffusivities were calculated. The harmonic potentials for the zeolite framework interactions were taken from Demontis et al. /82/:

$$V(r) = \frac{1}{2}k(r - r_o)^2 \tag{2.20}$$

Higher-order terms can be included. The constant k can be derived from spectroscopic data and r_o from structural data. The "ring effect" persisted when framework flexibility was included. The σ-values for the sorbent-sorbent interactions were varied between 1.5 Å and 4.5 Å. The diffusivities for the flexible framework turned out to be about 30–50% greater than for the rigid framework. Bandyopadhyay and Yashonath /83/ could confirm that the "ring effect" appears to be independent of the host zeolite and of the topological features of the zeolite micropores. The additional simulations were done for the VPI-5 zeolite which is an alumino-phosphate molecular sieve, the channel system of which comprises a straight 18-ring pore parallel to the z-axis, with a free diameter of 13 x 21 Å. The system temperature was taken to be 620 K. As the sorbate diameter approached that of the window, again a peak in the diffusivity could be observed. The "ring effect" or "superdiffusivity effect" (sometimes also called "levitation") can be explained by the fact that the radial force acting on a sorbate molecule is nearly zero when the size of the sorbate molecule is close to the diameter of the channel. The sorbate is "floating" through the channel. Yashonath and his coworkers /67, 69, 70, 71, 73/ investigated systematically the diffusion coefficients, rates of intercage diffusion and rates of cage passings of monoatomic spherical sorbates in NaY zeolites, the framework of which consists of cuboctahedral sodalite cages or β-cages, made up of eight 6-membered and six 4-membered rings, that are linked by 6-membered rings of oxygen atoms. This leads to the formation of a three-dimensional net of large cavities tetrahedrally connected by windows of 12 oxygen atoms. Structures and substructures of zeolites were described by van Koningsveld /84/. In their simulations, Yashonath and his coworkers used a Si/Al ratio of 3 and the charge balancing Na^+ cations fully occupied the SI and SII cation sites of the structure. Initially each supercage was occupied by one Xenon atom. The temperature was assumed to be 364 K. The Lennard-Jones potential parameters were taken from Kiselev and Du /55/. The authors detected that the potential to be surmounted for crossing the 12-ring window is a function of distance from the window center /67/. The potential minimum of -12 kJ/mol was observed 1.6 Å from the center of the 12-ring. A potential barrier of less than 1 kJ/mol was calculated to cross from one cage to another. The average time that a Xenon atom spends within a given cage was calculated to be 9.9 ps at 376 K /68/. The investigation of the trajectories of the diffusing atoms showed that the atoms move mostly closer to the wall than to the center. Increasing the loading to 2 or 3 atoms per supercage led to a partial dimerization of the xenon atoms /69-71/. About 15 % of the xenon atoms diffuse as dimers at a concentration of one xenon atom per supercage /62/. This figure increased at higher loadings. As expected, at higher temperatures the atoms were more evenly distributed over the supercages. Yashonath and Santikary /73, 85/ performed similar calculations for argon in NaCaA. The pore system of A-type zeolites is a cubic array of nearly spherical α-cages having a diameter of about 12 Å, interconnected

through 8-membered oxygen windows with diameters of about 4.3 Å when not blocked by a cation. The Si/Al ratio determines the diffusivity to a large extent. A Si/Al ratio of 2 was taken for the simulations. The Na^+ and Ca^{2+} cations did not occupy sites in the 8-ring windows, which connect to α-cages. A counter-intuitive observation was made: although the 8-rings in zeolite A are far smaller than the 12-rings in zeolite Y, the diffusion of the argon atoms was faster than xenon diffusion in zeolite Y. This anomalous result could be explained by the "*ring effect*".

Extensive investigations on diffusion in zeolites were executed for methane. Various relationships between the diffusivities and temperature, occupancy, rigid or flexible frameworks, presence of ions etc. were investigated. The groups of Yashonath, Demontis and Haberlandt published most of the MD papers on this subject. The simulation results were compared with PFG NMR and in some cases with quasi-elastic neutron scattering (QUENS) results. To sum up, it can be stated that the diffusivities obtained from MD simulations and PFG NMR or QUENS measurements agree quite well. In the subsequent paragraphs details of the results will be given.

Demontis et al. /52, 53, 86/ investigated the diffusion of CH_4 in silicalite. Demontis et al. /52/ adopted a harmonic model potential proposed in a previous paper on anhydrous natrolite and zeolite A. The model assumes that the potentials for Si-O and O-O interactions are represented by quadratic functions of the displacement from a given equilibrium bond distance /87, 88/. No other possible contacts are included, the initial topology of the framework bonds is retained during the MD simulations, and only first neighbors are considered as interacting atoms. Although this model is rather crude, it can reproduce the effects of the vibrations of the framework upon the diffusion of methane. As for the methane molecules, they were represented by soft spherical particles, mainly because attention was focused on the general features of the diffusion, so that a model as simple as possible allowing long simulation runs was desirable. The time step used in MD runs was 1 fs. This small value was chosen in order to ensure a good energy conservation, in view of the need for very long trajectories. The fluctuations of total energy were less than 0.1 %. Four MD simulations 200 ps long were performed. First the ability of the harmonic model to reproduce the most relevant structural and dynamical properties of silicalite was tested. For this purpose silicalite with empty channels was simulated. The second run was for the full system with 24 CH_4 molecules at a temperature of 298.1 K. The third run was with a monoclinic cell at 302.6 K as a consequence of the results of the second run. The last run was carried out with a fixed framework for comparison of the results with the flexible framework. Methane-methane interactions were represented by a 20-6 Lennard-Jones potential between the centers of the molecules, derived by Matthews and Smith /89/ from experimental data. The minimum falls at 3.88 Å, and is -0.431 kcal/mol deep. Methane-framework interactions were described according to Ruthven and Derrah /50/. The potential was slightly modified: as no cations are present in silicalite, the polarization term was dropped. The potentials were:

$$V_{CH_4\text{-}CH_4} = 1.0992 \cdot 10^{11} \cdot r^{-20} - 2.09835 \cdot 10^{3} r^{-6} \tag{2.21}$$

$$V_{CH_4\text{-}O} = 2.28 \cdot 10^{6} \cdot r^{-12} - 1.33 \cdot 10^{3} \cdot r^{-6}. \tag{2.22}$$

The usual minimum image convention was used, and the equations of motion were integrated by means of a modified Verlet algorithm. The diffusivities were calculated according to the

Einstein formula (eq. 1.1). The results of the MD simulation of the bare silicalite assuming a Pnma space group yielded mean values of the calculated coordinates in good agreement with the experimental ones, the standard deviation being 0.008 Å. The calculated diffusion coefficient was in very good agreement with a value found from NMR measurements by Caro et al. /90/. The simulated diffusivity was $D = 6.58 \cdot 10^{-9}$ m^2/s, which corresponds very well with the experimental value of $6.5 \cdot 10^{-9}$ m^2/s. For the fixed framework the diffusivity was approximately 20 % smaller ($D = 5.41 \cdot 10^{-9}$ m^2/s). The components of the diffusivities were (values of the fixed framework in brackets): $D_x = 3.59 \cdot 10^{-9}$ m^2/s ($4.93 \cdot 10^{-9}$ m^2/s); $D_y = 14.9 \cdot 10^{-9}$ m^2/s ($9.66 \cdot 10^{-9}$ m^2/s) (straight channel); $D_z = 1.22 \cdot 10^{-9}$ m^2/s ($1.64 \cdot 10^{-9}$ m^2/s). The authors argued that the CH_4 molecules float unhindered along the straight channel. The radial distribution functions revealed that the methane molecules move preferentially close to the axes of the channels. In the sinusoidal channel, the oscillating zeolite framework acts to tighten up the diameter of the channels. The result is a reduced diffusivity. The methane-methane radial distribution function exhibited a maximum at 3.75 Å, a distance slightly smaller than the minimum of the CH_4-CH_4 potential function. This maximum could reflect frequent collisions as well as permanent or transient methane dimers or clusters. A detailed analysis gave convincing hints that dimers and even clusters of three or four atoms occured. In a subsequent paper Demontis et al. /53/ investigated the temperature dependance of the diffusivity of CH_4 in silicalite. The potentials were adopted from the previous paper /52/. Three methane molecules per channel intersection were included in the MD system, i.e. 12 molecules per unit cell, 600 particles altogether. Simulations were executed for temperatures of 446, 290, 221 and 167 K. When the logarithms of the diffusivities were plotted against 1/T the characteristic Arrhenius behavior could be observed, suggesting that diffusion is an activated process. The activation energy was 2 kJ/mol, the corresponding experimental value is 4 kJ/mol /11/. The components of the diffusivities were close to measured values. A comparison of the diffusion coefficients obtained from fixed and vibrating framework simulations showed no regular trend, possibly because of statistical errors, but in any case they were similar, contrary to the results from the simulations of cation-free zeolite A. The activation energies and the radial distribution functions for the rigid and flexible framework were also similar, but by considering the velocity autocorrelation functions /41, 42/, relevant differences were detected. When methane molecules collide with the walls, backscattering can occur, resulting in negative velocity correlations. The effect of the rigid framework on the velocity relaxation is to cause a little shortening of the crossover time and to enhance the region of negative and positive correlation. Since the self-diffusion coefficient is proportional to the time integral of the velocity correlation function, the diffusion coefficients are quite similar for a fixed and a vibrating framework. Lattice vibrations enhance the number of binary collisions for temperatures higher than room temperature while multiple collisions are inhibited. On the contrary, in fixed framework simulations an exaggerated number of multiple collisions take place. To sum up, the energy exchange due to the vibrations of the framework in silicalite gives rise to significant effects on the motion of sorbate molecules. One should keep in mind that these considerations are for 12 CH_4 molecules per unit cell. Demontis et al. /91/ extended their investigations to the case of high dilution. In this case the influence of the vibrating framework on the diffusion mechanism of small molecules is not as dramatic as in the case of twelve molecules per unit cell. In the absence of collisions between sorbed particles, the diffusion is controlled by the interactions and collisions with channel walls, and the motion along the straight channels maintains on the average the initial direction. This

effect yields positive but oscillating velocity autocorrelation functions of unusual form.

June et al. /64/ performed simulations of the diffusive properties of CH_4 in silicalite for various temperatures and loadings. The computational details were the same as for the simulation of xenon diffusivities. At 200 K the diffusivity was nearly independent of the loading, but at higher temperatures the diffusion coefficient decreased with increasing occupation. The values of the diffusion coefficients were in good agreement with experimental results /92/, except at 200 K, where the simulations gave two times higher values than the measurements. June et al. /64/ also calculated the rotational diffusivity. As a result of sorbate-sorbate collisions, which act to decorrelate the molecular orientation, the rotational diffusivity was found to increase with concentration.

Bandyopadhyay and Yashonath /93/ also extended their calculations on xenon. The zeolite framework was assumed to be rigid. The zeolite-methane dispersive interaction term was taken from Bezus et al. /51/, and for the repulsive part the force on a pair of atoms was set to zero at the sum of their van der Waals radii. The time step was 10 fs for a total run time of 600 ps. They calculated the rate of diffusion from one α-cage to another to be $1.9 \cdot 10^{10}$ per sorbate atom per second in NaY zeolite and $24.3 \cdot 10^{10}$ per sorbate atom per second in NaCaA zeolite. Again, the "ring effect" was observed: methane diffuses faster through the zeolite with the smaller pores. The faster diffusion in zeolite A persists at higher temperatures, but was far less pronounced. This is caused by the larger amount of centralized diffusion at higher temperatures. For this case both zeolites present a potential well to centralized diffusion whereas at low temperatures diffusion close to the wall dominates, and this mode of diffusion presents a potential barrier for the NaY and a well for the NaCaA zeolite.

Fritzsche et al. /57, 58, 94, 95, 97/, Jost et al. /96/ and Haberlandt /98/ published papers on diffusion of CH_4, Xe and C_2H_6 in NaCaA and its cation-free analogue ZK4. In paper /58/ a fixed zeolite lattice was assumed, and the thermal equilibrium of the diffusing molecules was maintained by renormalizing the particle velocities after each step. This reduces the computing time compared to e.g. a Nosé-Hoover thermostat /42/, but is thermodynamically not completely correct. The authors detected that the diffusing molecules are able to thermalize their own kinetic energy to a Boltzmann distribution at any point within the zeolite lattice. This means that the energy exchange between the zeolite and the sorbent is almost negligible. In a subsequent paper /57/ the first four moments of the particle displacement profiles were calculated by MD simulations and compared with expressions derived from the solution of the diffusion equation. The n-th moment of the distribution curve of molecular displacement is defined by the relation

$$\left\langle \left| \mathbf{r} - \mathbf{r}_o \right|^n \right\rangle = \int \left| \mathbf{r} - \mathbf{r}_o \right|^n P(\mathbf{r}, \mathbf{r}_o, t) d\mathbf{r} \,. \tag{2.23}$$

Solving the diffusion equation for an infinite system, the probability density of finding a particular particle at time t at position $\mathbf{r}$, if it has been at position $\mathbf{r} = \mathbf{r}_o$ at time $t = 0$, is found to be

$$P(\mathbf{r}, \mathbf{r}_o, t) = (4\pi D t)^{-3/2} \exp\left(\frac{-(\mathbf{r} - \mathbf{r}_o)^2}{4Dt} \right), \tag{2.24}$$

where D is the diffusivity. Substituting eq. 2.24 in eq. 2.23 gives the following first four

moments:

$$\left\langle \left| \mathbf{r} - \mathbf{r}_o \right| \right\rangle = 4\sqrt{Dt/\pi} \tag{2.25}$$

$$\left\langle \left| \mathbf{r} - \mathbf{r}_o \right|^2 \right\rangle = 6Dt \tag{2.26}$$

$$\left\langle \left| \mathbf{r} - \mathbf{r}_o \right|^3 \right\rangle = \frac{32}{\sqrt{\pi}} (Dt)^{3/2} \tag{2.27}$$

$$\left\langle \left| \mathbf{r} - \mathbf{r}_o \right|^4 \right\rangle = 60(Dt)^2 . \tag{2.28}$$

These four moments can only coincide with the ones calculated from MD simulations if the distribution is indeed given by eq. 2.24. A comparison of the diffusivities derived from the four moments may serve as a test of the validity of the diffusion equation on intracrystalline zeolitic diffusion. Diffusivities calculated in this way at 300 K for mean occupation numbers of 1, 3 and 7 CH_4 molecules per cavity in ZK4 coincided after 30-60 ps molecular propagation. One has to conclude that for times larger than 30-60 ps molecular propagation is already described by distributions of the form of eq. 2.24, indicating that a kind of hydrodynamical stage has been reached. Diffusivities in ZKA were calculated as a function of concentration and for two sets of potential parameters σ, labeled A and B /94, 97, 98/. Set A was based on σ-values taken from Bezus et al. /51/, Kiselev and Du /55/ and Goodbody et al. /56/, set B from Ruthven and Derrah /50/, Demontis et al. /91/ and Cohen de Lara et al. /99/. Set A simulates slightly larger windows in zeolites than set B. Set B has a slightly larger value of σ_{CH_4-O} and a smaller value of ε_{CH_4-O} than set A. The authors computed for both sets isopotential surfaces of the center plane of an α-cage. These turned out to be quite similar. The center of a cage is a region of high potential energy and, therefore, nearly free of methane molecules at low or medium CH_4 concentrations. Set A gave a potential minimum in the plane of the 8-ring window, whereas set B predicted a smaller minimum near the inlet of the window, and the plane of the window corresponded to a saddle point. A methane loading of 1-7 molecules per cage was assumed. The MD runs were performed with a time step size of 5 fs over 0.75 ns. The residence time of a methane molecule in a cage was investigated by trajectory studies (see Fig. 2). With increased loading an increasing fraction of methane molecules that cross into a neighboring cage jump directly back into the cage from which they started (see Fig. 2b). This phenomenon occurred more often with decreasing temperature. The residence time in a cage was calculated to be 5-10 ps. At low concentrations it is difficult to "find" a window (see Fig. 2a). The more frequent intracavity collisions at higher loading lead to more passes through the window. On the other hand, the methane molecules will be more often knocked back into the cage where they came from. The diffusivities depend, as expected, on the parameter sets. Set A predicts a decrease of the diffusivity as loading increases, while set B predicts the opposite. Fritzsche et al. /95/ investigated the influence of extraframework cations Na^+ and Ca^{2+} in zeolite A. The windows were free from cations. The cations were situated near the hexagonal faces of the sodalite units in zeolite A. The parameter sets A and B were taken as in ZK4, augmented by a polarization term, which gives the inter-action energy of the induced dipole with the electric field while the dipole-dipole interaction of the induced dipoles of the guest molecules was considered to be a second order correction as well as a back-polarization effect. The aim of this investigation was to show the strong influence of the induction energy on diffusion of a small neutral molecule in a zeolite. The simple model proposed by Ruthven and Derrah /50/ was used to get effective cation diameters and effective

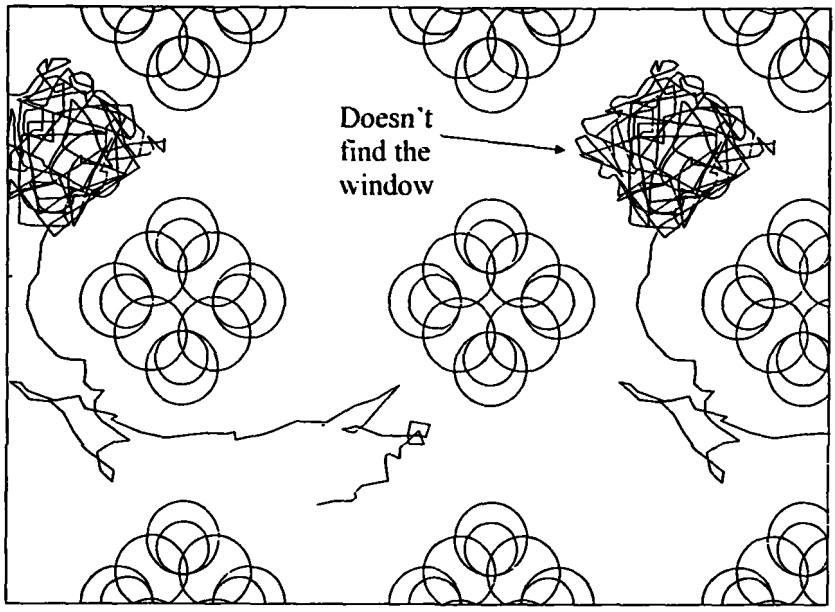

a)

b)

Fig. 2 Trajectories of methane within α-cages of ZK-4 for a) low and b) high loadings /118/.

charges of -0.25e on each oxygen. The other lattice atoms were treated as uncharged. The computational effort was much larger for NaCaA compared to ZKA, as much longer trajectories (up to 5-10 ns) were necessary to evaluate the small diffusivities which were found to be up to two orders of magnitude smaller than in ZK4. This was confirmed experimentally by Heink et al. /77, 100/. Parameter set A gave by far better results than set B. Increased loading leads to increase in the self-diffusivity at high loading (8 methane molecules). Between 6 and 7 CH_4 molecules per cage showed a shallow minimum in the diffusivity for set A. In Fig. 3 isopotential contour maps of NaCaA for the sets A and B are presented.

Catlow et al. /103, 104/ performed MD simulations of methane diffusion in silicalite in flexible zeolite frameworks based on a potential developed by Vessal et al. /105/. The parameters of this potential were derived by fitting to reproduce the static structural and elastic properties of α-quartz. The CH_4-CH_4 interaction potentials were taken from Kiselev et al. /66/ with methane treated as a flexible polyatomic molecule. The time steps in the simulations were 1 fs over 120 ps. The diffusion coefficient increased by a factor of 3 with increase of concentration from 1 to 2 methane molecules per cell, in contrast to experiments and other simulations. At lower temperatures the methane molecules occupied preferably the centers of the straight channels, whereas at higher temperatures also the zigzag channels were occupied.

Nicholas et al. /106/ investigated methane diffusion in silicalite, based on an MM2 /40/ force field. A simulation box of 27 unit cells was used, into which up to 216 methane molecules were placed. The zeolite lattice and the methane molecules were assumed to be rigid. Unlike other investigations, intermolecular interactions from the zeolite silicon atoms were included. Additionally, an electrostatic term was included in the potential energy. The calculated diffusivities at a temperature of 300 K were in good agreement with measurements, and showed a decrease with increasing concentration from 4 to 16 molecules per unit cell.

Nowak et al. /107/ found for short simulation time scales that methane is trapped inside pockets of the straight channel system of EU-1 zeolites, which have a unidimensional pore system with side pockets perpendicular to the main channel system.

As expected, the interaction potentials and their parameters play a dominant role for the quality of the simulation results. Ermoshin and Engel /108/ developed a new potential energy surface for methane in silicalite using a general approach to determine the molecule-framework interaction. Estimations based on general physical principles to describe intermolecular forces were presented. The developed potential was then used in MD calculations of diffusion coefficients and the heat of adsorption for methane adsorbed in silicalite. The potential energy of a spherical methane molecule being located at the coordinate origin and interacting with the atoms (i) of the zeolite framework at positions $\mathbf{r}_i$ can be written as a sum of electrostatic, V_E, inductive, V_I, dispersive, V_D, and repulsive, V_R, interactions:

$$V = V_E + V_I + V_D + V_R . \tag{2.29}$$

The electrostatic term is expressed in a multipole expansion (see e.g. /109/). Because of the spherical symmetry of CH_4, V_E is set equal to zero, $V_E = 0$. The inductive interaction is given by:

$$V_I = -0.5\alpha \mathbf{E}^2 , \tag{2.30}$$

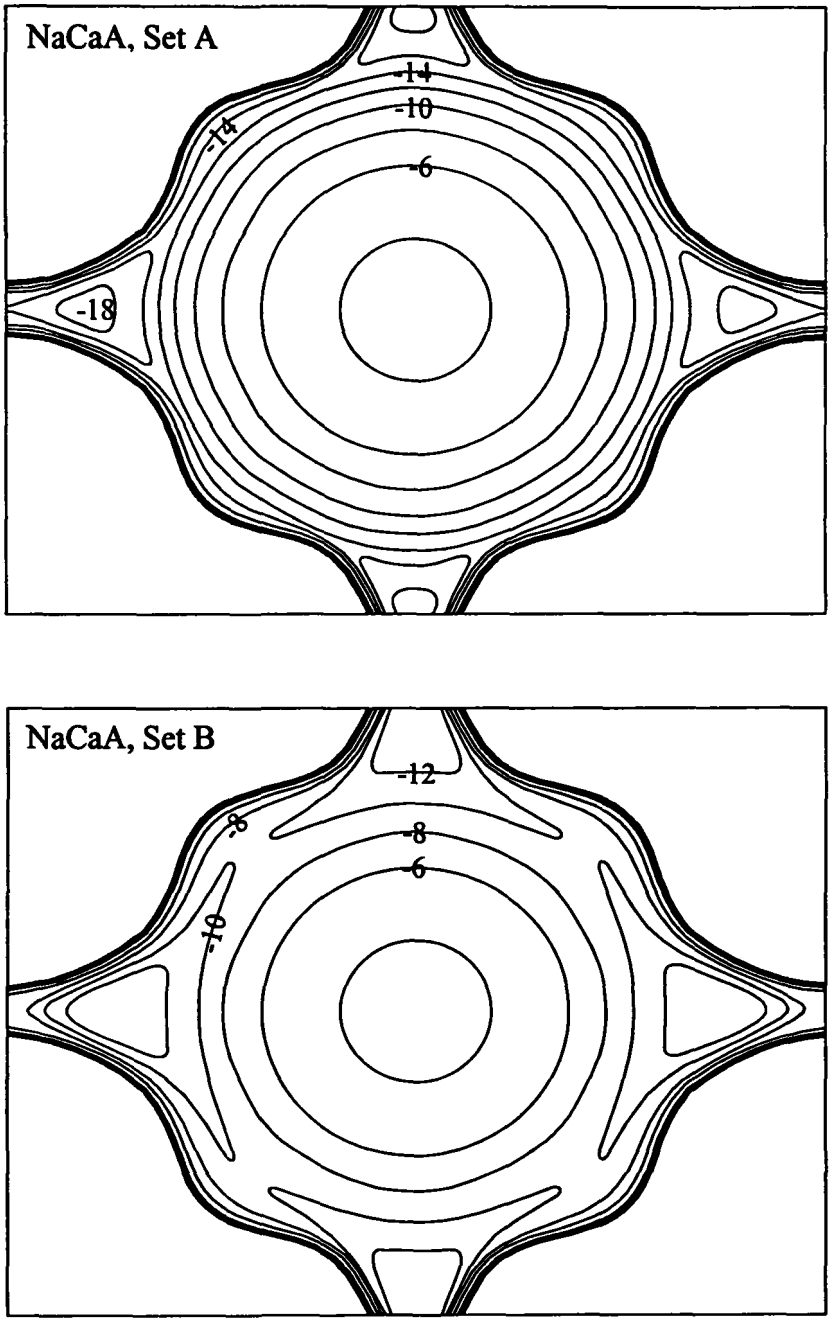

Fig. 3 Potential contour maps inside an α-cage of NaCaA zeolite for potential parameter a) set A and b) set B /97/.

where **E** is the electrostatic field vector at the position of the molecular center of mass and α is the static polarizability of the molecule. The polarizability of CH_4 is 2.593 $Å^3$ /92/. The polarizabilities of the framework atoms can be estimated with the help of the screening constants method /76/. The electrical field is a vector sum of fields originating from the ions:

$$\mathbf{E} = -\sum_i q_i \frac{\mathbf{r}_i}{|\mathbf{r}_i|^3} \tag{2.31}$$

Here $|\mathbf{r}_i|$ is the distance between the molecular center of mass and the ion i, and q_i is the respective charge. The dispersion interaction term is given by:

$$V_D = -\sum_i C_i r_i^{-6}, \tag{2.32}$$

where the van der Waals dipole-dipole coefficient was estimated via the Slater-Kirkwood combination rule /76/ (compare with eq. 2.17):

$$C_i = \frac{3}{2} \frac{\alpha \alpha_i}{(\alpha/n)^{1/2} + (\alpha_i/n_i)^{1/2}}. \tag{2.33}$$

Here α_i (α) is the static polarizability of the ion i (molecule), and n_i (n) is the number of valence electrons. The use of the number of valence electrons in eq. 2.33 in general overestimates the dispersion coefficient. Therefore, one should use effective values for this quantity /110/. For methane a $n_{CH_4} = 5.797$ was chosen. Eq. 2.33 can be transformed to the Lennard-Jones expression /76/ if the diamagnetic susceptibility is expressed via α_i and n_i, e.g. in atomic units (a.u.):

$$\chi_i = \sqrt{n_i \alpha_i} / 4c^2, \tag{2.34}$$

where c is the velocity of light. The repulsion energy is given as

$$V_R = \sum_i B_i r_i^{-12}, \tag{2.35}$$

where the coefficients B_i are calculated at the equilibrium distances between a framework atom (i) and the CH_4 molecule through the derivatives of V with respect to the intermolecular distance $|\mathbf{r}_i| = r_i$:

$$B_i = 0.5(R + R_i)^6 C_i - \frac{(R + R_i)^{13}}{12} \alpha |\mathbf{E}| \frac{d|\mathbf{E}|}{dr_i}\Big|_{r=R+R_i}, \tag{2.36}$$

where $r = R + R_i$ is the sum of the van der Waals radii of CH_4 and the ion i. The authors demonstrate that the induction energy can be neglected such that the second term in eq. 2.36 can be dropped. How to get the proper van der Waals radii, polarizabilities, ionic charges, valence electrons and Lennard-Jones parameters is demonstrated in the paper /108/. To test the potential, MD calculations were executed for a rigid and a flexible silicalite lattice. The influence of framework vibrations on the calculated quantities was investigated using the ab initio generalized valence force field (GVFF) model of the framework potential /111/. An MD box of 3456 framework atoms arranged in the zeolite structure (2 x 2 x 3 unit cells) was employed. The cutoff distance for the shifted potentials /41/ was taken as $R_{cut} = 19$ Å. The integration time step was 2 fs. During the first 20 ps the system was equilibrated at 300 K by scaling the velocities with a relaxation constant of 0.4 ps /112/. The positions of the methane

molecules were stored every fifth step during the 50 ps propagation, and the final positions and velocities were taken as initial conditions for a new run. An average of 16 uncorrelated runs was used in the calculation of the diffusion coefficients. The heat of adsorption H_{ads} was calculated as:

$$H_{ads} = \langle V \rangle - RT, \tag{2.37}$$

where $RT = 0.596$ kcal/mol at $T = 300$ K, and $\langle V \rangle$ is an ensemble averaged potential energy of the methane-framework interaction. The following results were obtained for the self-diffusivity $D = 1/3\ (D_{xx} + D_{yy} + D_{zz})$: $D[\text{Å}^2/\text{ps}] = 1.0 \pm 0.2$ (rigid framework), $D[\text{Å}^2/\text{ps}] = 1.4 \pm 0.25$ (flexible framework), $D[\text{Å}^2/\text{ps}] = 1.3 \pm 0.55$ (expt. /92/, extrapolated to zero loading); H_{ads} [kcal/mol] = −4.69 (rigid framework); H_{ads} [kcal/mol] = −4.76 (flexible framework); H_{ads} [kcal/mol] = −4.8 (expt. /113/). The authors stressed that the heat of adsorption provides a more sensitive measure for the quality of molecule-zeolite potentials than the diffusion coefficient.

The groups of Haberlandt /98, 115, 118/ and Bell /116/ published investigations on transport in zeolites in the presence of macroscopic transfer fluxes. Maginn et al. /116/ simulated methane in ZSM-5 in a rigid lattice. All interactions were described by Lennard-Jones potentials. The potential parameters were taken from Kiselev /66/. Two different non-equilibrium molecular dynamics (NEMD) techniques were developed. The first approach was called gradient relaxation molecular dynamics (GRMD). In this technique, a concentration gradient is set up within the zeolite simulation cell and the equations of motion are integrated using the same constant kinetic energy algorithm as is used in equilibrium molecular dynamics calculations. By monitoring the relaxation of the concentration gradient as a function of time and fitting this relaxation to the appropriate continuum solution of the diffusion equation, a transport diffusivity is obtained (see eq. 1.3). The GRMD method is an attempt to mimic as closely as possible the transient conditions prevailing in a macroscopic measurement, such as an uptake rate experiment. The method relies on Fick's first law to define the transport diffusivity (see eq. 1.2). The GRMD simulation corresponds to the following continuum one-dimensional diffusion problem

$$\frac{\partial c}{\partial t} = D_T \frac{\partial^2 c}{\partial y^2} \tag{2.38}$$

with boundary conditions

$$\left.\frac{\partial c}{\partial y}\right|_{y=0} = \left.\frac{\partial c}{\partial y}\right|_{y=L} = 0 \tag{2.39}$$

and initial condition (2.40)

$$c(y,0) = f(y).$$

Here, t is time, $c(y,t)$ the concentration as a function of position and time, L is half the length of the parent simulation box in the y-direction, and $f(y)$ is the initial concentration profile. The GRMD method is computationally intensive, because a large number of molecules must be tracked to obtain continuum-like behavior. To overcome this difficulty, a second technique, referred to as the "color field" NEMD method, was developed. In this technique the response

of the system to a perturbing field is measured and related to the corrected diffusivity (see also eq. 1.3), D_c, through the application of linear response theory. The corrected diffusivity is given by

$$D_c = \frac{1}{3N}\int_0^\infty dt' \sum_{i=1}^{V}\sum_{j=1}^{V}\left\langle \mathbf{v}_i(t')\cdot\mathbf{v}_j(0)\right\rangle . \tag{2.41}$$

For comparison the self-diffusivity is presented:

$$D_{self} = \frac{1}{3N}\int_0^\infty dt' \sum_{i=1}^{N}\left\langle \mathbf{v}_i(0)\cdot\mathbf{v}_i(t')\right\rangle , \tag{2.42}$$

where N is the number of sorbate molecules and $\mathbf{v}_i$ is the velocity of sorbate molecule i. By comparing eq. 2.41 with eq. 2.42, it can be seen that the corrected diffusivity, D_c, is a collective property that depends on the total flux of all sorbate molecules. D_{self}, on the other hand, depends only on the autocorrelation of individual molecule velocities. D_T and D_c are related via the thermodynamic correction factor, eq. 1.3:

$$D_T = D_c\left(\frac{\partial \ln f}{\partial \ln c}\right)_T . \tag{2.43}$$

Nonequilibrium molecular dynamics has been used to predict transport properties for a wide variety of systems. A review of NEMD techniques is given by Allen and Tildesley /41/, Cummings and Evans /117/ and Sadus /43/. A color conductivity algorithm analogous to the one used to calculate binary diffusivities in liquid systems can be applied to zeolites as well. The color field NEMD method allows for an arbitrarily small external field to be used. Fig. 4 presents the transport diffusivities of methane in silicalite as calculated by the color field

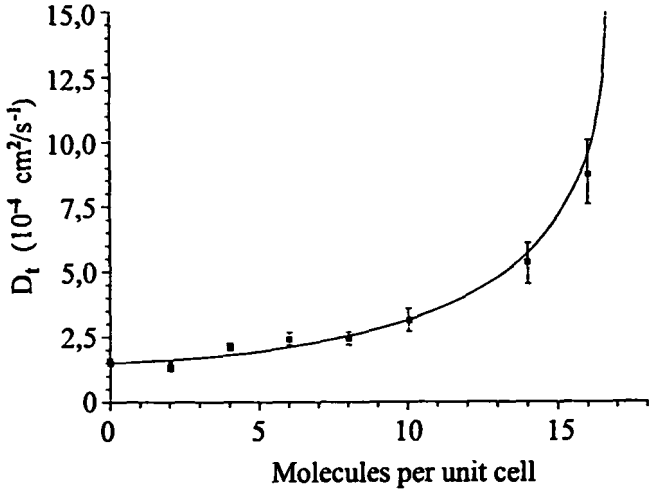

Fig. 4 Transport diffusivities of methane in silicalite as a function of loading at 300 K. The line was calculated by the Darken model. The points correspond to color field NEMD results /116/.

NEMD method. For comparison, the results of the Darken model are shown. The Darken correlation was calculated by making the approximation that $D_c(c) \approx D_{self}(0)$. As can be seen from Fig. 4 only at high loadings there are somewhat larger deviations between the two approaches. In Fig. 5, the self-diffusivities computed from equilibrium MD simulations are compared to the corrected diffusivities obtained from color field NEMD simulations. The corrected diffusivities remain nearly constant with increasing concentration, whereas the self-diffusivity decreases. Fritzsche et al. /115/ compared the different diffusivities of methane in silicalite.

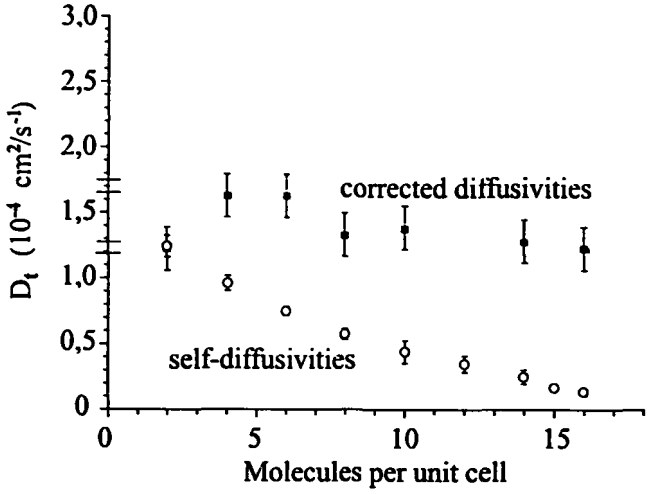

Fig. 5 Corrected diffusivities obtained from color field NEMD simulations, and self-diffusivities from equilibrium MD simulations /116/.

Using MD, Tepper et al. /119/ recently studied tracer diffusion of methane in the unidirectional channels of $AlPO_4$-5, which has straight nonconnected pores. To model methane, a Lennard-Jones potential was used. Dynamics runs were carried out in the canonical ensemble at a temperature of 300 K. The pores were filled to a density of 0.7 molecules per unit cell. A 50 ns production run was carried out after equilibration, and the mean square displacement of the particles was calculated for correlation times up to 30 ns. Next, a simple Monte-Carlo hop-and-cross model was introduced to mimic the MD simulations. The increased computational speed of the simplified model allowed for an in-depth investigation of system size effects. These effects turned out to be of great importance and hence very large system sizes were needed to eliminate the influence of periodic boundaries on the longer time scales. Since these large sizes are not easily accessible by normal molecular dynamics simulations, the simplified model proved to be of great use. An important result is that after elimination of system size effects, the motion of guest molecules is not strictly single file in nature. Although infrequent, crossing events may occur, and lead to a normal diffusive regime on large timescales. On short timescales, intermediate behavior was found, where the mean square displacement is proportional to $t^{0.64}$, while at a time of about 7

ns, a crossover to normal diffusion was found. These findings are in contrast with the experimental observation of single-file diffusion reported by Kukla et al. /122/ in 1996 using PFG NMR. The authors argue that this might be explained with pore blockages. This was confirmed by other PFG NMR /123/ and QUENS /124/ studies which detected normal diffusion on their time scales.

Sholl /120/ introduced MD methods that allow to study metastable adsorbed clusters at arbitrary temperatures. Diffusion and dissociation kinetics of clusters of SF_6 and CF_4 in $AlPO_4$-5 pores were simulated by this approach. These simulations confirm the observation of previous transition-state theory calculcations that the single-file diffusion of SF_6 and CF_4 in $AlPO_4$-5 is controlled not only by the motion of single adsorbed molecules, but also by dynamical events involving the concerted motion of multiple molecules. The mechanism that allows concerted cluster diffusion in $AlPO_4$-5 pores, namely the existence of a mismatch between the ideal adsorbate-adsorbate spacing and the pore's lattice spacing, is quite general. This observation suggests that concerted cluster diffusion and dissociation events could influence molecular diffusivities in a wide range of microporous materials with uni-dimensional pores. Therefore, it is important for the description of single file diffusion to include the formation and dissociation of clusters. As was pointed out by Sholl and Fichthorn in a previous paper /125/, concerted diffusion of molecular clusters can indeed be the dominant diffusion mechanism for molecular transport in these systems. One significant implication of this result is that single-particle models of single file diffusion cannot accurately describe particle mobilities during single-file diffusion.

Sholl and Fichthorn /126/ provided a general classification of the types of diffusion possible for multicomponent adsorbate mixtures in one-dimensional pores. The diffusion of mixtures of Ne and CF_4 in $AlPO_4$-5 pores was examined as an example of "dual-mode diffusion". "Dual-mode diffusion" means that the smaller (larger) species performs normal (single-file) diffusion, so that the long term behavior of tracer particles of the two species is very different. The usual criterion used to distinguish between normal and single-file diffusion is the scaling of the mean-square displacement with time. During normal diffusion in a one-dimensional pore the dependence $\langle x^2(t)\rangle = 2Dt$ can be observed where D is the tracer diffusivity. By contrast, if adsorbates are unable to pass one another in a pore, their mean square displacement is given by $\langle x^2(t)\rangle = 2Ft^{0.5}$. This type of diffusion is called single-file diffusion, and F is referred to as the single-file mobility. However, Keffer et al. /127/ showed that if adsorbates can pass one another infrequently, this criterion yields ambiguous results, even though as $t \to \infty$, $\langle x^2(t)\rangle \propto t$. Particle transport is this regime is said to occur by transitional diffusion. This case can be considered as a special case of normal diffusion. The alternative procedure for distinguishing between normal and single-file motion, namely to compare the particle sizes to the nominal pore diameter, can also lead to incorrect results /127/. Sholl and Fichthorn /126/ have shown that related criteria which use a slightly refined description of the pore structure and essentially approximate adsorbate particles as hard spheres can correctly account the diffusion modes of all of the species and mixtures studied in their paper. Hahn and Kärger /128/ discussed the results of Sholl and Fichthorn /125/, and gave indications that infinite dilution tracer diffusivities, D_{id}, and the single-file mobility, F, are related as follows:

$$D_{sd} = \pi \frac{F^2 \theta^2}{\sigma^2 (1-\theta)^2} \tag{2.44}$$

where σ is the nominal diameter of the sorbate and θ is the pore occupancy relative to a perfect one-dimensional arrangement of sorbates. Sholl and Fichthorn discuss this point in a subsequent paper /129/. Hahn and Kärger /130/ investigated deviations from ideal single-file behavior in zeolite host-guest systems with a one-dimensional channel structure. Deviations from ideal single-file behavior, i.e., from proportionality between the mean square displacement and the square root of the observation time, occur as soon as the finite length of the single-file system must be taken into consideration and the rate of mutual passages of the particles within the single-file system cannot be considered to be negligibly small anymore.

Schuring *et al.* /333/ carried out MD simulations of self-diffusion of linear and branched alkanes in mordenite and ZSM-22, amongst other zeolites. The diffusivities are strongly dependent on occupancy, but no single-file behavior was observed under any circumstance. They proposed the following mechanism to explain this observation: the activation barriers are too low for the individual molecules to really move in hops. No passings were observed, and the length of the simulation box did not seem to have an influence on the results. Therefore, a collective, resonant diffusion mechanism seems to occur, as is indicated by the chainlength dependency of the diffusivity and the activation energy. Such a mechanism was also proposed by Runnebaum and Maginn /136/ for diffusion along the straight pores of ZSM-5. Simulations by Sholl and Fichthorn /125, 334/ also indicated that collective motions of loosely bound clusters of adsorbates can play an important role, although the diffusion process was still considered to be activated by these researchers and single-file behavior was observed. Alkane-alkane collisions dominate the motion at high loadings. The barriers for diffusion of iso-butane and 2-methyl pentane in the large-pore mordenite are only 4.7 and 6.3 kJ/mol respectively, as opposed to a value around 30 kJ/mol in ZSM-5 and ZSM-22, which have tighter pores. In mordenite, the difference in diffusivity between iso-butane and n-butane is only a factor of 2, while it is three orders of magnitude in ZSM-5 and ZSM-22.

Recent simulations of diffusion in uni-dimensional pores often employ a hierarchical combination of molecular dynamics and dynamic Monte-Carlo to study long time scales. More results on this topic and on single-file diffusion in general can be found in Section 3.2.

Webster et al. /131/ investigated the effective catalytic pore sizes of zeolites, and discuss the apparent increase in effective catalytic channel intersection size with increasing temperature. Their approach presents an a priori description of relative pore sizes and can be used to investigate and describe numerous catalytic and adsorbent systems. Quantum chemical calculations (ZINDO) have been used for this purpose. The authors criticize the usage of van der Waals radii of oxygen or the oxide ion radius to calculate a window size for the large channel of HZSM-5 (or their Lennard-Jones corrected radii), since the values do not produce a pore of the necessary dimensions to allow for the passage of large aromatic molecules.

Gaub et al. /121/ determined explicitly the propagator of the motion which is closely related to the density autocorrelation function known as the van Hove function. This is done for the diffusion of methane in zeolites (ZK4, silicalite). Fourier transform in space of the van Hove function yields the intermediate scattering function, the decay of which is used to determine

the self-diffusion coefficient. Fourier transform in time yields the dynamic structure factor which can be compared with quasi-elastic neutron scattering results.

2.3 Molecular dynamics simulations of more complex molecules and mixtures

Many MD simulations are directed towards alkanes /132-137, 141, 145/, and a few towards alkenes and alkynes. Dumont and Bougeard /132/ simulated the diffusion of ethane, ethene, ethyne (acetylene) and propane in silicalites. The silicalite framework was held rigid, but the hydrocarbons were modeled as flexible molecules. The potential parameters could reproduce infrared spectra. The simulations showed that the molecules move along the center of the channels, while the channel intersections are avoided. The diffusivities obtained were $0.59 \cdot 10^{-8}$ m^2/s and $0.19 \cdot 10^{-8}$ m^2/s for ethyne and propane, respectively. A comparison of diffusivities of ethane (bent), ethene (flat), and ethyne in the zigzag channel revealed that ethane diffuses the slowest, ethene approximately 30 % faster, and ethyne three times as fast. In the straight channel, both ethene and ethyne diffuse about three times faster than ethane. This result is in accordance with the relative cross-sectional area of the three hydrocarbons. The authors obtained a diffusivity of $1.29 \cdot 10^{-8}$ m^2/s for ethene. Nicholas et al. /133/ calculated diffusivities for a concentration of 4 and 12 propane molecules per silicalite unit cell, and obtained values of $0.12 \cdot 10^{-8}$ m^2/s and $5 \cdot 10^{-11}$ m^2/s, respectively. These values are far below those computed by other researchers.

Diffusion of long-chain hydrocarbons (C_8-C_{20}) was investigated by June et al. /134/, Maginn et al. /135/, Runnebaum and Maginn /136/ and Webb et al. /137/. Extensive experimental investigations of the molecular dynamics of n-octane in ZSM-5 using solid-state NMR (^2H NMR) and QUENS were executed by Stepanov et al. /138/. June et al. /134/ calculated self-diffusivities for butane and hexane in silicalite, which were found to be monotonically decreasing function of sorbate loading. The anisotropy in the predicted diffusion tensor was similar to that found in smaller molecules such as methane. Two long-timescale dynamical processes detected during the simulations were the interchange of sorbate molecules between the straight and sinusoidal channels and the conformational isomerization of sorbate molecules about non-terminal carbon-carbon bonds. Both processes have time constants of the order of 100 ps. The longest among these time constants is associated with the interchange of molecules between the two channel systems and can exceed 500 ps for hexane. Such long-time relaxation phenomena require extremely long simulations to safely probe the dynamical behavior of hexane or longer alkanes in silicalite. Webb et al. /137/ obtained diffusion constants and activation energies for diffusion, E_a, for linear and branched alkanes inside the zeolites TON, EUO and MFI via molecular dynamics simulations. Molecules with carbon numbers in the range $n = 7$-30 were studied in the dilute limit. TON contains a system of one-dimensional uninterrupted channels with small periodic undulations in the walls. The channels run in the [001] direction so only the D_z component of the diffusion tensor is applicable for molecules in TON. EUO has as system of one-dimensional channels as well. These run in the [100] direction with a corresponding diffusion constant D_x. The channels in EUO differ from TON because their walls are periodically interrupted by 12-member rings on alternating sides of the channel. These windows open onto pockets in the wall that are large enough for segments of linear or branched alkanes to enter. Diffusion in the pocket direction, however, is not possible. MFI has two channel systems that run in the [100] and [010] directions (D_x and D_y). This zeolite differs from TON and EUO because the channel systems intersect. The intersections

are such that a path is created allowing diffusion in the third dimension as well (D_z). The alkane molecules were simulated using a united atom approach in which the CH_n groups are treated as single particles. Intramolecular interaction between particles, or united atoms, were represented by bonded and nonbonded forces. Bonded forces were of three types: constraint forces which keep intramolecular nearest neighbors at a fixed bond distance, bending forces arising from a term like

$$V_b(\theta) = \frac{k}{2}(\theta - \theta_b)^2 \tag{2.45}$$

which maintain the equilibrium angle, θ_b, between successive bonds, and torsional forces from

$$V_t(\phi) = \sum_i a_i \cos^i(\phi). \tag{2.46}$$

Nonbonded forces were described by Lennard-Jones potentials. The interaction parameters were taken from Siepman et al. /139/ with torsional potentials from Jorgensen et al. /140/. The zeolite lattice was held rigid throughout the simulations, and the Lennard-Jones potential was used for interaction between the CH_n groups and the zeolite. Simulations were done in the temperature range between 300 and 900 K, and all were in the dilute limit. Since the zeolite was static and the molecules did not interact with one another, a Langevin equation employing a damping term and a random noise term was used to thermostat the alkanes. The time constant for the thermostat was $\tau = 1$ ps. The bond lengths were kept constant using the RATTLE algorithm /41, 43/. Linear alkanes diffused the fastest in TON, and this was attributed to the absence of any channel features which pose a significant hindrance to diffusion, that is minimal lattice effects. In dilute gas, alkane diffusion scales as $1/n$. The length of the smallest molecule studied was already greater than the unit cell length of TON in the channel directions. Therefore, the whole length of the unit cell is experienced by even the smallest molecule. In Fig. 6 data for the mean square displacement (MSD) are shown for carbon numbers $n = 10, 16$

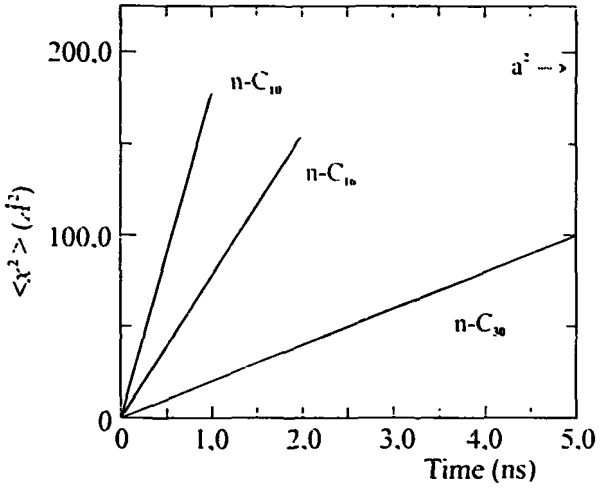

Fig. 6 Mean square displacements $\langle x^2 \rangle$ in EUO at $T = 600$ K as a function of time for n-alkanes ($n = 10, 16, 30$). The value of the unit cell parameter in the diffusion channel direction is indicated on the y-axis /137/.

and 30. The plots demonstrate the desired linearity for computing a reliable slope and, therefore, diffusivity. The value of the squared lattice parameter in the direction of diffusion is indicated on the y-axis. From this it can be seen that both C_{10} and C_{16} molecules move, on average, approximately the length of the unit cell within the duration of the MSD calculation. For linear alkanes, diffusion in EUO was the slowest among the three zeolites studied. In EUO there are large pockets off the diffusional channels that strongly influence linear alkane transport. Analysis of molecular trajectories demonstrated that diffusion in EUO occurs by molecules hopping from pocket to pocket. The first observed effect of this lattice feature is an overall decrease in diffusion relative to the other zeolites. The D_t-component dropped faster than a $1/n$ scaling. The authors explained this observation in terms of a lattice effect. Longer molecules are able to have both ends of the chain in a side pocket so diffusion can occur only when both ends come out of their pockes for a coordinated jump. As n increases so does the floppiness of the alkane molecule. That is, the motion at opposite ends of the chain is increasingly decorrelated, so the frequency of coordinated jumps is lowered. Monomethyl-branched alkanes diffuse slower than their linear counterparts, as expected. Branched molecules are bulkier, so that they interact more often with the channel walls. The anisotropy in the channel structure for MFI showed up in the data with regard to both magnitude and dependence on n. In connection with the n-alkanes some data from Heink et al. /77/ (see also Rees /12/) should be mentioned. As can be seen from Fig. 7, in all three zeolites, the self-diffusivity decreases with increasing chain length. This tendency was also experimentally observed by other authors, e.g., Cavalcante et al. /152/. The latter stress that the experimental evidence does not support the existence of a window effect for n-paraffins (C_6-C_{20}), as suggested by Gorring /153/.

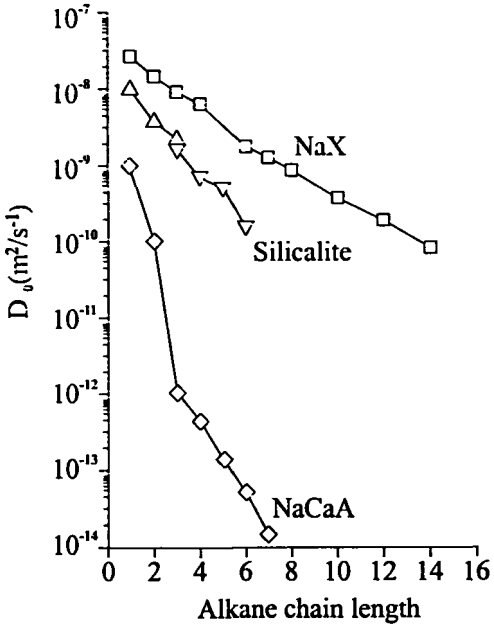

Fig. 7 Chain-length dependence of the self-diffusivities of n-alkanes in NaX, ZSM-5 and NaCaA at 298 K for a loading of one molecule per 24 (Si + Al) atoms /12/.

Corma et al. /141/ carried out atomistic MD simulations to calculate the diffusion of n-heptane and 2-methyl-hexane in purely silicious ITQ-1 which is a from of MCM-22, whose IZA code is MWW. This structure contains two independent pore systems formed by interconnected sinusoidal 10-member ring pores with a 4-5.5 Å diameter, and an independent 12-member ring system formed by large cages of 18.2 x 7.1 Å connected between them and with external surface through 10-member ring windows. The general purpose DL-POLY-2.0 parallel code /142/ was used throughout this study. The system comprised a 2 x 2 x 2 macrocell of ITQ-1 (1728 atoms) and 12 molecules of the C7 paraffin (276 atoms) located inside the macrocell. Two different simulations were executed: one with 12 molecules of n-heptane and the other one with 12 molecules of 2-methyl-hexane as the diffusing hydrocarbon. In each simulation, six molecules have been placed in the 10-member ring sinusoidal system and six molecules in the 12-member ring supercage void system. Time steps of 1 fs and an equilibration temperature of 450 K have been used in all the simulations. During the equilibration stage 20 ps runs were performed to ensure that the energy was stationary, and thereafter the simulations were additionally extended over 200 ps within the NVE ensemble. History files were saved every 1 ps, and from these, data analysis of the diffusion process was carried out. Explicit dynamical treatment of all the atoms of the system – 2004 in total – was included in the simulation. The DL-POLY code in its fully parallellized implementation was run on the 512 PE CRAY-T3D MPP computer at the EPCC (Edinburgh Parallel Computing Centre). The present simulations were run on 64 processors. The computer time used to complete all the simulations was 200 x 64 h. Four types of interatomic potentials were needed to model the system:

$$V_{total} = V_{zeolite} + V_{hydrocarb} + V_{hc-hc} + V_{zeolite-hc}. \tag{2.47}$$

The potential for the framework, $V_{zeolite}$, was originally derived by Catlow et al. /143/ and is essentially a Born model potential comprising three-body interactions, short-range terms, and long-range Coulomb interactions. The potential for the sorbates, $V_{hydrocarb}$, was taken from Oie et al. /144/ and comprises two-(bond), three-(angle), and four-body (dihedral) interactions together with Coulomb terms. The V_{hc-hc} and $V_{zeolite-hc}$ potentials were taken from /143/. Diffusion of 2-methyl-hexane through the 10-member ring sinusoidal systems presents serious steric restrictions, which make the molecules stick to the minimum energy locations of the channels. A slightly different picture appears for the branched alkane in the larger cavities in which, although extensive local motion is still the dominant feature, the larger void spaces together with the presence of some larger mobilities indicated that the process was activated and, therefore, larger mobilities can be expected at higher temperatures. The linear n-heptane showed a very different picture with respect to the branched isomer regarding diffusion through the simusoidal 10-member ring channel, the former diffusing without any steric restriction.

It is useful to present the main results of Stepanov et al. /138/ on NMR and QUENS investigations of n-octane in ZSM-5. The authors drew the following conclusions from their measurements. The peculiarity of the dynamic behavior of n-octane adsorbed in ZSM-5 depends on the loading. Upon exposure under vacuum of a ZSM-5 sample at room temperature to the vapor of n-octane, corresponding to a loading of 1.8 molecules per unit cell, the adsorption of this linear alkane occurs exclusively inside the straight channels of the zeolite lattice. N-octane molecules located in the straight channels of the zeolite diffuse essentially along the direction of the straight channels with a diffusion coefficient $D = 12 \cdot 10^{-n}$

m^2/s at 300 K. In the course of translational motion along the straight channels, some coupled rotational or librational motions of all CH_n ($n=2,3$) groups of the hydrocarbon skeleton in the molecule take place, which may correspond to the fast interconversions between trans and gauche conformations in the adsorbed alkane molecule. This "rotational" motion is reflected in the ^2H NMR spectra as fast rotations of the separate methylene and methyl groups simultaneously around two and three C-C bonds. Upon heating at 373 K for 1 h, n-octane molecules formerly located in the straight channels become redistributed over the straight and zigzag channels. Subsequent translational motion of n-octane consists of two independent modes of motion. One of them represents the movement along the tortuous zigzag channel. Another mode of translational motion represents the movement along the straight channels. This movement of the molecule is disturbed by collisions with the other molecules located mainly in the zigzag channels and in part at the channel intersections. For loadings equal to or higher than 3.5 molecules per unit cell the molecules showed isotropic reorientation inside the zeolite channel system, which may arise from collisions of the molecules at the channel intersections, thereby changing the direction of their translational motion.

Hernández and Catlow /145/ reported MD simulations of n-butane and n-hexane in silicalite. The framework was kept rigid. With regard to the adsorbate molecules, the authors have adopted a version of the Rijckaert-Bellemans model /154/. In this model both the CH_2 and CH_3 groups are represented as united atoms or beads, each one of the appropriate mass, i.e. 14 or 15 g/mol respectively. Directly bonded beads were maintained at a distance of 1.53 Å from each other through the use of constraints, which were imposed using Andersen's RATTLE algorithm. The diffusion of n-butane turned out to be slightly faster than that of n-hexane under similar conditions of temperature and loading. A general conclusion that could be drawn from the simulations was the observation that variations in the temperature have stronger effects than variations in the loading. The distribution of the dihedral angle in n-butane remains almost unaffected when the loading is varied from 2 to 8 molecules per unit cell, while it was seen to change drastically as the temperature was varied.

Diffusion of aromatics, especially benzene, was also simulated. Nowak /156/ carried out one of the first calculations of benzene and toluene in silicalite and theta-1, which has a uni-dimensional medium-sized pore window surrounded by 10-member rings. Only the straight channel of silicalite was considered. Both the zeolite framework and the aromatics were held rigid during the simulations. Activation energies for diffusion were calculated from differences in energy on the potential ways. Demontis et al. /157/ modeled the diffusion of benzene in zeolite NaY. A rigid framework was assumed. Benzene-benzene interactions were described with a Buckingham potential. Benzene–zeolite interactions were modeled by a short-range Lennard-Jones term and a long-range electrostatic term. Sixteen benzene molecules were simulated in a unit cell of zeolite Y. The diffusivities were calculated for 300 K. The MD simulations were initiated with benzene exclusively atop SII cations. In the subsequent simulation, the benzene molecules migrated to occupy window sites. This is in agreement with neutron diffraction studies of sorption location as a function of loading. Bull et al. /158/ performed MD simulations for one molecule of benzene adsorbed in a single unit cell of faujasite. The zeolite framework was flexible. The potential parameters were taken from the Cff91 force field from MSI (Molecular Simulations). Simulations were performed for diffusion at 298, 350, 400 and 450 K. An integration time step of 1 fs was employed. The total simulation

time was 25 ps. The agreement between the calculated diffusivities and ^2H NMR measurements was good.

Nakazaki et al. /155/ carried out MD simulations based on Dreiding force fields of benzene, toluene and xylene in ZSM-5. The results were visualized by means of computer graphics. The energy level of p-xylene entering the pores of ZSM-5 with the methyl group in front was the lowest among the molecules studied in all positions of the pore channels. The interaction of the methyl groups of the aromatics with the pore walls of ZSM-5 was fairly large.

Over the last few years some examples of MD calculations of binary mixtures were published. Jost et al. /96/ simulated the diffusion of mixtures of methane and xenon in silicalite. A rigid framework was used. For the interactions a 6-12 Lennard-Jones potential was used, and Methane was modeled by a simple spherical potential. A Verlet algorithm with a time step of 10 fs was applied. Each run contained a thermalization part of 10 000 steps (100 ps) and an evaluation part of 500 000 steps (5 ns). The MD box contained 128 guest molecules, equivalent to 16 unit cells for a loading of 8 molecules per unit cell. All simulations were carried out for a temperature of $T = 300$ K. At first it was demonstrated for the pure substances that methane diffuses much faster than xenon in silicalite. This is due to the mass ratio xenon/methane and to the different Lennard-Jones parameters, especially the different ε-parameters of the LJ interactions Xe–O and CH_4–O. In the mixtures xenon atoms obstruct diffusion more strongly than methane molecules. Having the same total amount of guest molecules in different mixtures the diffusion coefficient decreases with increasing fraction of xenon. The diffusion coefficients of methane and xenon are nearly the same for high xenon loadings, while for high methane loadings the xenon diffusion coefficients are much smaller than the methane diffusion coefficients. The reason for the very strong influence of the slower xenon atoms on the faster methane molecules is found in the topology of the channel system. The diameter of the channels is too small to allow a passing of the particles within the same channel. Therefore, the xenon atoms barricade the channels for the methane molecules. With increasing xenon fraction in the mixture more and more channels get blocked, and, from eight or nine xenon atoms per unit cell on, nearly all channels are occupied by xenon atoms and the methane molecules can only move within a cage of nearest xenon neighbors. Therefore, the methane molecules can no longer diffuse faster than the xenon atoms, they only rattle within the cages. Jost et al. /148/ compared MD simulations for the system methane/xenon in silicalite with PFG NMR measurements. The MD simulations were executed as in ref. /96/. The experimental results were in good agreement with the simulations. The diffusion coefficients for methane are a bit lower than the simulated values, but they were already within the error bars. The xenon diffusivity is nearly unaffected by the composition of the mixture. Xenon was not measurable at room temperature. At $T = 152$ K, the xenon diffusion could be measured. The measured absolute values of the xenon diffusivities were higher than the ones from simulations (up to twice the value).

Grillo and de Agudelo /150/ studied the relationship between structure and catalytic performance of Pt-HMOR model catalysts towards the n-butane hydroisomerization reaction employing a combination of simulation strategies. The procedure combined Monte Carlo (MC), MD and energy minimization techniques (EM). It was evidenced that the pore structure of mordenite not only affects the size and location of Pt particles, but also provides molecular sieve properties for the intermediates and products to be formed selectively in the reactions.

Gergidis and Theodorou /149/ studied the transport of n-butane-methane mixtures in the zeolite silicalite. Long MD simulations (up to 20 ns) for the calculation of diffusion tensor components for both species over a wide range of loadings (0 – 14 molecules per unit cell) and compositions were carried out. Self-diffusivities were seen to decrease monotonically with loading of either species. Raising the loading of n-butane from 2 to 9 molecules per unit cell caused the diffusivity of methane to drop by a factor of 60. The spatial distribution of molecules of the two co-adsorbed species showed that, at high occupancies, n-butane molecules force methanes to partially abandon straight channels and occupy the intersection regions. At high methane concentrations, n-butane molecules are forced to preferentially populate the gauche conformation. At high loadings, anomalous diffusion was detected for both species. Anomalous effects were more pronounced for methane than n-butane in all three directions, but most strongly in the z-direction. The distribution of sorbate-sorbate and sorbate-zeolite interaction energies showed a clear occupancy dependence. Increasing the loading from 4 methane and 4 n-butane to 4 methane and 7 n-butane molecules per unit cell, total interaction energies shifted to more attractive energies. Methane was modeled as a spherical molecule. For n-butane, bond lengths were assumed to be rigid and constrained to a length of 1.53 Å. Bond and torsion angles were allowed to fluctuate under the influence of potentials. The zeolite framework was rigid. Chitra and Yashonath /159/ have reported MD simulations for binary mixtures of Lennard-Jones spheres having identical masses but different diameters in the zeolite NaY. Their study showed that the larger sorbate would diffuse faster than the smaller sorbate. This is possible when the sorbate diameter approaches the diameter of the window ("ring effect"). A direct comparison between MD simulations and self-diffusivities from PFG NMR for a binary mixture of CH_4–CF_4 was made by Snurr and Kärger /160/. The reported self-diffusivities from simulations were in good agreement with experimental measurements. The authors observed that the diffusivities for both components, at constant total loading, decreased as the fraction of the larger and less mobile CF_4 increased.

Sastre et al. /146/ simulated diffusion of o/p-xylene inside the siliceous zeolite CIT-1, which contains channels formed by rings containing 12 and 10 Si atoms. The dimensions of these two channel systems are sufficient to cause substantial differences in the diffusion of para-xylene and ortho-xylene. Ortho-xylene trajectory plots showed diffusion through the 12-membered ring channels of CIT-1 only, the higher loading making the diffusivity decrease due to increasing intermolecular interactions. Para-xylene trajectory plots showed that diffusion through both 12-membered and 10-membered ring channels of CIT is possible. The effect of also using the 10-membered ring channels made the loading in the 12-membered ring channels decrease, and the smaller size of the p-xylene made its mobility higher with respect to the larger ortho-isomer. The results showed higher diffusion coefficients for the p-xylene compared to the o-xylene, and a decreasing diffusivity as the loading increases. A somewhat more complex picture appears in the mixture, where both o-xylene and p-xylene are allowed to diffuse simultaneously in the framework. The corresponding MD simulations reveal a reduction in the diffusivity of the slower isomer (o-xylene) and an increase in the diffusivity of the isomer whose diffusivity is higher (p-xylene), those results being in agreement with recent experiments.

Sastre et al. /147/ performed MD studies of the diffusion of a mixture of benzene and propylene, for the cumene synthesis process in purely siliceous MCM-22 (MWW). The

diffusion processes in each channel system of MWW at 650 K were studied independently. The authors found that in order to obtain quantitative or semiquantitative diffusion coefficients, the framework should be optimized. The optimization was done using the BFGS technique /161/, and the result was used as input for a 25 ps equilibration stage of the zeolite + sorbate system. After this period, runs of 200 ps with a time step of 1 fs were carried out within the NVE microcanonical ensemble at 650 K. The MD simulations were carried out using the general purpose DL-POLY-2-0 code. Trajectories of the diffusing molecules were calculated. Fig. 8 shows, e.g., the trajectory of an individual propylene molecule, which allows us to see in more detail the large part of the structure explored by a molecule in the 200 ps run.

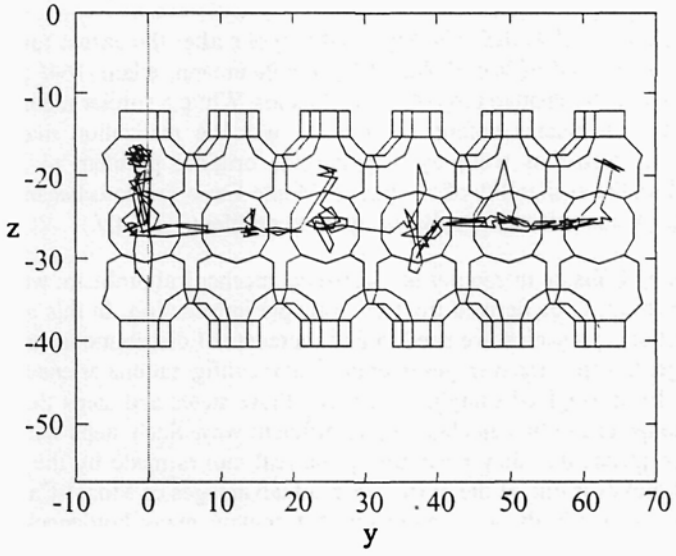

Fig. 8 Trajectory of an individual propylene molecule diffusing through the supercages of MCM-22 /147/.

The simulations showed that benzene diffused slowly in both of the two pore systems which is due to the small size of the 10-membered ring openings of the sinusoidal systems and to the location of the 10-membered ring windows in the supercages that are perpendicular to the direction of motion. On the other hand, the mean square displacement plots also show a large diffusivity for propylene in both channel systems and especially in the supercage system. The trajectory analysis for benzene showed little motion around the energy minima in the 10-membered ring sinusoidal channels and an intercage diffusion in the supercage system. In the case of propylene, the diffusion occurs throughout both channels in all their extension.

Demontis et al. /151/ carried out computer simulations of the dissociation – recombination reaction of diatomic molecules in silicalite and ZK4. The guest-host dynamical coupling at the level of the recombination reactions of photodissociated radical species and diffusion of diatomic molecules in two topologically different zeolites were investigated. In particular, two factors ruled the mechanism of the reactive and diffusive phenomena: lattice dynamics,

acting as an effective heat bath for the sorbed molecules, and the effects of two different crystal structures. Greater recombination percentages in ZK4, in particular for the larger atoms, result from the more effective confinement compared to the more "open" silicalite structure. The cage structure of ZK4, characterized by narrow windows with a diameter comparable to the dimensions of the guest species determined its ability to hold the photo-dissociated radicals inside the same α-cage, in particular for the larger iodine atoms.

3. DYNAMIC MONTE-CARLO SIMULATIONS

3.1 Introduction

The Monte-Carlo method, called this way by Metropolis after the casino town in Monaco, was developed near the end of World War II by von Neumann, Ulam /164/ and Metropolis /165, 166/ as part of the Manhattan project at Los Alamos. While a similar method of sampling had been used by statisticians before, the novelty was the realization that deterministic problems could be treated as well, by mapping the original problem to a probabilistic equivalent one. With the availability of computers, Monte-Carlo methods became increasingly used in mathematical analysis and to solve many-body problems /41, 42/.

The simulation of diffusion in zeolites is a statistical mechanical problem: we are interested in a macroscopic result, to be derived from microscopic information. In this and many other problems in statistical mechanics, we need to find moments of distributions, and in particular "ensemble averages", which are averages over particular configurations or ensembles in phase space /167, 168/. By a weighted sampling, stressing those states and steps that are the most important, the moments can be calculated in an efficient way. Such steps will in general be unphysical, which means that they need not be the real moves made by the molecules. To allow unphysical moves is one of the most important advantages of Monte-Carlo simulations over molecular dynamics in dynamic problems that contain many bottlenecks, such as the diffusion in zeolites.

This section reviews dynamic Monte-Carlo studies of diffusion on lattice models of zeolites. The adjective *dynamic* indicates that the trajectory of molecules and properties over time are studied, in order to derive the diffusivity. Other types of Monte-Carlo, like Grand-Canonical Monte-Carlo (GCMC) and Configurational-Bias Grand-Canonical Monte-Carlo (CBMC) /169, 170, 42/, are extensively used to investigate adsorption in zeolites, and will not be discussed here /36, 38/. In dynamic Monte-Carlo simulations of diffusion, the pore space through which molecules diffuse is simplified to a lattice, consisting of a grid of coarse-grained adsorption sites, which are connected by bonds. Molecules occupy a certain fraction θ of the sites, and are assumed to hop from site to site, normally along bonds connecting neighboring sites. Their movement is therefore described by the set of master equations for each site, eq. (1.4). A large enough number of molecular trajectories is followed, and statistics for quantitities of interest are collected after the system has equilibrated. If the lattice contains random features, which in the case of zeolites would be a result of a distribution of adsorption strengths, simulations need to be repeated for a sufficiently large number of randomly generated lattice realizations. Diffusivities and other properties are then calculated based on ensemble averaged statistics.

Before discussing the application of Monte-Carlo simulations to diffusion in zeolites, it is

important to review various dynamic Monte-Carlo algorithms and the definition of *Monte-Carlo time*. It is useful to note that dynamic Monte-Carlo of diffusion on lattice models of zeolites is mathematically equivalent to that of defects in crystals and of chemisorbed adatoms over crystal surfaces; only the lattice topology and the simulation conditions of interest differ. Because of this similitude, a lot can be learnt from results obtained in these areas.

Many simulations, especially the earlier ones, did not sufficiently account for the effect of the jump time distribution. Its importance was noted by several authors, including Scogin /171/, Nelson et al. /172/ and Fichthorn and Weinberg /173/: molecules should not all be moved at the same time during the simulations, one after the other, or according to some other fixed scheme, as this is not only unrealistic but may also lead to long-time errors. It is better to think in terms of *events* /171/, which are Poisson-distributed in time /172/. Such an approach was also used by Coppens et al. in their Monte-Carlo simulations of self-diffusion and transport diffusion in zeolites /174-176/. A list of events, e.g., only hops in the simple case of one-component diffusion, is scheduled at the beginning of the simulation. Jump times are randomly drawn from an exponential distribution with average time equal to the adsorption time τ on a site before a jump is attempted, $t_i = \Delta t_i \sim -\tau \ln(u)$, with $u \in (0, 1)$ a uniform random deviate. The average τ may be a constant, depend on the type of site (weak, strong) or even differ from site to site. For n molecules, there are n events (attempted hops) scheduled at times $t_i = \Delta t_i$. These events are ordered according to increasing time t_i. At the time t_m indicated by the head of the list, say molecule m, this molecule is temporarily removed from the list and the first event is executed. A new event is scheduled for molecule m (whether its jump or other event was successful or not); the list is updated by including its new event, keeping the list ordered; after which the process starts all over again.

This problem has been studied in detail by the group of Jansen and Lukkien, who compared different Monte-Carlo algorithms to solve the master equation, eq. (1.4), and applied these methods to the general situation of multi-component diffusion and reaction on surfaces /177-180/. The *first reaction method* or *discrete event simulation* /181, 177/, which was found to be the most generally applicable one, is similar to the just described method. When hopping probabilities are time independent, good results are also obtained with the often used *random selection method*, where sites and possible jumps are randomly selected at each Monte-Carlo time step. One Monte-Carlo step corresponds to one trial per lattice site on average. This is in effect a time-discretized solution method for the master equation. However, the last method leads us to another important problem of Monte-Carlo simulations, and one that has often been cited as a disadvantage of the method: the definition of Monte-Carlo time. When does the evolution of the system during a Monte-Carlo simulation correspond to real-time evolution? Older dynamic Monte-Carlo methods usually pick a site, then pick a reaction or diffusion jump at that site, which is executed with some probability /182/. There is no definiton of time in such a description. This problem was discussed by Fichthorn and Weinberg /173/, who introduced a *variable-step size method*, with the assumption that the time when an event (a reaction or change in configuration) occurs is Poisson distributed. Reaction probabilities are replaced by rate constants. If time is incremented using a deterministic average step size, equal to the expectation value of the next event, errors may be introduced, especially for non-equilibrium processes /179, 180/, since temporal fluctuations are neglected. An adaptation of the variable-step size method was suggested by Lukkien et al. /179/. The method is more complex, but may be the method of choice for large models.

With an event-oriented approach and knowledge of the times needed for each microscopic event, problems can be avoided, as the clock is advanced every time an event occurs, and the event list is updated. If the microscopic events are unknown, some reference time needs to be defined, e.g., the average time for an attempted hop, and all the other times should be referred to this time. In this case, Monte-Carlo time advances only proportionally with real time. This is also the case with the random selection method.

Which method is to be prefered, depends on the problem: a variable-step size method is the best general method when the rate constants do not change over time; otherwise, the first reaction method should be used. If computer memory is an issue or if only a few trials need to be performed per reaction, the random selection method may be the method of choice. Even more efficient is the combination of different methods in one simulation, when there are different types of jumps or reactions /179/. The time of the next event for each of the groups is determined and an event out of the group with the smallest time is selected; if an event occurs, new times are determined for each group.

In this context, the recent work by Huitema and van der Eerden /183/ is of interest; they estimated the physical time per Monte-Carlo step by requiring equality between the self-diffusion coefficients measured by dynamic Monte-Carlo and by molecular dynamics. This is done by comparing velocity auto-correlation functions. Based on results with liquid Lennard-Jones systems, they found that processes with rate-determining steps at time scales smaller than 1 ps may show deviations between MC and MD, but when the time scales are larger than about 1 ps and the length scales larger than 0.40 pm, they can be simulated with Monte-Carlo. Although it is not evident that this can be directly translated to diffusion in zeolites, these orders of magnitude give some confidence in the applicability of dynamic Monte-Carlo.

3.2 Diffusion in zeolites

After this mathematical background, we can now focus on the applications. As mentioned earlier, a lot on diffusion in zeolites can already be learnt from the many studies of diffusion of adatoms on surfaces and of defects in crystals. There also exists a large body of literature on general random walks on regular lattices, usually specifically discussing diffusion at low occupancies $\theta \rightarrow 0$, where diffusion can be treated as an uncorrelated random walk /184-189/. In those situations, exact or approximate solutions of the master equations can be found. When the occupancy θ is higher and sites cannot be multiply occupied, the problem is more complex, because the molecules influence each other. Any attempt to hop to an already occupied site will fail. Molecules therefore have a higher probability to retrace their path and reoccupy recently vacated sites. This leads to negative correlations in the molecular trajectories and to deviations of the diffusivity from mean-field results, in which correlations are neglected. Mean-field behavior is one where the only effect of forbidden hops is to reduce the diffusivity by a factor resulting from the average, instead of the local occupancy. As a result, it is only correct in the limit of an infinite connectivity, where the probability to hop to a neighboring site may well be approximated by the average. For lattices with one type of site, the mean-field self-diffusivity drops in a linear way with θ:

$$D_t = D_0(1-\theta), \tag{3.1}$$

where D_0 is the diffusivity in the limit of zero occupancy /19, 20/. More complex results can be derived for lattices with different types of sites. The smaller the connectivity of the sites, the larger the expected deviations from mean-field theory, because the local environment is not representative for the global average. This effect is very important for zeolites, in which the pore network is often poorly connected. An extreme case is a one-dimensional chain of sites, where correlations become infinitely long-range, leading to a deviation from Einstein's law of diffusion, $\langle r^2(t)\rangle \sim t$, and replacing it by $\langle r^2(t)\rangle \sim t^{1/2}$. Some examples of this anomalous diffusion, called *single-file diffusion,* were already discussed in Section 2 and more will follow at the end of this section. For motion on other regular, non-fractal lattices, Einstein's law for self-diffusion is still valid, yet short-range correlations exist.

Assessing these correlations is important for the study of diffusion in zeolites, in which we are interested in the dependence of diffusivity on loading or occupancy. A large body of information can be drawn from the literature on defect diffusion in metals and alloys: two limits, the already mentioned occupancy θ close to 0, and also θ close to 1, have received special attention. The first corresponds to the diffusion of a low concentration of interstices, and the second to the diffusion of a low concentration of vacancies. Analytical results can be obtained for $\theta \rightarrow 1$, because the environment is constant, and are expressed as a correction to mean-field called the correlation factor:

$$f = D/D_1 = D/D_0(1-\theta) \tag{3.2}$$

/190/. More information on the calculation of the correlation factor in this limit can be found in various books on defect diffusion /191-193/. This limit is useful for comparison with Monte-Carlo simulations.

Since diffusion on lattices with a finite occupancy and a finite connectivity is a true many-body problem, accurate (semi-)analytical solutions are difficult to obtain, and Monte-Carlo simulations are needed. It should nevertheless be mentioned that diagramatic relations for the occupancy and particle correlation functions were derived and applied to a cubic lattice by Fedders and Sankey /194-196/, and a second-order approximation for the diffusivity was derived by Tahir-Kheli and Elliott /247/. In general, however, Monte-Carlo methods should be used. These become more and more feasible with the advent of ever faster computers. As was noticed early on, the Monte-Carlo method is highly flexible, allowing for different conditions at different sites, depending on their local environment. For example, the hopping frequency of a molecule from its present site to a neighboring vacant site may depend on the presence of other neighboring occupied sites, which may influence the depth of the potential energy well in which the molecule resides /197/. The hopping frequency is proportional to $\exp(-\Delta E/kT)$, ΔE being the energy difference between the site and the transition-state leading to a neighbor. Attractive and repulsive interactions between the diffusing atoms can thus easily be accounted for, and lead to cooperative effects, which increase with increasing concentration. Murch and Thorn /197/ quantitatively showed that, when compared with non-interacting atoms, attraction between solute atoms retards diffusion (because molecules are restrained), whereas repulsion can considerably enhance it (because molecules are expelled) (see Fig. 9). In the latter case, the diffusivity may increase with concentration and show a maximum. A special situation around $\theta = 0.5$ occurs when an ordered phase is formed.

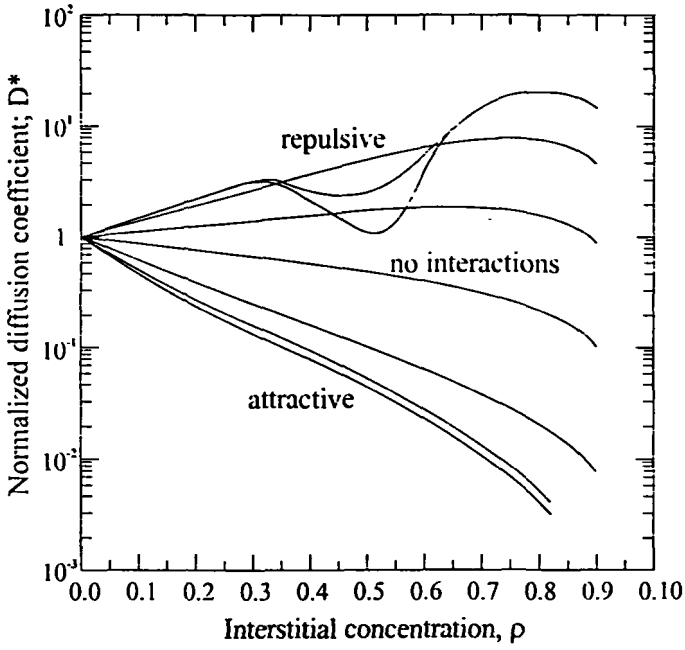

Fig. 9 The composition dependence of the normalized diffusion coefficient D^* at various values of $\tilde{T}$ /197/.

Clearly, similar results should hold for diffusion in zeolites. The pioneering Monte-Carlo and analytical studies by Reed and Ehrlich /198/ on surfaces are equally interesting. They studied the connection between surface diffusion of chemisorbed gases and atomic jump rates at arbitrary occupancy. In an ideal Langmuir layer, i.e., in the absence of interactions between the adatoms, the surface diffusivity in the presence of a concentration gradient is simply given by $D_T(\theta) = \Gamma(0)\,\lambda^2$ at all coverages, where $D_T(\theta)$ is the surface diffusivity at occupancy θ, $\Gamma(0)$ is the rate of atom jumps, and λ is the jump distance. For interacting adatoms, a thermodynamic correction is needed, because the diffusion really occurs under the influence of a gradient of chemical potential, not concentration, and the effective jump rate $\Gamma(\theta)$ may be a complex function of θ. The resulting equation is formally identical to the "Darken" equation, eq. (1.3), where $\Gamma(\theta)$ plays the role of the corrected diffusivity D_C. Knowledge of the thermodynamics, as characterized by the adsorption isotherm or by the concentration fluctuations, is therefore very important in deriving the transport diffusivity. A similar model as the one used by Murch and Thorn /197/ was employed to study diffusion on a lattice in the presence of nearest-neighbor attractive or repulsive interactions. Using a mean-field approximation (quasi-chemical approximation), analytical expressions for the diffusivity, the effective jump rate and the thermodynamic factor could be derived. In particular, for repulsive interactions, the correlation factor f [in the terminology of vacancy diffusion, viz. eq. (3.2)] strongly decreases with coverage, and the thermodynamic factor is largest around $\theta = 0.5$, where the deviations from a non-interacting lattice gas are largest. The surface diffusivity versus coverage

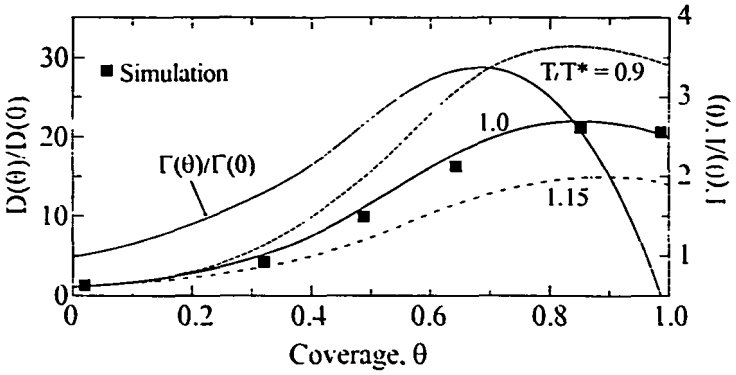

Fig. 10 Coverage dependence of the diffusivity in the quasi-chemical approximation /198/.

graph shows a maximum at high coverages as well (see Fig. 10). The case of attractive interactions is very similar, except that a decrease and minima are observed. The quality of the approximation and the effects of interactions beyond nearest neighbors were studied with Monte-Carlo simulations, using different Morse potentials. Interesting behavior is observed when the interactions between nearest neighbors are repulsive and those between second-nearest neighbors are attractive. In this case, an ordered phase is formed, leading to a sudden increase of the diffusivity around $\theta = 0.4$–0.5 as a result of a peak in the thermo-dynamic factor, after which the diffusivity remains more or less constant, because of an increased jump rate. Such results could easily be understood based on the Monte-Carlo simulations, which showed the energetically favored c(2x2) ordering with alternating occupied and vacant sites (see Fig. 11). Under such conditions, the time-correlation formalism for diffusion does not hold /199/.

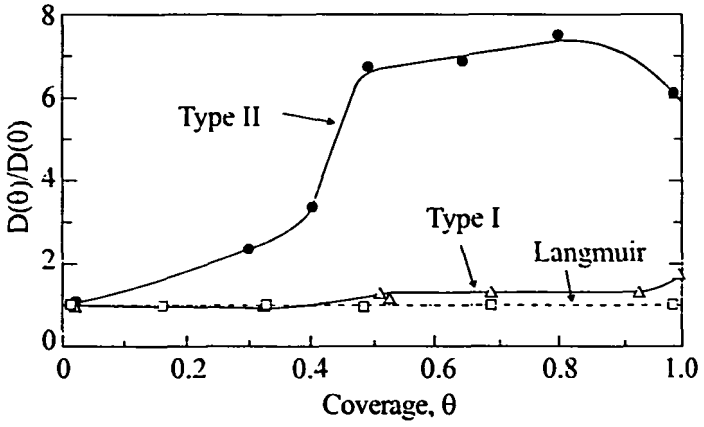

Fig. 11 Coverage dependence of the diffusivity, obtained from the product of the thermodynamic factor and the jump rate /199/.

One of the implications of the just summarized work for understanding diffusion in zeolites, is that the thermodynamics of adsorption are of the greatest importance. Although we have chosen to focus ourselves on diffusion in this review, adsorption studies are essential in simulating diffusion. Where and in which configuration the molecules preferentially adsorb, how they interact, whether segregation effects occur, provides the input for the computational techniques to study diffusion and reaction.

A detailed MC study of diffusion on an fcc lattice was conducted by Kehr et al. /200/, who also derived a correlated-jump model with a general waiting time distribution. They showed that strong correlations exist between two consecutive jumps. There is a marked influence on the waiting time, i.e., the time spent on a site /184/, especially on the time to jump backward to a site it has just vacated. Only correlations between two consecutive steps were accounted for, which was sufficient to describe diffusion on an fcc lattice, where each site has 12 neighbors.

Diffusion in lattice gas models has been reviewed by Kehr and Binder /201/. While a lot can be learnt from the methodology developed in solid state physics, care should be exercised when transferring these results to zeolites. Indeed, the lattices considered there are usually better connected than those representing the coarse-grained pore space of zeolites. Diffusion of defects is typically studied on the relevant cubic, fcc and bcc atomic lattices, which are well-connected. The connectivity of the zeolite pore space is often lower. In ZSM-5, e.g., there are sites in the channels connecting neighboring pore intersections. Channel sites therefore have a connectivity of only 2. Four channels meet in each of these intersections, so that the connectivity of sites in those intersections is 4 or possibly more, depending on the number of sites in an intersection. ZSM-5 with one site per intersection has an average connectivity of $8/3 \approx 2.67$, much less than the 6 for a normal cubic lattice, 12 for an fcc lattice or even 4 for a square lattice or diamond lattice. The importance of such topological effects has recently been studied using dynamic Monte-Carlo simulations. Poor connectivity leads to more significant restrictions on the motion of molecules compared to well-connected lattices. This is of interest to the application of zeolites as sorbents, catalysts and catalyst supports, as it may also influence effective reaction rates of diffusion controlled processes. It is therefore important to study the effect of the lattice topology on the results. Coppens et al. /174/ found that the diffusivity in silicalite decreases more significantly with loading than would be expected from either a cubic or a square lattice model (Fig. 12). A time-correlation formalism, similar to the one used for vacancy diffusion in solids, was used to predict the deviations from mean-field theory, and led to a concentration independent renormalized correlation function:

$$C'(n)/C_\infty = 1 - \exp\left\{\left[-(n-1)/n_c\right]^\gamma\right\} \tag{3.3}$$

where $C'(n)$ expresses the correlation of the first step, $\mathbf{r}_1 - \mathbf{r}_0$, with the displacement after n steps, $\mathbf{r}_n - \mathbf{r}_1$:

$$C'(n) = \frac{\langle(\mathbf{r}_1 - \mathbf{r}_o)\cdot(\mathbf{r}_n - \mathbf{r}_1)\rangle}{\left\langle|\mathbf{r}_1 - \mathbf{r}_o|^2\right\rangle},$$

and C_∞ is the limit of this function for $n \to \infty$. It can be shown that the diffusivity:

$$D = f D_1 = 2(C_\infty + 1)D_1, \tag{3.4}$$

where f is the correlation factor introduced earlier. Correlations decay as a stretched

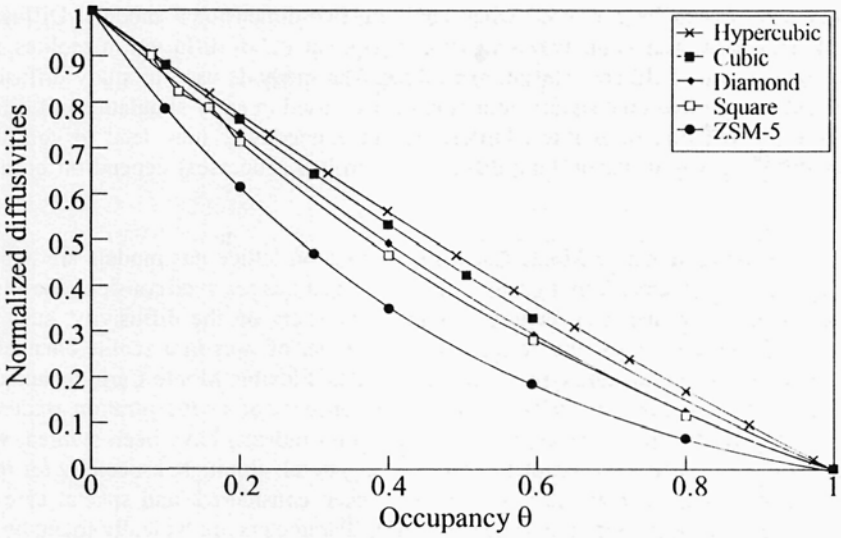

Fig. 12 Self-diffusivities in various lattices, as a function of occupancy. The results are normalized with respect to D_0, the diffusivity in the limit of zero coverage /174/.

exponential function of the number of steps n taken by a molecule, where the exponent γ is representative for the lattice, e.g., $\gamma = 0.9$ for a cubic lattice and 0.55 for silicalite. The lower the value, the stronger the correlations and the deviation from mean-field. While only two consecutive steps are significantly correlated on an fcc lattice /200/, 7 steps are needed to decorrelate the motion for more than 90 % on a ZSM-5 silicalite lattice (Fig. 13).

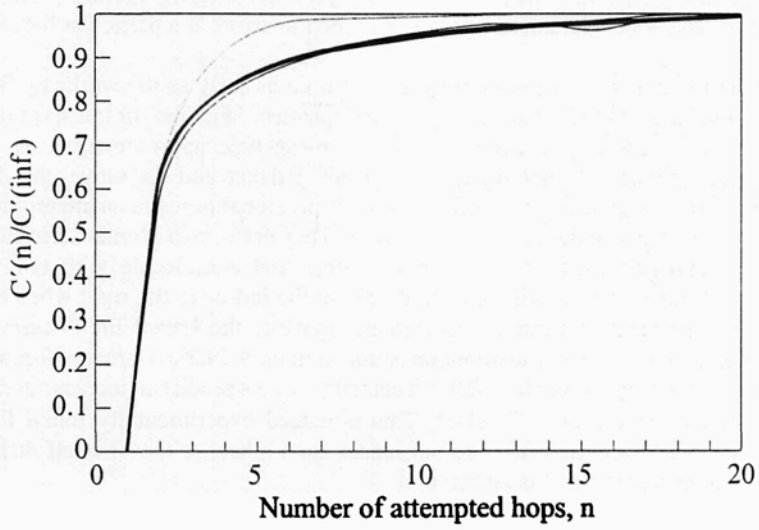

Fig. 13 Renormalized displacement-time correlation functions for the ZSM-5/silicalite lattice /174/.

Similar care should be exercised when applying two-dimensional models. Diffusion on lattice models of surfaces is the two-dimensional "equivalent" of diffusion in zeolites, so that developments in this field are relevant to zeolites. The methods used to study diffusion are similar, and two-dimensional square lattices have been used in early simulations of diffusion, adsorption and reaction in zeolites. Differences in connectivity may lead to considerable differences in the way diffusion (and diffusion controlled processes) depend on occupancy, however.

Broadly speaking, dynamic Monte-Carlo simulations on lattice gas models are applied to two categories of problems. A *first group of problems*, that has received considerable attention, is the study of the influence of different lattice parameters on the diffusivity, such as the topology of the pore network, the occupancy, the number of sites in a zeolite channel intersection, and the distribution and type of adsorption sites. Flexible Monte-Carlo techniques are particularly suited for this. Both self-diffusion (in the absence of a concentration gradient) and transport diffusion (in the presence of a concentration gradient) have been studied, with or without reactions. Usually, the simulations are quite general, although, especially for reaction problems, applications to particular systems have been considered, and special care to the lattice topology has been paid in more recent papers. Parameters are typically found by fitting to macroscopic results or from separate adsorption and/or kinetic experiments. A *second group of problems* concerns specific molecule-zeolite systems, for which an appropriate, detailed model is set up, which is coarse-grained to study the long-range diffusion properties. Several of these studies will be described under the header "transition-state theory" (Section 4), because the main issue in these methods is the derivation of fundamental (corrected) transition rates which are then substituted into a simple dynamic Monte-Carlo simulation, usually at infinite dilution. The groups of Auerbach and Metiu also developed analytical methods to be used in parallel with Monte-Carlo simulations, and their work will be discussed under the present header. Note that both types of studies are of interest, the second type for practical applications, the first type to see which parameters really matter, which level of detail is needed, and which parameters need to be tuned to arrive at a particular behavior.

Lattice models to study diffusion in zeolites were used as early as the works by Barrer and Jost /19, 20/, and Riekert /202/. A concentration independent "Fickian" or transport diffusivity is predicted on the basis of these models, using a mean-field approximation, as described earlier. Many experiments do not support this result. Palekar and Rajadhyaksha /203, 204/ therefore simulated diffusion and adsorption in one-dimensional pores in an attempt to find the concentration dependence of the transport diffusivity. They performed Monte-Carlo simulations on a line of equidistant sites, in which they assume that a molecule with two occupied neighbors cannot move, that it will move randomly to the left or to the right when either one of the neighbors is vacant, and that it will certainly move to the vacant site in case there is a single vacant neighbor. The latter assumption is uncommon. A Markov process formulation of this problem was given by Patwardhan /205/. Their simulations predict an increase in diffusivity with sorbate concentration, $D_T = D_0/(1-\theta)$. This is indeed experimentally found for certain systems in which diffusing molecules do not hinder each other, so that the self-diffusivity is concentration independent, yet it is not general.

The relationship between the binary diffusivities and single-component diffusivities was also investigated by the same group /204, 206/. They found that the sorption of the species

with the higher diffusivity is slowed down as a result of the presence of the species with the lower diffusivity. The latter, however, can become faster than when it is sorbing alone, due to the contribution of the cross term. At a given composition of the sorbate phase, all the diffusivities decrease with a decrease in diffusivity of the slower component.

While useful for one-dimensional pores, extrapolation of such results to three-dimensional zeolites is not warranted. It is indeed known that the diffusion behavior in a one-dimensional channel is qualitatively different from diffusion in higher dimensional systems. In particular, anomalous single-file diffusion can occur. Using the same one-dimensional model, Pitale and Rajadhyaksha /207/ indeed found a non-constant tracer diffusivity at fixed sorbate concentration.

Simulations on higher dimensional lattices are therefore needed. Of special interest is whether continuum models can be used and how the diffusivity depends on various lattice parameters. Theodorou and Wei /208/ simulated diffusion and reaction of two components with the same diffusivity on a two-dimensional lattice. This work is further discussed in the subsection on diffusion and reaction in zeolites. Amongst other things, they found that continuum models are inaccurate at higher loadings as a result of site blocking. More extensive Monte-Carlo simulations of tracer and transport diffusion on a two-dimensional lattice were carried out by Aust et al. /209/, Dahlke and Emig /210/ and Frank et al. /211/ who studied both single components and binary mixtures. There are no interactions between molecules. Each cage can contain a maximum number of molecules. This number was found to have a great impact on the results as is seen in Figure 14 and 15 /209/. The cages are activated at random,

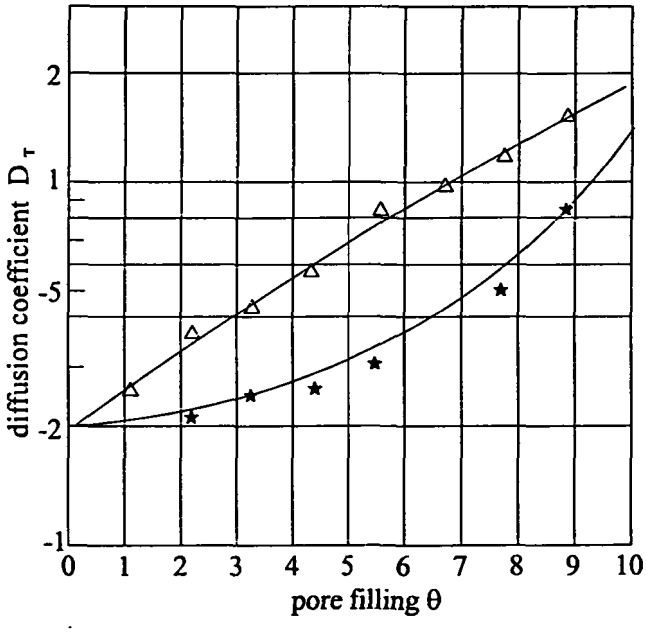

Fig. 14 Concentration dependence of transport diffusion coefficient; one molecule per cage and event allowed to jump, no passing in windows, Δ: max 1 particle; *: max 2 particles/cage /209/.

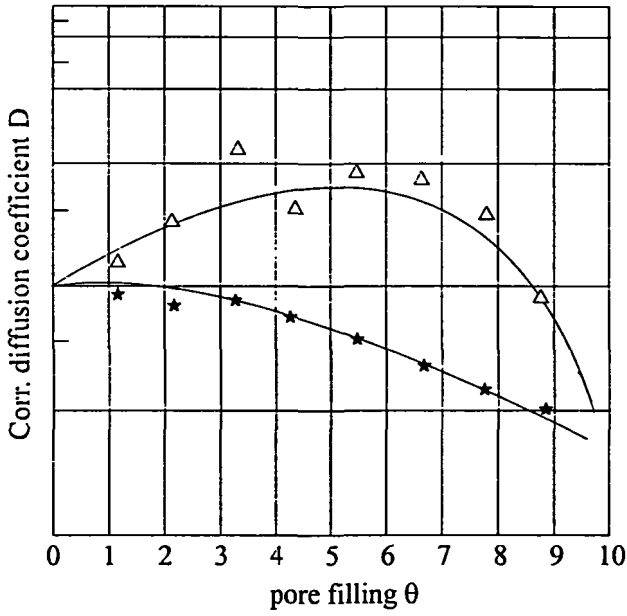

Fig. 15 Concentration dependence of corrected diffusion coefficient; 1 molecule per cage and event permitted to jump, no passing in windows, Δ: max 1 particle per cage; *: max 2 particles per cage.

but each of them only once during a single Monte-Carlo step. Different hopping models were implemented, but a (more accurate) Poisson distribution of event times was not accounted for. Binary diffusion was also simulated by Nelson and Wei /212/. These authors report qualitative agreement with experiments, but the results are especially useful to investigate the dependence of the results on model assumptions. At the same time, this means that a good understanding of the microscopic behavior is essential to make appropriate assumptions in the mesoscopic Monte-Carlo simulations. For example, Aust et al. /209/ report a diffusivity increase with loading under the assumption that a molecule will jump when there is at least one vacant neighbor; when the assumption is modified so that a molecule will not move if it attempts to move to an occupied neighbor, a concentration independent diffusivity is found.

More surface Monte-Carlo simulations of multi-component diffusion were carried out by Van den Broeke et al. /213/, using a Langmuir and a repulsive sorbate-sorbate interaction model. The modeling and assumptions are similar to those in the work of Aust et al. /209/, but the main objective was to verify the applicability of a surface diffusion model in terms of the Maxwell-Stefan equations for zeolites, as discussed in Section 5 of this review. Simple Langmuir adsorption models led to results consistent with a number of experiments. Monte-Carlo simulations of the counter-diffusion of a binary mixture clearly indicated that this process is not symmetrical. Transient uptake of binary and ternary mixtures showed that the properties of the fast moving species are the most affected by the presence of other sorbates, while the uptake behavior of the slowest moving component is similar to single-component uptake.

Faux et al. /214/ studied the effect of a directional bias in the diffusion on a square lattice. In zig-zagged pore networks like the one of ZSM-5, nonspherical sorbate molecules may indeed prefer to hop forward or backward instead of making a 90° turn. This directional bias can lead to considerable anisotropy of the self-diffusivity, but the effects decrease with concentration.

Rajadhyaksha et al. /215/ found deviations from Einstein's relation for self-diffusion on a square lattice at high loadings, for a vacancy concentration close to zero. Diffusion seemed to be anomalous, similar to the single-file diffusion observed in one-dimensional pores. These results have been contradicted by other authors /209, 213/ and may be a result of the relatively short time of the Monte-Carlo simulations, since moves of the tracer are extremely rare in this limit and the assumption that time is proportional to the number of jumps made by the tracer is not warranted.

First steps toward the study of self-diffusion on more detailed lattice models of zeolites were made by Van Tassel et al. /216/ and Keffer et al. /127/, who did not only consider cage-to-cage hopping, but also intra-cage motion (Fig. 16). Several molecules can occupy several sites within a single cage. The energetics of the motion between sites of the "sublattice" representing a cage can be very different from the energetics of intra-cage motion, as indicated by transition-state theory and molecular dynamics. An analytical model, exact at low loading and approximate at higher loadings, was also derived (Fig. 17). Keffer et al. /127/ studied the percolation properties of such more complex lattices, with different types of bond-blockers, and found regular percolation theory and the effective medium approximation to be quite easy to generalize.

The previous papers considered lattices with equivalent sites, occupied by interacting or non-interacting molecules. Coppens et al. /174, 176/ studied the effect of a distribution of weak and strong adsorption sites on self-diffusion and transport diffusion on lattice models of zeolites. Apart from a cubic lattice, a realistic model for the pore network of ZSM-5 was used as a test example, since it was shown earlier /174/ that the connectivity of the network plays an important role (Fig. 18). The influence was studied of the fraction of strong adsorption sites, the relative strengths of strong and weak sites, τ_s/τ_w, the number of sites per zeolite cage or pore intersection, and the ratio of intra- to extra-cage hopping probabilities. A mean-field theory was also presented, showing good agreement at sufficiently low occupancies, high enough connectivity, and a sufficiently homogeneous site strength distribution. Because of correlation effects, qualitative discrepancies may occur in other cases. Experimentally observed trends of the dependency of diffusivity on loading could be reproduced. Strong adsorption sites become occupied or are "titrated" first when increasing the loading, so that the self-diffusivity may increase with occupancy, opening up more tortuous paths along weaker adsorption sites to other molecules, herewith facilitating their motion. A maximum occurs, because at even higher occupancies, the constrictions imposed on the molecular motion start to dominate, leading to a decrease in diffusivity (Figs. 19, 20). Such behavior was also found experimentally /11/. An important conclusion of the work on transport diffusion is that a small fraction of strong adsorption sites leads to a sharp increase of the transport diffusivity already at small loading. Further loading has little effect on the diffusivity.

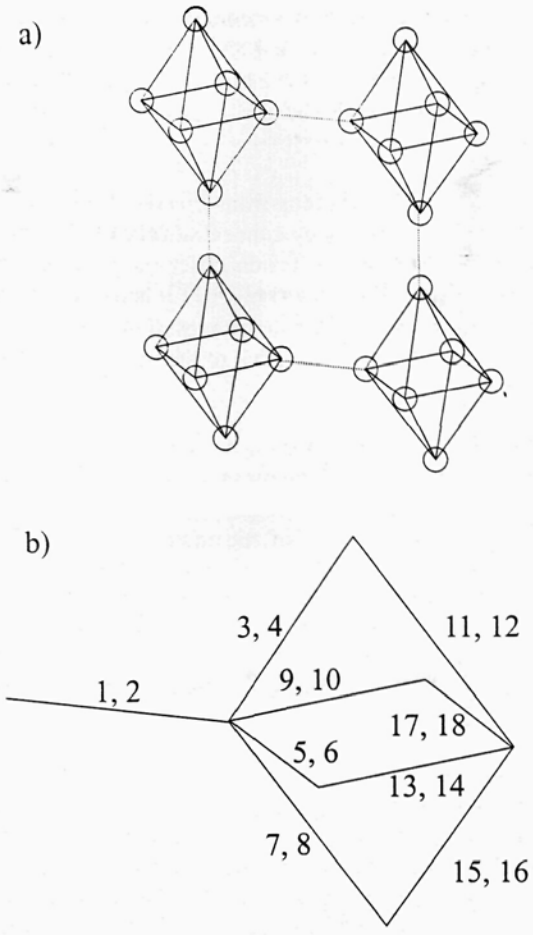

Fig. 16 a) A lattice of adsorption sites (circles) composed of connected octahedral sublattices. Solid lines represent possible hops within each sublattice (site hops) and dotted lines represent possible leaps between neighboring sublattices (window hops). b) The hops on the lattice which have a component in the x-direction, taken to be the direction of hop 1 (a window hop). Odd numbered hops have a component in the positive x-direction and even numbered hops have a component in the negative x-direction /216/.

Bhide and Yashonath /217/ studied the effects of the spatial distribution (plain, square, clustered or chessboard) and acid strength distribution of adsorption sites on self-diffusion on a two-dimensional lattice. Also sorbate-sorbate interactions and hop length (single hops, double hops) were varied. Again, experimental trends of diffusivity versus occupancy could be qualitatively reproduced by changing these parameters.

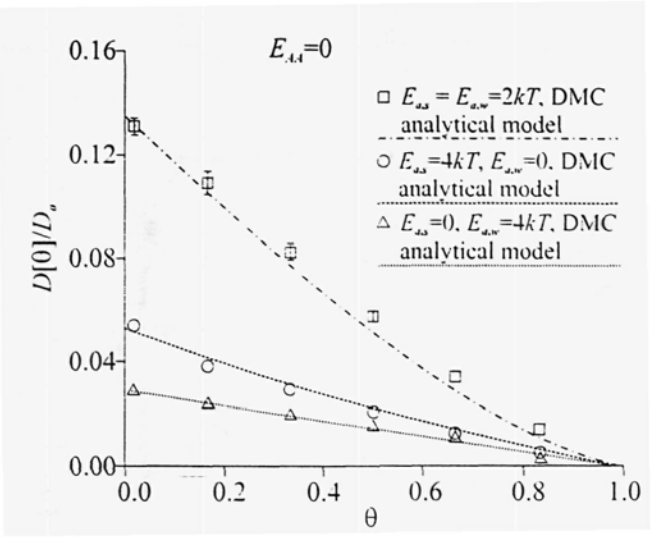

Fig. 17 The self-diffusivity vs. loading fraction as computed by dynamic MC and an analytical model /216/ for various values of the activation energy for window hops ($E_{a,w}$) and for site hops ($E_{a,s}$).

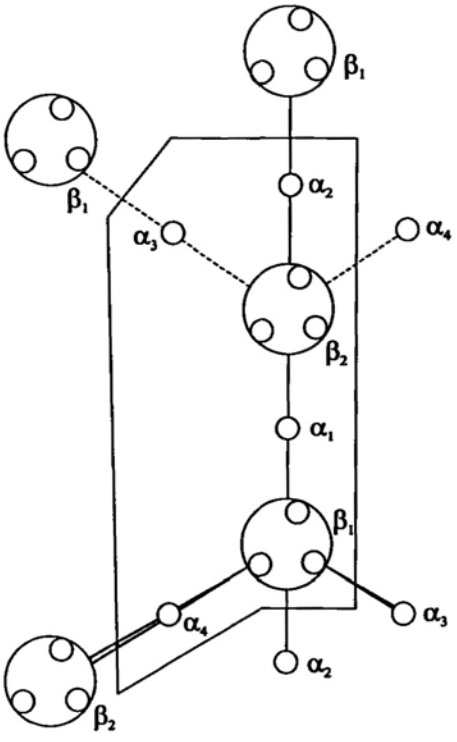

Fig. 18 Lattice representation of the unit cell for the ZSM-5 pore space: 2q β sites in the channel intersections, which can be weak or strong, and 4 weak α sites in the channels /175/.

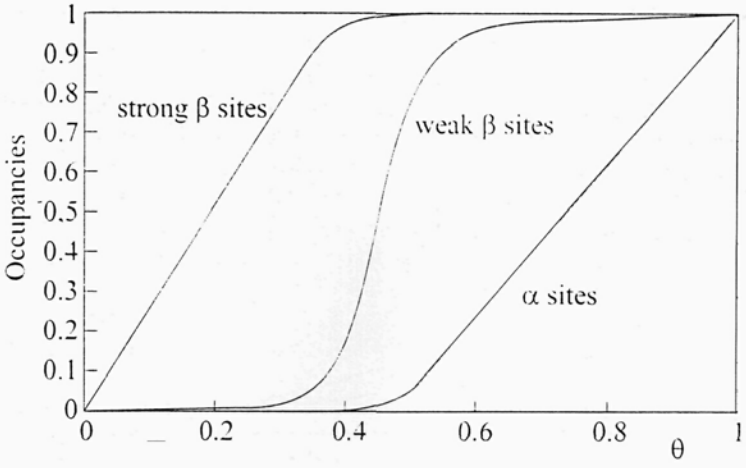

Fig. 19 Occupancies of the strong β and the weak β and α adsorption sites in ZSM-5, as a function of the total loading θ /175/.

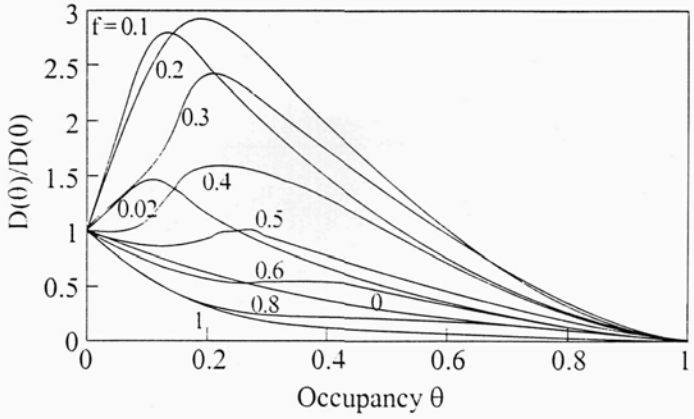

Fig. 20 Self-diffusivity in ZSM-5 with 1 site per cage, as predicted by Monte-Carlo simulations, $\tau_s/\tau_w = 100$ /175/.

Also very recently, Gladden et al. /218/ developed a kinetic Monte-Carlo code to study binary diffusion and adsorption on realistic representations of coarse-grained zeolite networks. The necessary parameters can be found from ^{2}H NMR experiments, and/or molecular dynamics and grand-canonical Monte-Carlo (GCMC). An example was shown for ethane-ethene binary adsorption on silicalite. Experiments at one temperature were used to find the missing parameters needed to successfully predict the sorption behavior at another temperature.

As mentioned earlier, a somewhat different approach was taken by Auerbach and co-workers, who studied a particular model system in more detail in an attempt to improve our understanding of diffusion in zeolites. In a series of papers, Auerbach, Metiu et al. /219-228/ conducted a systematic study of benzene tracer diffusion in Na-Y and Na-X zeolites. They performed systematic dynamic Monte-Carlo simulations and developed increasingly comprehensive analytical and semi-analytical theories. Benzene diffusion in the synthetic, cationic faujasite Na-Y is a typical example of a practical system to which MD cannot be applied, because the molecules are trapped at strong binding sites for most of the time. Nucleophilic benzene molecules hop from one site to another, so that dynamic Monte-Carlo is the method of choice to investigate the long-range mobility. There are two types of sites in Na-Y (Si:Al = 2) (Fig. 21). The first type consists of "S_{II} sites" in cages, where benzene binds to a Na^+ ion coordinated to a zeolite 6-ring. Hops between such sites lead to a randomization of the benzene plane orientation, but not to (translational) diffusion. Cages are tetrahedrally connected; in between there are 12-ring windows, which represent the second type of sites, the so-called "*W*-sites". The S_{II} sites are the strongest ones. Since it is a nucleophile, benzene diffusion in Na-Y can be represented by a succession of jumps in between the two kinds of sites; *W*-*W*, *W*-S_{II} and S_{II}-*W* moves need to be considered. Molecular dynamics simulations as well as spin-relaxation NMR are only able to probe the intra-cage S_{II}-S_{II} motion, and not the cage-to-cage motion which is responsible for the long-range diffusion that is experimentally measured using, typically, PFG-NMR /227/.

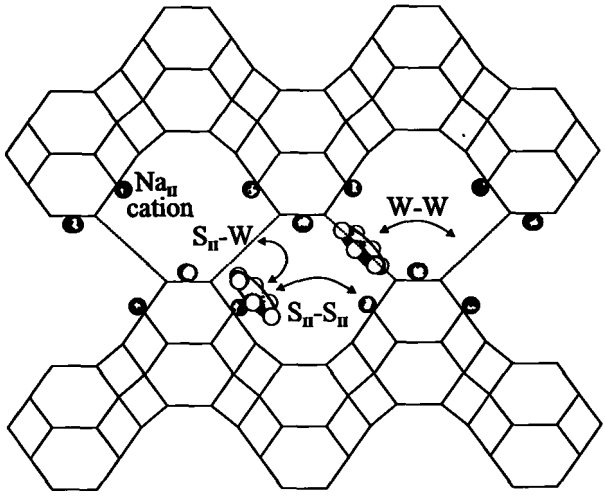

Fig. 21 Benzene molecules in NaY /226/.

The dynamic Monte-Carlo simulations of this group are in principal similar to the ones discussed earlier, but with the important difference that they are much more detailed and quantitative. In particular, the fundamental parameters, the jump activation energies, are determined and serve as input for the Monte-Carlo simulations or analytical expressions for the diffusivity. To represent the zeolite-benzene potential energy surface, an average

tetrahedral (T)-site approximation with partial charges was employed and the potential parameters were determined /219/. The location of the two types of binding sites and their energies were calculated: –75 kJ/mol for the S_{II} binding energy and –50 kJ/mol for the weaker W window sites. It is interesting to go over the methodology used by this group as it is quite general, so that much can be translated, in principal, to other systems. Unfortunately, the study and behavior of other less symmetrical systems (*e.g.*, benzene in silicalite), may well be more complicated in practice, because of the large number of sites and jumps (there are, *e.g.*, 27 potential minima for benzene in silicalite /229/). For more details, including values for the parameters, we refer to the orginal papers.

Auerbach, Metiu et al. first studied diffusion of a single benzene molecule, i.e., benzene in Na-Y at infinite dilution /219/. The variable-step size Monte-Carlo method was used to estimate the self-diffusivity and activation energy over the 100 to 500 K temperature range. The activation energies of the jumps were found from a minimum energy path method. This method consists in locating the transition state by following a minimum energy path, calculated using a constrained optimization approach, from one site to another. Both the S_{II}-S_{II} and the S_{II}-W hops occur according to a "cartwheel" mechanism, in which benzene remains roughly orthogonal to intermediate 4-rings (Fig. 22). The W-W hopping process, bypassing the cage sites, gains in importance at higher benzene loadings, e.g., about 4 per supercage, and is somewhat analogous to interstitial diffusion in solids.

The principal idea behind the method of Auerbach et al. is to reduce the site-to-site diffusion problem to a simpler cage-to-cage diffusion problem, for which only the cage-to-cage hopping rate needs to be determined (Fig. 23). Such a hierarchical approach makes the diffusion process easier to understand and characterize, and enables much quicker calculations of diffusivities (~N instead of ~N^2). Hierarchical methods are typically used when the jump rates are determined by transition-state theory (see Section 4). Auerbach and Metiu /221/ derived the following expression for the self-diffusivity at infinite dilution:

$$D = \frac{1}{6} k a^2, \tag{3.5}$$

where the hopping length a is approximately equal to the cage-to-cage distance, or better the root mean square cage-to-cage hopping length, and the hopping frequency k can be expressed in terms of fundamental site-to-site hops. This expression is the same as the well-known one for a simple cubic lattice, despite the different lattice topology. The cage residence time is found to decay exponentially, so that cage-to-cage hopping is indeed a first-order process. A first approximation in terms of the hopping rate from S_{II} to W sites was refined in later work to include W-W hops /223/:

$$k = k_{S_{II} \to W} (1/2)\, 3 \left[1 + \alpha(T)\right] = k_{S_{II} \to W} (1/2)\, 3 \left(1 + k_{W \to W} / k_{W \to S_{II}}\right). \tag{3.6}$$

This is an exact solution of the master equation. When $\alpha(T)$ lies between 0 and 1, the factor $3[1+\alpha(T)]$ counts the number of allowed target sites for cage-to-cage motion. For $\alpha(T) \gg 1$, benzene mobility is more like interstitial diffusion, and the rate is controlled by W-W hops and the probability of W site occupancy, following a move from S_{II} to W to start the W-W hops.

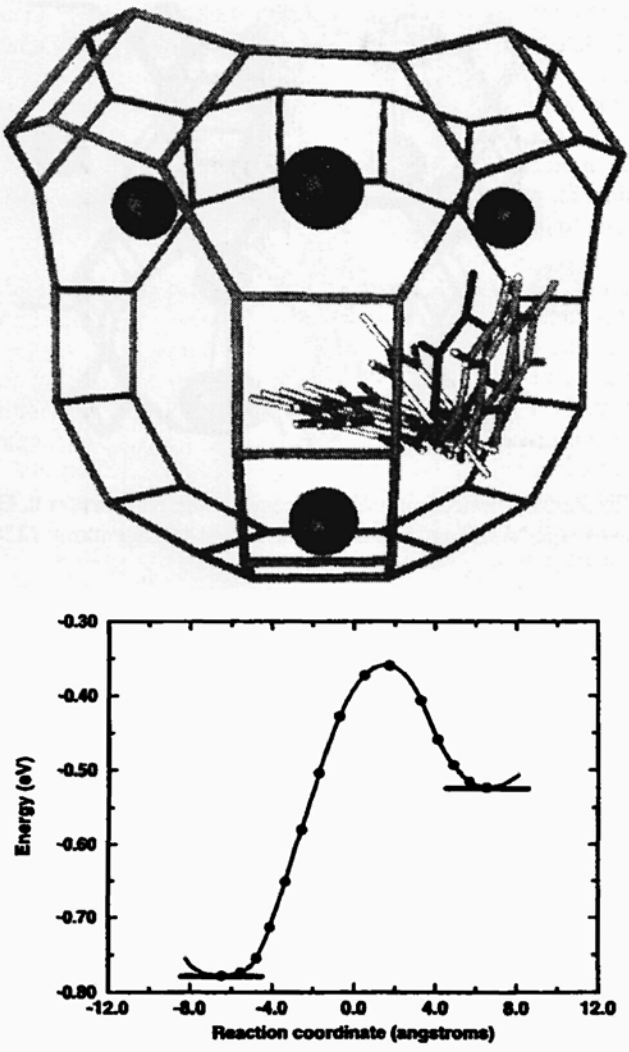

Fig. 22 $S_{II} \leftrightarrow W$ minimum energy path showing cartwheel motion, with transition state (bold) /219/.

Auerbach et al. /220/ also studied diffusion in Na-X to investigate the influence of the Si:Al composition ratio on the results (Fig. 24). Since the Si:Al ratio of Na-X is about 1, the number of Na^+ ions is larger than in Na-Y, so that a lower benzene mobility is expected. While an increase of the Si:Al ratio in Na-Y indeed leads to the expected increase in mobility /222/, the opposite is seen for Na-X: room temperature benzene mobilities increase by nearly two orders of magnitude and the activation energy for benzene in Na-Y is half that for benzene in Na-X. ^2H NMR and binding site, energy and hopping path calculations, as described above for Na-Y

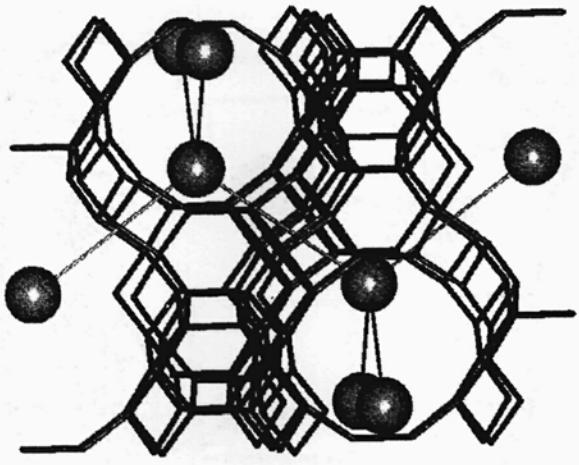

Fig. 23 Tetrahedral connectivity of supercages in the NaY unit cell. Balls represent supercage "sites" and sticks represent cage-to-cage jumps /226/.

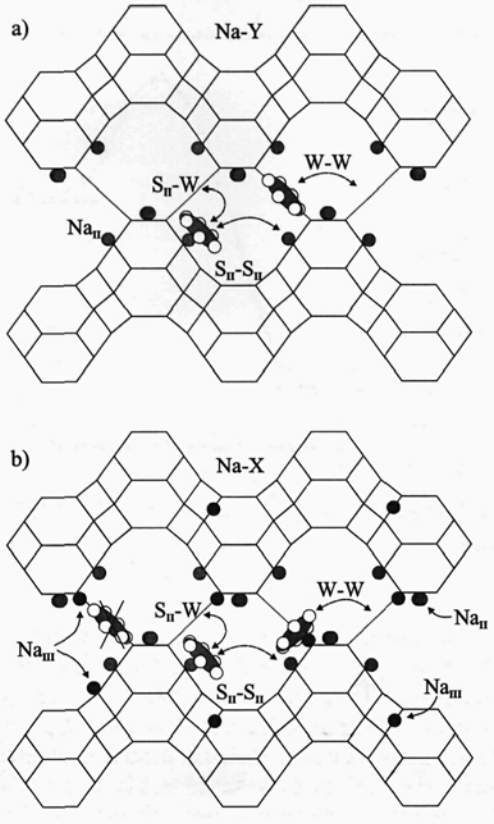

Fig. 24 Sorption sites and jumps for benzene in a) NaY and b) NaX /228/.

clarify this seeming paradox: new, to benzene accessible S_{III} sites, are indeed created, but they lie close to the windows. Because of this, attractive interactions from S_{III} sites overlap with those from adjacent S_{II} sites, which reduces the activation energy by splitting the large S_{II}-W energy barrier up into two smaller barriers S_{II}(close)-S_{III} and S_{III}-W. As a result benzene is more mobile in Na-X than in Na-Y (Fig. 25).

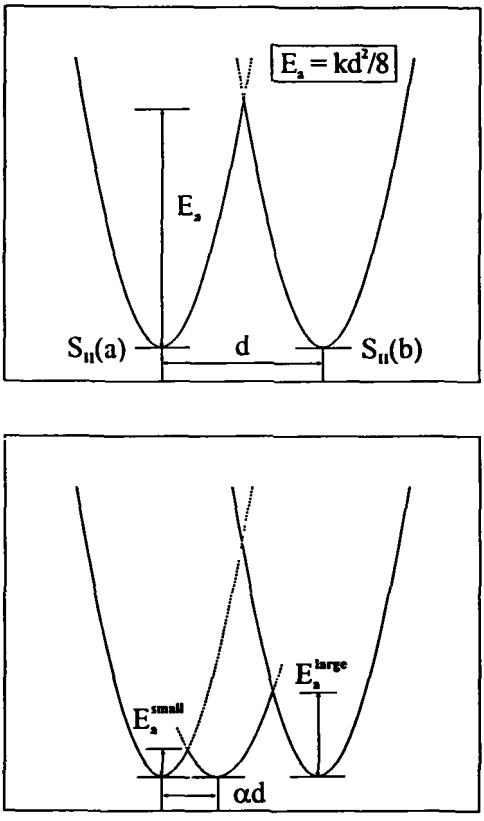

Fig. 25 a) One-dimensional harmonic model of adjacent S_{II} sites in NaY, parametrized as $V_a(x) = 0.5kx^2, V_b = 0.5k(x-d)^2$; b) Na-Y model of adjacent S_{II} sites applied to NaX, which adds the S_{III} site parametrized as $V_c = 0.5k(x-\alpha d)^2$ /220/.

The previous results were at infinite dilution. At higher benzene occupancy, θ, some stable sites are blocked and intracage molecule-molecule interactions modify adsorption and activation energies, leading to correlations. These correlations complicate the benzene motion, preventing the derivation of a rigorous analytical solution in closed form. For the benzene in Na-Y system, an analytical mean field approximation nevertheless turns out to give surprisingly good results, as Saravanan and Auerbach showed /224, 225/. The diffusivity can still be written in the same form as at infinite solution, eq. (3.5), but the mean supercage residence time $1/k$ is

now a non-trivial function of the occupancy. The mean-field approximation consists in assuming that instantaneous occupancies in neighboring supercages are identical. In deriving the analytical expression for the diffusivity, it was also assumed that the occupancy of a site is either 0 or 1 (vacant or blocked site). The cage-to-cage hopping frequency can then be written as a product of a transmission factor κ (assumed to be 1/2, because all cages are identical on average, and this is a mean-field approximation); the probability of occupying a W-site, P_W; and the total rate of leaving a W site, k_W:

$$k = \kappa P_W k_W \tag{3.7}$$

in which it is quite straightforward to show that

$$P_W = 1/\left[1 + K_{eq}(W \rightarrow S_{II})\right],$$

where the equilibrium coefficient

$$K_{eq} = < n_W > / < n_{S_{II}} > \tag{3.8}$$

is the ratio of the averages of the fluctuating numbers of molecules populating the W and the S_{II} sites respectively. Much less straightforward is the calculation of those averages. This can be done more easily in the grand canonical (constant μVT) ensemble, because of an analogy with a fermion gas consisting of two classes of fermions with different energies. This corresponds to the two types of sites. The population of the energy levels is well-known for such a system, and so is K_{eq}. The link with the canonical ensemble (constant NVT), which is needed here and for which an expression for K_{eq} can also be derived, is complex and can only be done numerically. A leading order approximation can be derived analytically, however, and, after a lot of algebra, yields two expressions for K_{eq}, depending on whether the number of molecules is larger or smaller than the number of S_{II} sites. The numerical results as well as the Monte-Carlo simulations are useful to have a better idea about the quality of the approximation, which was found to be excellent away from $\theta = 2/3$. An estimate for the average window residence time $<\tau_W> = 1/k_W$ can be made under the mean-field approximation, MFA, assuming either full occupancy of neighboring supercages (for $N > N_{SII}$) or all empty window sites except for the one under consideration, for $N < N_{SII}$. In summary, a quite simple result follows for $N < N_{SII}$ and an infinite volume ($\theta < 2/3$):

$$k(\theta) = (3/2)\left\{\left[2/(2-3\theta)\right]\left(k_{W\rightarrow W} / k_{W\rightarrow S_{II}}\right) + 1\right\} k_{S_I \rightarrow W}. \tag{3.9}$$

In this approximation, the factor $2/(2-3\theta)$ is the only difference with eq. (3.6), valid at infinite dilution. For $N > N_{SII}$ ($\theta > 2/3$), all S_{II} sites are blocked in the approximation, and the result is:

$$k(\theta) = 3(1-\theta)\left[(3\theta - 2)/\theta\right] k_{W\rightarrow W}. \tag{3.10}$$

This site blocking model predicts that the diffusivity $D(\theta) = (1/6)k(\theta)a^2$ is highest at $\theta \approx 0.82$, corresponding to approximately four S_{II} sites and one W site blocked per supercage. Quantitative agreement was found with Monte-Carlo simulations, using fundamental rate coefficients calculated at infinite dilution /225, 226/ (Fig. 26). It is seen in these simulations that the intercage jump length, a, slightly but gradually increases with loading, and is not constant as is assumed in the mean-field approximation, because molecules enter and exit cages through different W sites. The agreement between diffusivities calculated using MC and the mean-field approximation is almost perfect for loadings smaller than 2/3, but increases

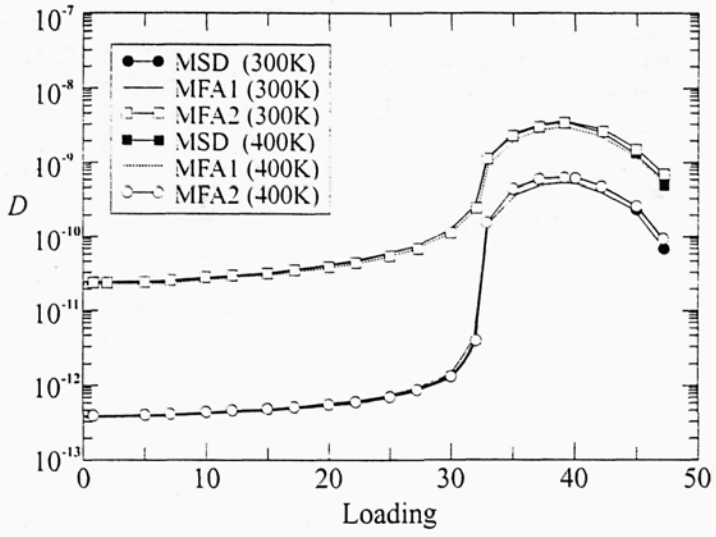

Fig. 26 **Diffusion coefficients versus loading for 300 and 400 K calculated by the three methods explained in the text /226/.**

roughly linearly to about 25-30 % at higher loadings (Fig. 27). Calculation of the correlation factor $f = D/D_1$ (eq. 3.4) shows this discrepancy in a different way.

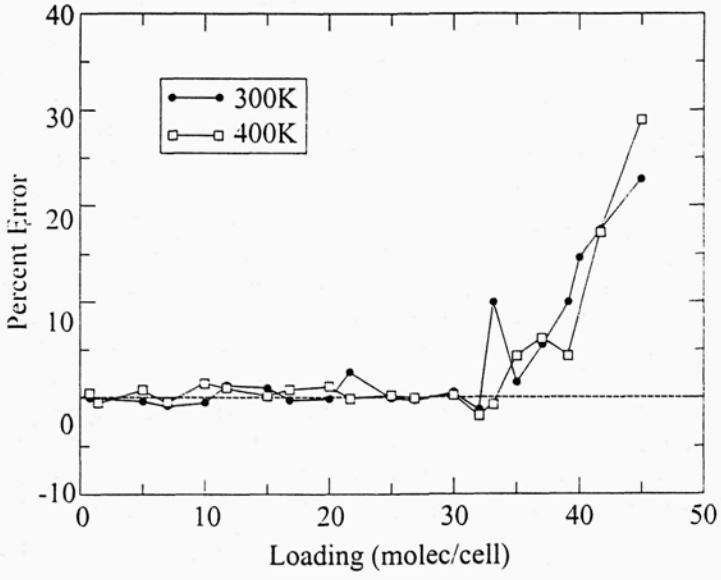

Fig. 27 **Percent error between MFA and MFD diffusion coefficients calculated as $(D_{MFA2} - D_{MSD})/D_{MSD} \cdot 100\%$ /226/.**

Because there was quite some deviation between the calculated and the experimentally measured diffusivities, the theory for benzene diffusion in Na-Y and Na-X was further refined to include nearest neighbor adsorbate-adsorbate interactions /227, 228/. Now, qualitative agreement with PFG-NMR was found (decrease with loading) and disagreement with tracer ZLC (increase with loading) (Fig. 28). An Ising lattice of binding sites was used as a

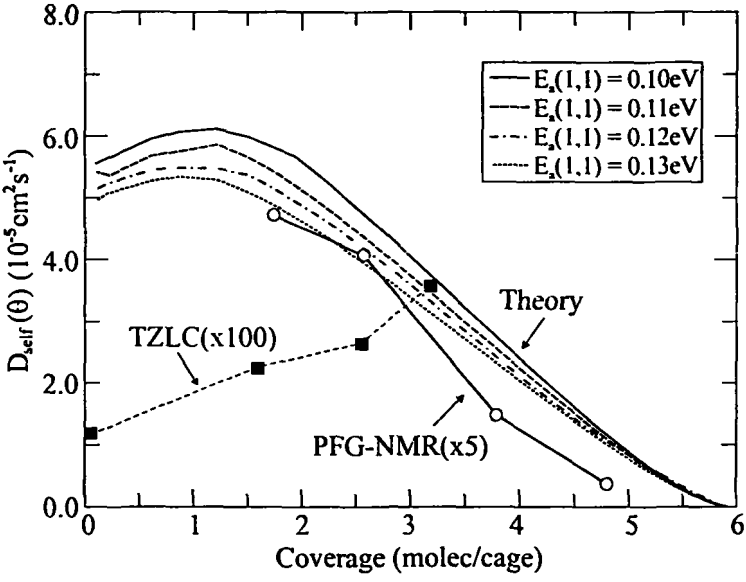

Fig. 28 Benzene diffusivities in NaY as a function of loading /227/.

representation of the system. The Hamiltonian contains the site free energies and the coupling between nearest neighbor sites S_{II}-S_{II} and S_{II}-W (the W sites are too far from each other to interact significantly). By varying the fundamental energy scales, the system is seen to exhibit four of the five loading dependencies of self-diffusion reported by Kärger and Pfeifer /11, 306/ (see also Fig. 68). The adsorbate-adsorbate interactions modify the jump activation energies. These modifications are calculated using a simple parabolic jump model: the minimum energy hopping path connecting adjacent sorption sites is characterized by intersecting parabolas. This model is most accurate when the spatial paths of the jumping molecules are not drastically changed by sorbate-sorbate interactions, although the energies can change. An analytical mean-field theory can then be derived, based on calculations of the probability of occuying a site and the rate of leaving it. Monte-Carlo simulations of these parameters can also be performed. The loading dependence of the diffusivity is mostly controlled by these parameters. The mean-field theory is very quick and predicts the activation energy fairly well. At low to moderate couplings, diffusivities can also be calculated using the theory, but deviations from the Monte-Carlo simulated values are important at stronger couplings. The diffusivity can either be calculated directly from the mean-square displacements found from Monte-Carlo simulations (MSD) or from Monte-Carlo simulations of the hopping rates and the use of the mean-field approximation discussed earlier. Making

the coupling more negative leads to a shift of the position of the maximum diffusivity from high loading to low loading to infinite dilution. The mean-field approximation works very well at low loadings, because the cage-to-cage motion is essentially uncorrelated. At higher loadings, stronger deviations are seen, which are attributed to phase transitions from a low to a high density of adsorbed benzene, similar to the vapor-liquid equilibrium of bulk benzene. For strong coupling, the diffusion moves from super-critical to sub-critical. Significant correlations exist, because the distribution of molecules is very inhomogeneous ("evaporation" along cluster boundaries). In this region, the simulated self-diffusivity is almost constant over a wide range of occupancies.

Experimental measurements of benzene diffusion in Na-Y and Na-X exhibit a remarkably gentle dependence on occupancy, for low to moderate loadings, and the benzene molecule can easily rotate within a cage, hereby removing auto-correlations in its motion. This may explain the success of Saravanan and Auerbach's analytical approximation. For many other systems, the dependence is much more pronounced /11/, and mean-field approximations have to be used with caution, especially when the connectivity is low and there is a clear distribution of adsorption strengths, leading to more strongly correlated motion /175/.

Jousse et al. /230, 231/ studied the diffusion of trans-2-betene as a function of loading in silicalite-2, the all-silica member of the MEL family, a three-dimensional zeolite with straight 5.3 x 5.4 Å channels that run along perpendicular directions and are connected by two types of intersections: small more or less spherical ones, and elongated ones, looking like channels in the z-direction (Fig. 29). The diffusion of trans-2-butene as well as of other butene isomers could be simulated at low loading using molecular dynamics or kinetic Monte-Carlo, the latter despite the fact that the energy barriers are rather small /230/. At higher loadings, the diffusivity decreases with increased loading as a result of slightly attractive intermolecular interactions for each of the isomers, except for trans-2-butene, where a more complex behavior is seen: the diffusivity as a function of loading is not monotonic but goes through a maximum at about 2 molecules per unit cell (Fig. 30). This could be interpreted as a result of repulsive interactions at low loadings, and attractive interactions at higher loadings. To study the effect of intermolecular interactions present at higher loadings, kinetic Monte-Carlo

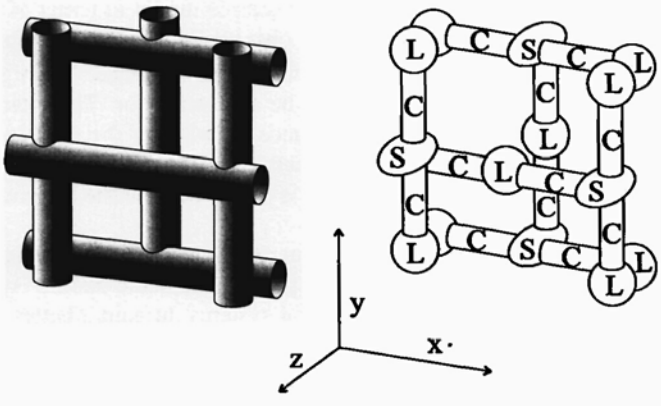

Fig. 29 Pore structure of MEL /230/.

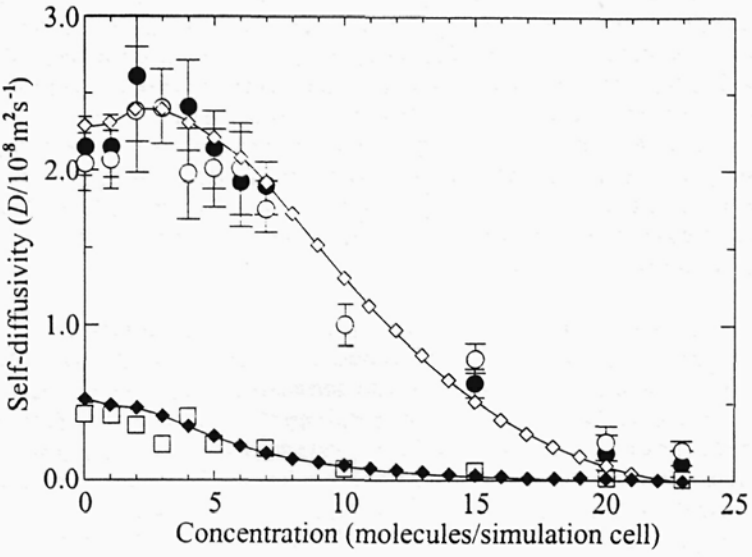

Fig. 30 Self-diffusivity as a function of loading for trans-2-betene in silicalite-2 (MEL family) /230/.

simulations were performed and a semi-analytical theory for the hopping rates was proposed /231/. Molecular dynamics is not so appropriate for this purpose, because only quantities averaged over many configurations are observed. Molecular dynamics shows that there are three types of sites for this system – large intersections, small intersections and channel sites –, but it suffices to consider hops between the intersections, where siting is preferred. The small intersections are elongated and can contain several molecules, while the larger intersection can only contain one. The maximum number of molecules per site can be evaluated from MD. Rate constants k_{ij} for hopping from any site i to any site j can then be calculated. The energy barriers to cross from one site to another are written as a function of two parameters, which depend on the intermolecular interaction energies. A simple model in terms of hops between spherical, symmetric sites is unable to simulate the observed diffusion behavior, because the larger intersection sites are channel-like and therefore asymmetric. At higher loadings, packing of molecules inside the channels needs to be accounted for. The interaction energy between two molecules in a large intersection depends on whether the molecules lie next to each other or whether there is another molecule in between. If this effect is accounted for, the maximum in the diffusivity as a function of loading is observed from the hopping simulations.

An important advantage of the method by Auerbach and co-workers is the level of quantitative detail that can be obtained for a specific molecule-zeolite system. Others performed Monte-Carlo simulations for more general systems, to gain a better understanding about the parameters that influence the way in which the diffusivity depends on occupancy.

A special situation occurs when the intracrystalline pore space consists of parallel or one-dimensional pores, such as is the case for, *e.g.*, ZSM-12, -22, -23, -48, and for $AlPO_4$-5, -8, -11,

L, Omega, EU-1 and VPI-5. Large enough molecules may not be able to pass each other anymore, so that the molecular propagation may become strongly correlated over long distances and Einstein's relation for self-diffusion, $<r^2(t)> \sim t$ no longer holds. This has been called single-file diffusion /316/. Early work modeled movement in one-dimensional zeolites assuming a hopping model, where molecules hop from site to site along a line; molecules cannot hop to already occupied sites. Based on this, it can be shown that $<r^2(t)> = 2 F t^{1/2}$, where F is called the mobility factor. The mean square displacement is proportional to the square root of time rather than to time itself /317, 194–196, 318–322/. Such anomalous diffusion is also observed on self-similar fractals, diffusion in random media with traps, and in various fields /323–326/.

Recently, computational studies of single-file diffusion in zeolites have become a hot topic, as direct and unambiguous experimental evidence has been difficult to obtain. PFG-NMR and QUENS studies with methane in $AlPO_4$-5 showed ordinary diffusion according to some /123,124/, but single-file behavior according to others /122, 327/ (see also Section 2.2). To this date, there seems to be no unambiguous and uncontested experimental proof for single-file diffusion, possibly due to different time scales (varying from ns to 0.1 s) and sample details in different investigations. An indication of single-file diffusion for methane in VPI-5 has also been suggested on the basis of smaller diffusivities than for ZSM-5, which has much narrower pores /328/, in contrast with some of the observations for $AlPO_4$-5, which also has narrower pores /329/.

In recent years, detailed numerical simulations have been carried out to explain if and when single-file diffusion occurs, and how it could be observed. Several examples were already discussed in Section 2.2. Modeling of diffusion in one-dimensional pores sometimes employs a combination of MC and MD techniques, and the reader is therefore also referred to Section 2.2 for more details. If molecules have a nonzero probability to pass each other, single-file diffusion may be observed on short time scales, but is absent over longer times, so that the diffusion becomes ordinary again. When two or more molecules can occupy a site, they can also pass each other more easily and anomalous diffusion is only observed at short times /330/.

MD simulations (see, e.g., /321/ and Section 2.2) show $<r^2(t)> \sim t^{1/2}$ after an initial ballistic phase, i.e., when a significant number of mutual encounters between molecules have occurred. Crystallite boundaries, however, appear to influence diffusion of a single-file system, as it stops being anomalous under the condition of fast particle exchange at the ends /128/. Under these conditions, the previous expressions indicate a time of tracer exchange proportional to the third power of sample length for long channels /331/, in contrast to previous Monte-Carlo simulations /332/ on channels of length 25-75 l, in which an exponent of 3.3-3.4 was found.

Tepper et al. /119/ studied methane diffusion in $AlPO_4$-5, and found anomalous diffusion at short times and a system-size independent cross-over at long times, which are inaccessible to MD. A simple "hop-and-cross" model was able to reproduce the MD results rather accurately and study the phenomena more in depth over very long times. The "cross" involves an interchange of the molecule with its neighbor, when it attempts to move to a site occupied by this neighbor. The closest approximation of the MD results was found for a very low crossing

probability, $p_{cross} = 0.0008$. Even such a small value has a profound influence on the results. At a time of 7 ns, a crossover from anomalous diffusion with an exponent of 0.64 (not 0.5, due to infrequent crossing events) to normal diffusion (exponent 1) was observed. Based on their results, the authors disagree with the experiments of Kukla et al. /122/, which may have been influenced by channel blockages caused by imperfections and impurities. The results agree with the experiments of Nivarthi et al. /123/ and Jobic et al. /124/.

Several results obtained by MD indicate the importance of collective or resonant motions of molecular clusters; some authors observed single-file behavior /125, 334/, some not /333/. This was discussed in more detail in Section 2.2. Sholl and co-workers have performed hierarchical simulations of adsorbed molecules in $AlPO_4$-5 that allow to study the rare adsorbate passages and close the gap between the atomic scale and the macroscale /120, 335, 336/. Kinetic Monte-Carlo simulations on a lattice gas model can be used, because it was shown by free energy calculations that not only the diffusion of isolated molecules but also the passing of molecules in a pore are activated processes. The free energy barriers for adsorbate passage are entirely due to entropic effects when the adsorbate-adsorbate interactions are hard wall potentials, but contain an energetic component when they are of the Lennard-Jones type. The order of magnitude of the energetic contribution is essential, as single-file diffusion will occur when it is much larger than k_BT. In the kinetic Monte-Carlo simulations, the effects of adsorbate passage were modeled as neighboring particle exchanges.

Recent work by Sholl and Lee indicates that concerted cluster diffusion can play an important role at higher loadings /336/. A hierarchical method was used to include atomic-scale information in coarse-grained kinetic Monte-Carlo simulations on microsecond time scales. Building upon the observations of Sholl and Fichthorn that show the significant influence of concerted cluster diffusion /125, 126/, molecular dynamics simulations of CF_4 clusters in $AlPO_4$-5 and of Xe clusters in $AlPO_4$-31 were carried out, to characterize the diffusion and dissociation mechanisms and rates of these clusters as a function of temperature and cluster size /335, 336/. The information from these simulations was then used to obtain parameters for the kinetic Monte-Carlo simulations. In these simulations, clusters are represented by their size and center of mass, and particles making up a cluster are equidistant and do not have to lie on a lattice. The clusters can dissociate and coalesce. Such simulations enable to accurately account for the detailed effects of clusters on time scales difficult or as yet impossible to access by MD. It was found that as much as 70 % of the total single-file mobility could be attributed to concerted cluster motions, so that formulas like eq. (2.44) underestimate single-file mobilities.

Okino et al. /337/ argue that more detailed modeling while introducing minimal complexity is necessary, because any realistic channel will have a variety of defects that may lead to deviations from the $t^{1/2}$ dependence. A hierarchical approach was therefore advocated by these researchers as well, although the challenge remains the proper linking between the different levels. In order to develop such an approach and gain better understanding of single-file diffusion when single-site hops dominate the diffusion, a deterministic model describing jumps between configurations was proposed. This model is similar to the model of Tsikoyiannis and Wei /237/ discussed further on, but with a corrected definition for the conditional hopping probabilities. In a second-order approximation to the complex problem of M species in a length-N pore, configurations are described in terms of all possible $(M + 1)^2(N - 1)$ doublets,

more in particular all pairs of adjacent sites. This allows to include the most important correlations for large systems. The doublet approximation does not directly assume the absence of any correlations between non-neighboring sites, but it does assume that such correlations are the result of correlations between neighboring sites. Better approximations can be obtained by considering triplets, and so on. A full model with all $(M+1)^N$ variables can only be solved for very short pores /338/. The doublet approximation could capture the anomalous single-file diffusion behavior even for very long pores, and the results were in agreement with the full model results by Rödenbeck et al. /338/ for short pores. Reactions and further correlations can easily be incorporated.

It is clear from this review that the results are very sensitive to the model details. Additional experimentation on more systems, together with more extensive simulations will be necessary to find a consensus on the actual diffusion behavior for a broader range of one-dimensional zeolites and nanoporous materials.

3.3 Monte-Carlo simulations of diffusion and reaction in zeolites

There are not many publications on the modelling of diffusion and reaction in zeolites, using other than a continuum approach. Continuum models are a good approximation when there are no long-range correlations present in the system and the diffusion and reaction phenomena can effectively be decoupled. This means that diffusivities measured in the absence of reaction are used in *macroscopic* differential equations describing diffusion and reaction in a catalyst pellet. Close to a percolation threshold, when molecules with sizes close to the pore size are diffusing, or for intrinsically very fast reactions, there is a need for more detailed network models that account for the correct topology of the pore network /232, 233/. For zeolites, one or all of these situations may occur, so that it should at least be verified whether diffusion and reaction can be decoupled, using network models.

With present day supercomputers, *microscopic* molecular dynamics simulations are not suitable because the necessary simulation times on the order of microseconds or more are prohibitively long. Somewhat less detailed *mesoscopic* Monte-Carlo simulations, on the other hand, are a good alternative, and this is the statistical mechanical method that has been most commonly used to study diffusion and reaction in zeolites. Considerable progress has been made, as some successes have been booked in studying industrially important processes, including xylene isomerization, alkylation of toluene, and methanol to olefines (MTO).

Continuum models may help us to get a first qualitative idea about the solution of a problem, but many simplifying approximations need to be made, which are unnecessary in Monte-Carlo simulations. These approximations make the solutions less accurate, and sometimes even make them qualitatively incorrect, in particular when correlations are important. It is only in recent years, with the advent of faster computers, that three-dimensional Monte-Carlo simulations are performed more routinely. Most authors have used small simplified two-dimensional grids, nevertheless obtaining qualitatively useful results and sometimes remarkably good agreement with experiments.

Theodorou and Wei /208/ developed a Monte-Carlo approach to investigate an isomerization reaction and the effect of catalyst deactivation by pore blocking. A two-dimensional, square

grid was used as a simplified model for the ZSM-5 pore space. The para-selectivity in the isomerization of xylene, e.g., is strongly influenced by catalyst modifications, such as those resulting from coking, which blocks some of the pores, leading to retardation of intra-crystalline transport and potential diffusion limitations. The simulations allowed to quantify these effects, by studying the influence of random blocking of pore entrances or of pores in the bulk (Figs. 31, 32). The authors found that bulk pore blocking led to a much sharper,

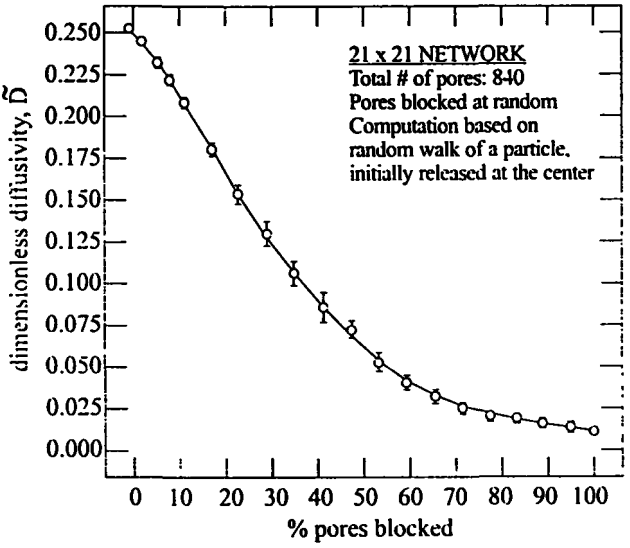

Fig. 31 Effect of bulk blocking of pores on diffusivity /208/.

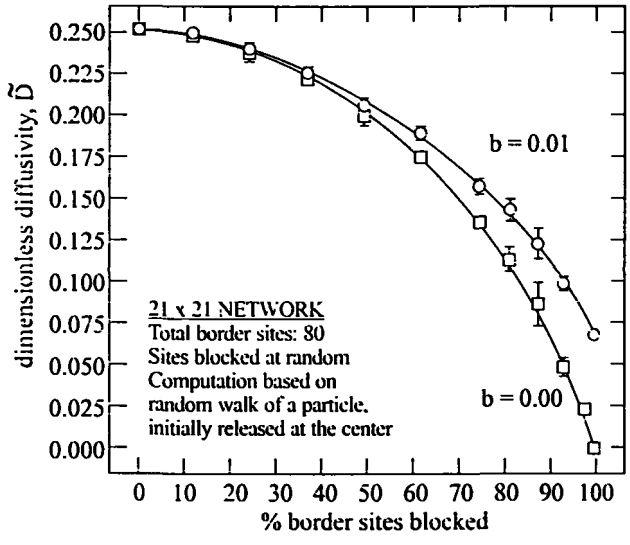

Fig. 32 Effects of border blocking on diffusivity /208/.

convex decrease than pore entrance (surface) blocking, for which the diffusivity-blockage curve is concave. This can be rationalised by noting that, as long as not too many pores at the external surface are blocked, molecules can migrate to a free entrance and reach the interior, after which they move more freely than if the pores in the bulk were blocked. The effects of loading were also studied, assuming equal activity of all sites. Higher occupancies lead to more retardation, as discussed earlier. Comparison with a continuum model showed that the decrease of the effectiveness factor with occupancy is well described by such a model for occupancies lower than about 50 % (Fig. 33). At higher occupancies, the continuum, mean-field approximation underestimates the effectiveness factor, as calculated from Monte-Carlo simulations. Especially noteworthy is the incomplete occupancy and the non-zero limit of the effectiveness factor at maximum loading, because of the nonuniform distribution of catalytic activity and the finiteness of the grid (Fig. 34).

These results were extended by Mo and Wei /234/, who used percolation theory and an effective medium approximation (EMA) to study the effect of random pore blocking on the effective diffusivity. Sundaresan and Hall /235/ incorporated the effect of nonidealities arising from interactions between sorbed molecules as well: molecules may be more likely to jump to a neighboring vacant site if some of its other neighbors are occupied. These repulsive interactions are similar to those included in the surface diffusion studies of Murch /197/ and of Reed and Ehrlich /198, 199/. The activation energy for migration of a molecule is

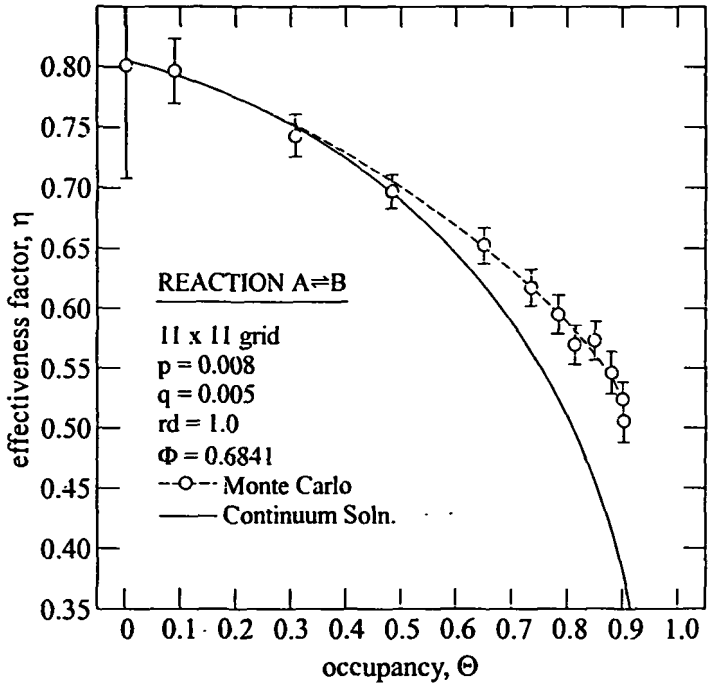

Fig. 33 Variation of effectiveness factor with global occupancy (comparison between Monte Carlo and continuum approaches) /208/.

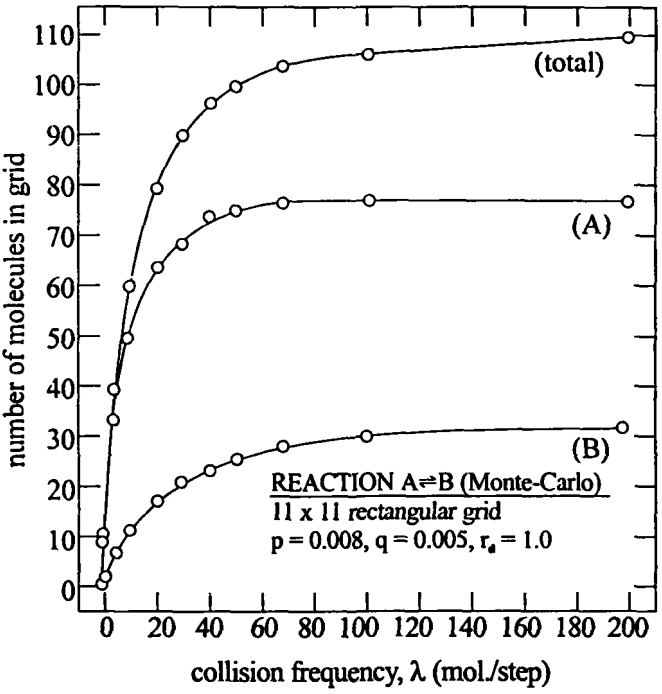

Fig. 34 Monte Carlo model: number of particles in a grid as a function of collision frequency /208/.

proportionally reduced by the interaction with molecules occuping an adjacent site; a different repulsive interaction energy is used depending on whether the pore in between these sites is open or blocked (e.g., because of coking). Based on the lattice gas model, they derived a continuum model for large crystals and not too severe internal pore blocking alone. Such a model can only be used when the pore blocking is sufficiently below the percolation threshold. Moreover, pairs of sites are treated independently, i.e., the quasi-chemical approximation is made, to enable a continuum description without having to resort to Monte-Carlo simulations. The results will not be discussed in detail, as we are limiting ourselves to Monte-Carlo simulations in this review, but one of the important conclusions from the simulations was that the effect of pore blocking is more pronounced in the presence of repulsive lateral interactions between sorbate molecules. As experiments of toluene alkylation in blocked ZSM-5 suggest such strong effects, this may mean that interactions indeed constitute an important factor.

Pore blocking or pore size reduction also has an influence on the ion exchange in zeolite A, as shown by Ruthven /236/ in Monte-Carlo simulations on a three-dimensional cubic grid. Tsikoyiannis and Wei /237/ developed a model for diffusion and reaction in zeolites using a cubic grid with one type of site, using the same assumptions as Theodorou and Wei /208/, but in continuous time. A Markovian formalism was developed, which allows to derive approximate solutions to the master equation describing diffusion and reaction in the zeolite.

In the absence of intermolecular interactions, the transient uptake or transport diffusivity is found to be independent on occupancy. The significant effect of attractive or repulsive intermolecular interactions on multi-component diffusion was studied as well.

Xylene isomerization in ZSM-5, again using a two-dimensional lattice, was considered by Frank et al. /211, 238/, and by Wang et al. /239, 240/, who also studied the alkylation of alcohols. Frank et al. tuned the hopping ratios of ortho-, meta and para-xylene to measure their effect on the reaction path. This enabled them to get an idea of the ratios of hopping rates needed to match the experimental observations; they found that a ratio o:m:p of 1:1:10 of diffusion coefficients led to a better correspondence with experiments than the often assumed ratio 1:1:1000 (Figs 35, 36). Since there is a debate on this ratio, simulations can give better insights into its effect. To convert Monte-Carlo time steps into real time, the average adsorption time on a site was approximated by a harmonic oscillator of which the frequency is chosen such that the oscillator's energy equals the activation energy. Wang et al. /239, 240/ obtained remarkably good correspondence of simulated conversions and selectivities with experiments, when using experimentally determined parameters for the diffusivities, adsorption constants and the intrinsic reaction rate constants (Fig. 37). In view of the known problems in measuring diffusivities, the limitations in using single-component diffusivities only, and the use of a small two-dimensional grid, it would be interesting to study whether the excellent agreement is a coincidence or whether the reaction results are not very sensitive to some parameters.

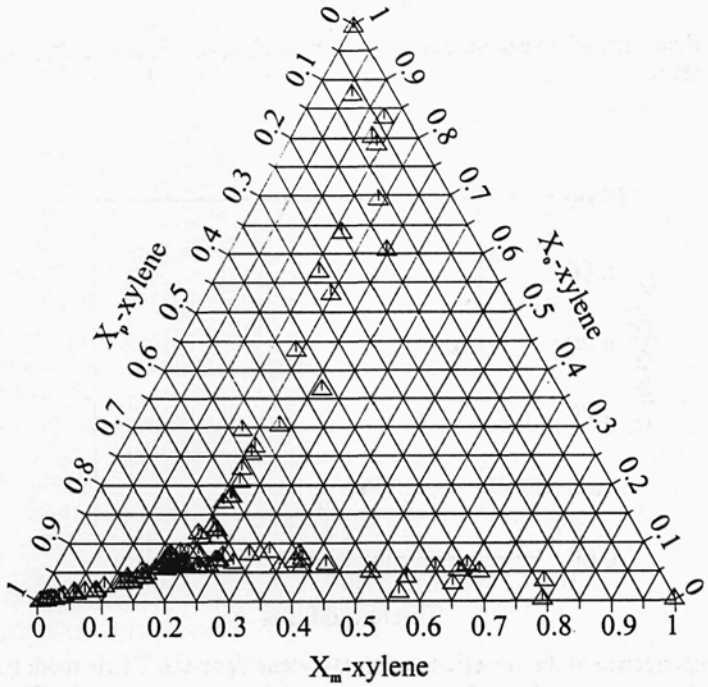

Fig. 35 Reaction path of isomerization of xylenes: $P_{Do\text{-}xylene}$: $P_{Dm\text{-}xylene}$: $P_{Dp\text{-}xylene}$ = 1:1:10 /211/.

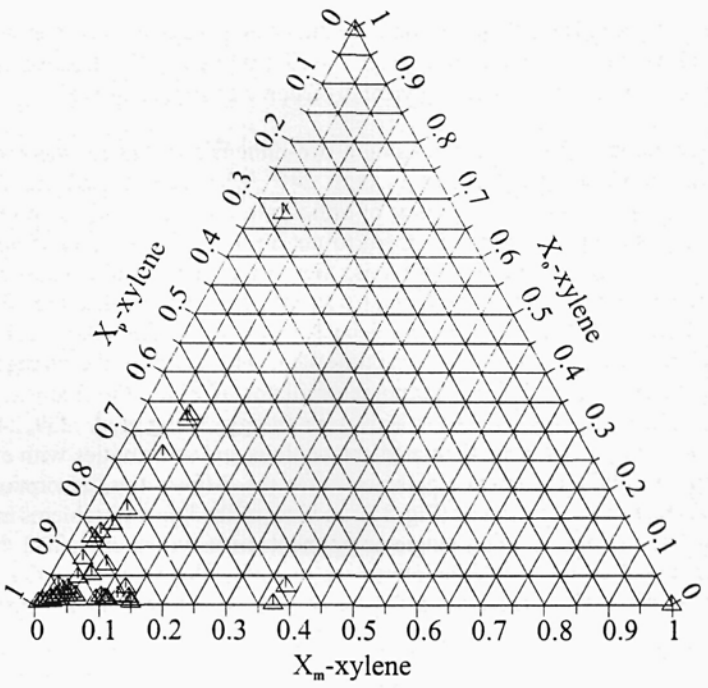

Fig. 36 Reaction path of isomerization of xylenes: $P_{Do\text{-}xylene}$: $P_{Dm\text{-}xylene}$: $P_{Dp\text{-}xylene}$ = 1:1:100 /211/.

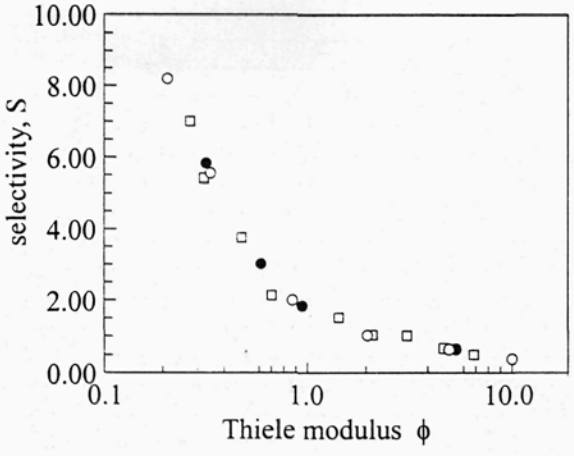

Fig. 37 Dependence of the selectivity of meta-xylene upon the Thiele modulus for ortho-xylene isomerization. (○) continuous model; (●) experimental; (□) cit. /239/.

Ethylation and disproportionation of ethylbenzene on ZSM-5 was studied by Klemm et al. /241/ to explain experiments and to provide suggestions to enhance para-selectivity. Comparison with experimental results taught that para-selectivity could be mainly attributed to product shape selectivity (i.e., products with a bulky structure cannot diffuse out quickly enough) rather than transition state shape selectivity (i.e., products are not formed at all), while the opposite holds for the disproportionation reaction. A continuum and a Monte-Carlo approach led to similar results (Fig. 38). The advantage of the Monte-Carlo approach is once again the ease with which parameters can be tuned and their effects simulated. It is an attractive method to understand the nature of structure selectivity.

Caution is needed with the interpretation of all these simulations, however, since it was observed in pure diffusion experiments and simulations that the diffusivities are very dependent on the pore network topology, so that results obtained with two-dimensional grids may not be generally valid.

Trout et al. /242/ used the true topology of the coarse-grained pore network of ZSM-5 to study its percolation transition, as well as the influence of the constraints on diffusion and isomerization at arbitrary loading (Fig. 39). In their model, there is one site per intersection and per channel in between two neighboring intersections. Sites are weak or strong. A reaction can occur on the strong sites. The diffusivity decreases more sharply with occupancy than on a square lattice, because of the reduced connectivity of the lattice. The reaction rate is higher when the occupancy is lower, as this reduces the fraction of blocked reaction sites. When all sites are assumed to be equal, they showed that there is an optimal fraction of reaction sites as a result of the subtle trade-off between the availability of enough reaction sites, on the one hand, and a decreased diffusivity and effectiveness at higher fractions of reaction sites, on the other (Fig. 40).

Recently, Hinderer and Keil /243/, and Keil et al. /244/ used a three-dimensional network with a fine grid to simulate the conversion of methanol into olefines (MTO) in a ZSM-5 catalyst; their Monte-Carlo approach enables to include complex chemical reaction networks between a large number of components, and does not assume the knowledge of the single component diffusivities. The latter is important, because even the single component diffusivities are not available in the temperature range of interest. The network is not simply a coarse-grained network containing bonds between sites. Instead, the complete crystallite space is divided by a fine cubic grid (Fig. 41). Each cube can be one of four different lattice elements: rigid zeolite framework, free intracrystalline pore space, active site or window site. A molecule can occupy any vacant element in the pore space or an active site. Sorbate-sorbate interactions are accounted for. During one Monte-Carlo step, each molecule is chosen in a random sequence, and a random direction is chosen. If the movement in that direction is possible, the molecule moves until it collides with another molecule or with the rigid zeolite framework. When molecules cross a window, they have to surmount a potential barrier. A Lennard-Jones potential is commonly used to describe the interactions; the sensitivity of the Lennard-Jones length constants σ turns out to be very high, leading to a tenfold increase in diffusivity when σ is reduced by only 10 %. The accuracy of the method was checked by comparison with MD and available experimental data for some test diffusion cases, and was found to be satisfactory. Simulations were then carried out for the MTO synthesis, using a simplified

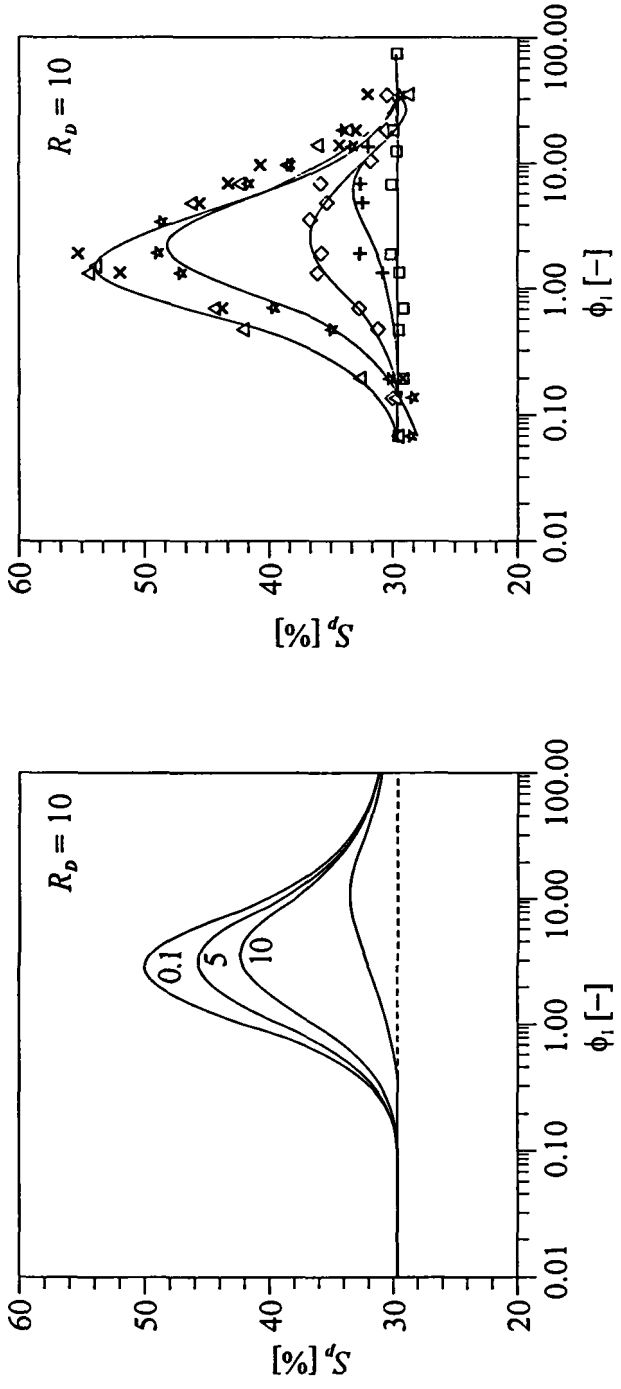

Fig. 38 Dependence of para-selectivity S_p on Thiele modulus ϕ of isomerization at different values of ϕ_F /241/.

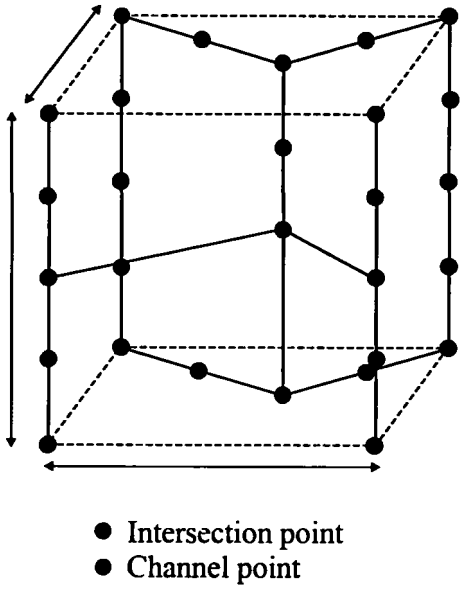

Fig. 39 Lattice model of ZSM-5 /242/.

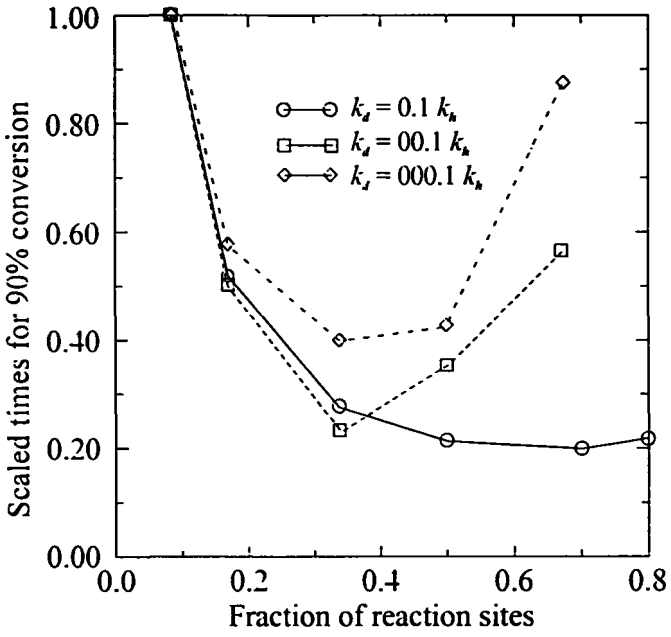

Fig. 40 Effects of the strength and fraction of reaction sites on the dynamics of diffusion and reaction when 33.33 % of the weakly adsorbed sites are occupied. The graph shows times for the product to reach 90 % of the steady-state concentration /242/.

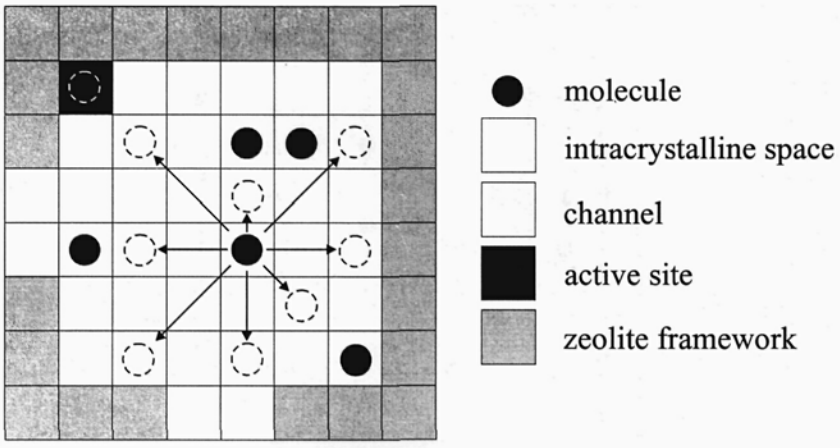

Fig. 41 Movements of molecules during MC calculations /243/.

reaction scheme with 6 or 7 reactions, and reaction probabilities specified to approximate experimentally determined product distributions. Keil et al. /244/ did not only consider the zeolite particles, but complete composite catalyst particles consisting of small catalytically active zeolite particles embedded in an inert, amorphous matrix. Such particles have become of increasing industrial importance in recent years as they offer several advantages related to reducing deactivation and attrition, amongst others. Both the multi-component zeolite diffusion and the molecular, Knudsen and surface diffusion through the matrix were accounted for in their model, which enabled them to obtain the composition of the reaction mixture as a function of MC steps, as well as the effectiveness factors as a function of particle size and zeolite fraction (Fig. 42).

3.4 Conclusion

Even with the advent of more powerful computers, it is expected that dynamic Monte-Carlo methods will continue to play a prominent role in the field of diffusion and reaction in zeolites. Among the many advantages are its flexibility, speed and ability to efficiently probe the configuration space, by allowing non-physical moves. Important is also the simplicity of the method and the possibility to hierarchically combine it with more detailed, microscopic methods. The basic parameters in the mesoscopic Monte-Carlo technique can also be found from detailed experiments.

First-principle-based dynamic Monte-Carlo methods, in which parameters are calculated by *ab initio* quantum chemical methods and interactions between neighboring adsorbates can be included, are already applied to simulate catalytic kinetics on surfaces /245/ and thin film growth /246/. Truly *ab initio* calculations on zeolites are even more complex, but could possibly be performed through such hierarchical methods. In such a method, microscopic simulations, such as molecular dynamics or dynamically corrected transition-state theory, and quantum-chemical calculations to calculate the elementary kinetic parameters, form the input to a mesoscopic Monte-Carlo method. While this has not yet been done to date, the databases that are currently built make this not inconceivable in the near future.

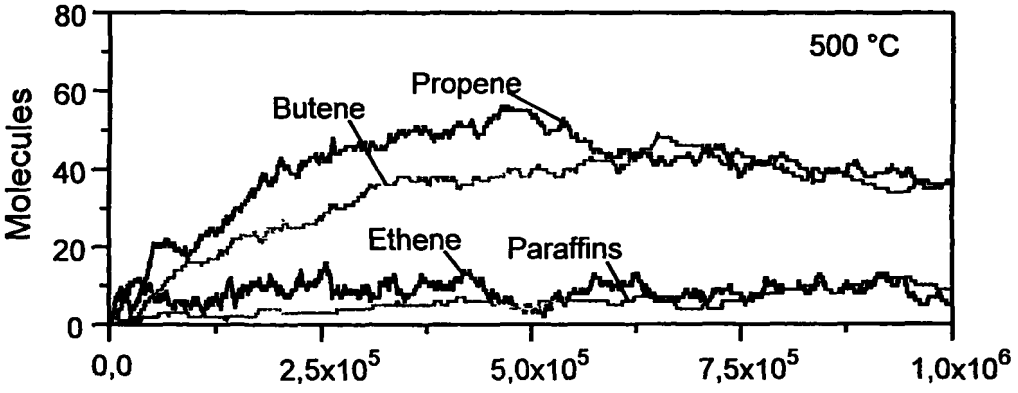

Fig. 42 Number of olefin and paraffin molecules within a lattice of 4096 intersections /244/.

4. TRANSITION-STATE THEORY

4.1 Introduction

Transition-state theory (TST) is very useful to characterize the sluggish, activated motion of tightly fitting molecules in zeolites. In these cases, the motion can be accurately described by a succession of hops between sites, which are coarse-grained potential energy minima. Once these sites have been localized, knowledge of the jump or transition rates between them allows to calculate the diffusivity using the dynamic Monte-Carlo method or, if possible, an analytical technique. Long molecular dynamics calculations can be avoided, as the kinetic problem is converted into an equilibrium problem. Only short, local molecular dynamics may be required to correct the transition rates for multi-step transitions or recrossings of the transition state.

As already stated in Section 1, transition-state theory (TST) and dynamic Monte-Carlo (MC) can be related to a master equation. The derivation of the master equation (ME) starts with a phase space density ρ and a probability P_j of finding the system in configuration j. For the derivation of the master equation, we need to express how P_j changes with time. This leads, by means of the Liouville equation, to a relation between dP_j/dt and the Hamiltonian of the system /23, 24/. Finally, one obtains an equation of the form of eq. 1.4.

Substitution of the Boltzmann distribution for the phase space density leads to the well-known expressions for the transition probabilities:

$$W_{ij} = (k_B T/h) Z^{\ddagger}/Z, \qquad (4.1)$$

in which T is the absolute temperature, k_B is the Boltzmann constant, h is the Planck constant, and $Z^{\ddagger}$ and Z are the partition functions for the transition state between i and j and for the initial configuration j respectively /42/. The transition probabilities W_{ij} can also be written as rates k_{ij}, when the probabilities P_j are probabilities of occupancy. Transition-state theory (TST) is concerned with calculating the transition probabilities or rates k_{ij}^{TST}. As is clear from eq.

(4.1), calculation of these rates is only based on the equilibrium phase space distribution of the system at the initial states and at the transition states or hypersurfaces separating states. It is assumed that molecules are coupled to a heat bath: while residing near a potential minimum (initial state) or at a saddle point of the potential energy hypersurface (transition state), energy is distributed uniformly over all their degrees of freedom as determined by the canonical ensemble density function. The final state does not appear in the equation for the rate. The theory assumes that molecules approaching the transition state with sufficient kinetic energy to cross this barrier between initial and final state will always cross it /163/. In reality, this need not be so: if the molecule fails to thermalize in the destination state, it will recross into either the initial reactant state or quickly cross to a second product state. Corrections for dynamical recrossings or multistate transition events may therefore be necessary, as we will see furtheron in simulations of diffusion in zeolites. To allow for such events, jump rates needs to be corrected, using a transmission coefficient:

$$k_{ij} = \kappa_{ij} k_{ij}^{TST} . \tag{4.2}$$

The transmission coefficients κ_{ij} are found from short molecular dynamics simulations (MD). Once the transition rates are known, the master equation can be solved either analytically or by a dynamic Monte-Carlo simulation, as discussed in Section 3.

We shall now discuss the application of TST to diffusion in zeolites. This subject has also been reviewed by Theodorou et al. /21/, Bell et al. /36/ and Bates and van Santen /38/.

4.2 Diffusion in zeolites

The first application of TST to diffusion in zeolites was by Sargent and Whitford in 1971 /248/, who used it to calculate the diffusivity of CO_2 in zeolite 5A, which has a cubic pore network. However, the errors in the diffusivities were very large, probably due to the neglect of the preferred molecular orientation for the linear CO_2 molecule when crossing the transition state. A TST-study by Bétemps and Jutard /249/ of the diffusion of Ar in 5A led to poor estimates as well; this time, the errors could be attributed to uncertainties in the location of the Na^+ ions.

In 1972, Ruthven and Derrah /250/ derived a transition-state theory to compute the diffusivity of the approximately spherical molecules CH_4 and CF_4 in the same zeolite 5A. Diffusion in this system can be modeled by a cavity-to-cavity motion, easily amenable to a transition-state theory. The 8-membered oxygen windows between the cavities form transition barriers that molecules have to pass in order to move from one cavity to another. They do this at a transition rate k. Since the cavities form a cubic array, the diffusivity at infinite dilution can simply be estimated by $1/6\, k\, a^2$, where a is the lattice constant, see also eq. (3.5) (Ruthven and Derrah actually used an alternative derivation using a flux expression with the transport diffusivity, linked to the self-diffusivity by the Darken equation). Excellent agreement with sorption experiments was found, under the condition that a high degree of rotational freedom is associated to CF_4 in the transition state, yet not to CH_4. This leads to different partition functions for the transition state configurations of these molecules, and therefore to different transition rates, eq. (1.4).

Despite the agreement with sorption uptake experiments, the results are at odds with PFG

NMR experiments, which are likely to be more accurate, according to Kärger et al. /251/. These investigators derived a slightly different, yet similar expression for the self-diffusivity, based on eq. (4.1), and an adsorption isotherm. The latter relates the partition function in the cavities to the partition function in the gas phase, which is useful to avoid the calculation of the former and use an experimental isotherm. At low loadings, the isotherm corresponds to Henry's law, making the diffusivity inversely proportional to Henry's constant $K = K_0 \cdot \exp(V_0/k_BT)$. The only assumptions necessary for calculating diffusivities in the given model are now the changes in the degrees of freedom when comparing free molecules in the gas phase with molecules in the transition state between neighboring cavities. This allows to calculate the ratio of partition functions:

$$Z^{\ddagger}/Z^{g} = Z_{\mathrm{int}} Z_{w} Z_{rot} / Z_{g,\mathrm{int}} Z_{g,trans} Z_{g,rot} \tag{4.3}$$

from which the prefactor of the diffusivity, D_0, follows:

$$D_0 = a^2/(h K_0) Z^{\ddagger}/Z^{g}. \tag{4.4}$$

Note that a transmission factor $\kappa = 1$ was chosen, which may not be valid anymore at higher loadings. These partition functions refer to internal degrees of freedom (Z_{int}, $Z_{g,int} \approx 1$), translation in the gas phase ($Z_{g,trans}$), two-dimensional vibration in a window (Z_w) and rotation (Z_{rot}, $Z_{g,rot}$). Contrarily to Ruthven and Derrah, Kärger et al. /251/ find it more likely that the windows do not impose significant restrictions to the molecular rotation of spherical molecules ($Z_{rot}/Z_{g,rot} = 1$). They applied this TST expression to diffusion of methane and ethane in zeolite NaCaA zeolite, obtaining good agreement with PFG-NMR measurements.

The transition-state theory of many other molecule-zeolite systems is in principal the same, but its application is more complex. What simplified the treatment for zeolite A was the high degree of symmetry of its lattice, leading to only one type of site and one type of transition state. June et al. /252/ made the first TST study of diffusion in a zeolite with several types of sites and jump rates between sites, namely silicalite. Because a high number of degrees of freedom of the diffusing molecule complicates the problem (there are up to 3N-6 vibrational degrees of freedom for an N-atom molecule), diffusion of Lennard-Jones spheres, represented by Xe and SF_6, with only 3 translational degrees of freedom was studied. Twelve sites per unit cell, and 3 different types of adsorption sites were found: one in each straight channel section, one in each sinusoidal (zig-zag) channel section, and one in each intersection. Although there are actually several energy minima in a channel, the barrier between them is too small ($< k_BT$) to consider them separately, so that they can be combined to form a *macrostate*. By locating the saddle points of the potential energy surface the transition states can be located; for Xe there are 6 topologically distinct transition paths between (macro)states, while for the larger SF_6 there are only 3 (Fig. 43). It turns out that for Xe (but not for SF_6) not only the obvious transitions between topologically neighboring sites are *possible, but also direct transitions from straight channels to sinusoidal channels can occur*, although these are less probable (their jump frequency is lower). For the larger SF_6, the volume of the intersection sites is larger and the volume of the channel (macro)states smaller. The influence of temperature is interesting, as the occupancy of the sites, P_i or θ_i, is strongly temperature dependent: at higher temperatures, more uniformization is seen. A larger molecule like SF_6 will prefer to occupy the more spacious although energetically less favorable intersection sites, because of entropic effects. In any case, equilibrium occupancies should be

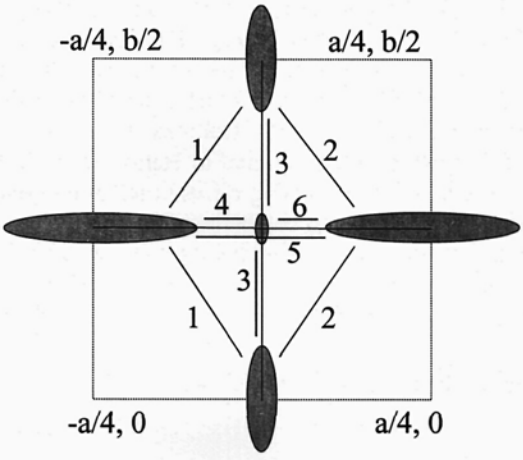

Fig. 43 Special layout and connectivity of the xenon sorption states located around the silicalite channel intersection. The figure is a view of 1/4 unit cell down the [001] crystallographic axis /252/.

such that the condition of detailed balance or microscopic reversibility is satisfied:

$$k_{ij}^{TST} P_j = k_{ji}^{TST} P_i , \tag{4.5}$$

in which k_{ij}^{TST} is the transition rate from site j to site i (note that another common notation for this rate is $k_{j\to i}^{TST}$). The transition rates are calculated as before, from the ratio of the NVT (canonical ensemble) configurational integrals over the transition hypersurface S_{ij} and the (macro)state volume V_j:

$$k_{ij}^{TST} = (k_B T/h) Z^{\ddagger} / Z = (k_B T/2\pi)^{1/2} \int_{S_{ij}} d^{N-1}x \, \exp[-v/k_B T] / \int_{V_j} d^N x \, \exp[-v/k_B T] \tag{4.6}$$

For a nice overview on how to compute the rates, see Theodorou et al. /21/.

The work by June et al. illustrates the possibilities offered by TST with different levels of complexity. It is the first work to include a dynamical correction factor κ, and a successful comparison with molecular dynamics was made for the Xe-silicalite system. The latter is very important, since the molecular dynamics are up to 2 orders of magnitude slower, especially at lower temperatures, and could not even be completed within a reasonable amount of time for the slower SF_6 diffusion, showing the importance and success of dynamically corrected TST.

Dynamical corrections were calculated using the formalism of Voter and Doll for multistate systems with many degrees of freedom /253/, based on a theory first presented by Chandler /254/. This theory only assumes that the time scale for thermalization after a barrier crossing is separated from the time scale between barrier crossings. It is the latter time scale that is especially large, making molecular dynamics often prohibitively long. Within the framework of dynamically corrected TST, molecular dynamics only need to be performed over the time scales needed for thermalization, to study whether, after a short time t, a molecule starting in

state i will end up in state j, return to i or move on to a state j' beyond j (multiple crossings when no thermalization in the intermediate state is possible).

In the case of Xe-silicalite, an additional comparison was made between results obtained using a rigid and an animated (flexible) lattice, where all the silicalite atoms are allowed to relax during the sorbate motion. Monte-Carlo simulations were used to calculate the self-diffusivities at infinite dilution, based on the calculated jump rates. Simulations using a flexible lattice led to lower, but not much lower, values of the diffusivity: a 40 % decrease was found at 100 K. The dynamical corrections suggest that the weak coupling of a small sorbate molecule such as Xe with the lattice enhances recrossings of the transition state. These effects are expected to become more important for larger molecules, as is also suggested from simulations of benzene in silicalite /255/. Diffusion is anisotropic in silicalite, and the temperature dependence of the anisotropy of SF_6 diffusion could be revealed. The anisotropy is increased by multistate jumps between adjacent straight channel sites, bypassing intersections. Such jumps become more frequent at higher temperatures.

Snurr et al. /255/ studied the activated diffusion of benzene in silicalite, which introduces a next level of complexity: the diffusing sorbate is not spherically symmetrical anymore, so that its orientation matters. The result is that there are not three, but six degrees of freedom, including three translational and three orientational degrees of freedom. A potential energy map for benzene diffusion in silicalite was calculated by Nowak et al. /256/, showing the variation in potential energy of a benzene molecule as it moves along the center of a silicalite channel (Auerbach et al. /219/ used a similar approach for Na-Y, *cf. supra*). TST for this system has also been used by Schröder and Sauer /257/, starting with a minimum-energy path calculation of the motion of benzene through the straight channels of silicalite; the sinusoidal channels were neglected in this simulation. While simpler, such minimum-energy path calculations have the serious drawback that the paths through the channels are not unique and that a molecule stepping along one path may abruptly switch to another one. This is for example the case for benzene in silicalite, so that a minimum-energy path calculation may not be satisfactory. Snurr et al. /255/ conducted an exhaustive search for all the minima (sites) and saddle points (transition states) of the six-dimensional potential energy hypersurface. They found 27 unique minima and 100 unique transition states in the asymmetric unit of silicalite (one-eighth of a unit cell). The diffusion paths in six dimensions were constructed using Fukui's intrinsic reaction coordinate approach /258/, which consists of determining pairs of gradient-following paths from each saddle point, until two minima, corresponding to the microstates, are reached. The transition rates associated to paths connecting minima were then calculated, approximating the transition states by hyperplanes perpendicular to the paths, and the potential energies by quadratic approximation functions (harmonic approximation) /259/. A rigid silicalite framework was assumed. To facilitate the calculations, based on the values for the rates, minima could be grouped into microstates and macrostates. This is somewhat similar to the lumping of components in kinetic studies of complex chemical processes. Within a macrostate, the motion between sites is much quicker than in between sites belonging to different macrostates, so that equilibrium may be assumed within each macrostate, and only the jumps between macrostates need to be considered in the dynamic Monte-Carlo simulations used to estimate the diffusivity. Note that this is again quite similar to the findings of Auerbach et al. /222, 223/ for benzene in Na-Y, although the number of states is much smaller in the latter case. The macrostates found for benzene in silicalite correspond to intersection, sinusoidal

(zig-zag) and straight channel adsorption sites, just like for Xe and SF_6. Benzene molecules are found to spend most of their time in the channel intersections, and to move mainly in the direction of the straight channels and less, but significantly, in the direction of the sinusoidal channels. Jumps between macrostates are strongly temperature dependent, while jumps between microstates within a macrostate are not. The latter correspond to small displacements or fast rotations of a molecule. While all these results corroborate experimental findings, the TST-predicted orientationally averaged diffusivities themselves ($1.1x10^{-12}$ m^2/s at 300 K) are 1-2 orders of magnitude below the experimentally reported values. The activation energy is too large and the preexponential factor appears to be slightly underestimated (Fig. 44). This is probably a result of the assumption of a rigid lattice. June et al. /252/ showed that including the flexibility of the lattice plays an important role for tight fitting molecules. The presence of a large molecule may change the breathing motions of the silicalite structure. A similar discrepancy is found for diffusion through polymers, where including the network flexibility is essential to match experimental results /260/.

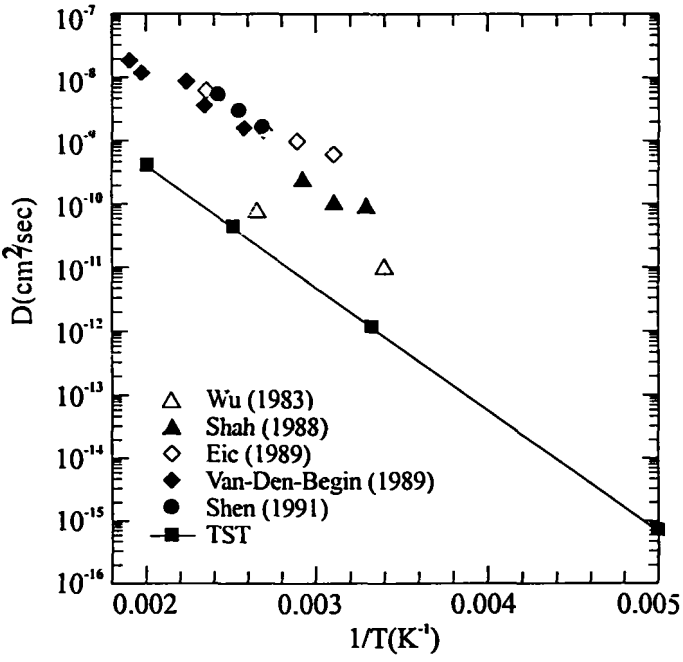

Fig. 44 Comparison between TST predictions and experimental results for the self-diffusivity of benzene in silicalite at low loadings /255/.

The diffusion of Xe in Na-Y was simulated by Mosell, Schrimpf and Brickmann, who employed both MD and TST /261-263/. They considered only cage-to-cage motion in their TST calculations, because the intra-cage motion is much more rapid. The novelty was a detailed consideration of the dynamical corrections to the transition rate, in order to separately determine a local transmission coefficient and the probability for the continuation of a jump event. A

higher number of barrier crossings per jump was observed with increasing temperature. The effect of dynamical corrections remained small, however, except at higher temperatures where they led to an increase of the diffusivity by approximately 30 % at 210 K, the highest temperature considered. Little influence on the activation energy was observed. Agreement with conventional MD was excellent.

Maginn et al. /264, 265/ took a hierarchical approach to simulate diffusion of long n-alkanes (up to C_{20}) in silicalite. Their method combines Brownian motion theory (BD) with transition-state theory (TST). Diffusivities of such long molecules could not be obtained by molecular dynamics, because the molecules move too slowly, or traditional transition-state theory, because the number of degrees of freedom is so high. Coarse-graining is applied to reduce the effective dimensionality of the system and minimize the necessary computer resources. A coarse-grained representation of the zeolite is obtained by defining straight channel (S), zigzag (Z) and intersection (I) regions. The alkane chain is coarse-grained by representing it by the projected coordinates X_1 and X_2 of the ends, together with the "macrostate" in which the molecule resides and which is either intersection-terminated or channel-terminated. The macrostate is represented as a sequence of I, Zi (zig), Za (zag) or S; the channel segments can be traversed either upward or downward (+ or –). An example is [Zi^+IS^-], which means the tail lies in a straight line segment, the head in a zig-segment, and the molecule crosses the intersection in between them. It can move through an intermediate macrostate [Zi^+I] (here, only X_1 is needed to characterize it) to reach a macrostate [Zi^+], when the molecule lies completely within a zig-segment of a zig-zag channel (Fig. 45). The dynamics are now characterized by a

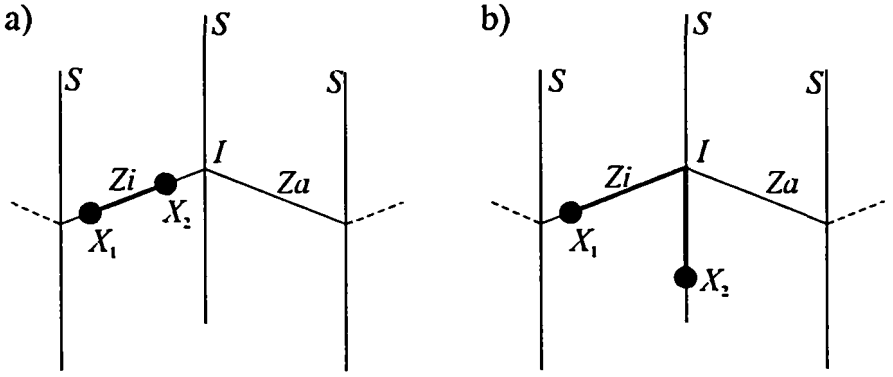

Fig. 45 Positions of a molecule in a zig-zag channel /265/.

succession of intra-macrostate movements and transitions between macrostates. The former occur when a molecule crosses an intersection and are calculated using Brownian dynamics, the latter are calculated by TST. Configurational integrals (partition functions) need to be evaluated for the different macrostates, using configurational-biased MC (CBMC). This allows to calculate the potential of mean force felt by a molecule in this macrostate, as a function of the projected end positions. The most probable configuration of a molecule is discovered from such calculations, and it is found that chains prefer to reside largely in extended conformations.

The transition rate constants between two macrostates are calculated in the usual way, described earlier, but a transition from a channel- to an intersection-terminated rate is followed by a placement of the end X_2 using a conditional probability that X_2 lies on the dividing surface in between the two states. The motion of a molecule within a macrostate is tracked by integrating a two-particle (channel-terminated) or one-particle (intersection-terminated) Langevin equation, in which the friction factors are assumed to be sums of factors proportional to the contour lengths in each state. Short-time MD calculations are used to calculate correlation functions for a chain in a macrostate and match the corresponding correlation function based on the BD calculations. This allows to adjust the magnitude of the mobility matrix, without having to perform MD on many systems. The fitting calculations show that friction scales linearly with chain length for chains longer than C_8. The motion is a combination of gliding of one or both ends (BD) and jumping of one end (TST). Using this hierarchical method, the computation time is virtually independent of chain length for long-chain alkanes. From the calculations, it was found that long-chain alkane molecules favor the straight channels, along which diffusion is fastest, and that the self-diffusivity at infinite dilution declines as a function of alkane chain length until about C_8-C_{10}, after which it levels off. The same trend was seen in macroscopic ZLC experiments, although the predictions were much higher (Fig. 46). There was relatively good agreement with MD and available

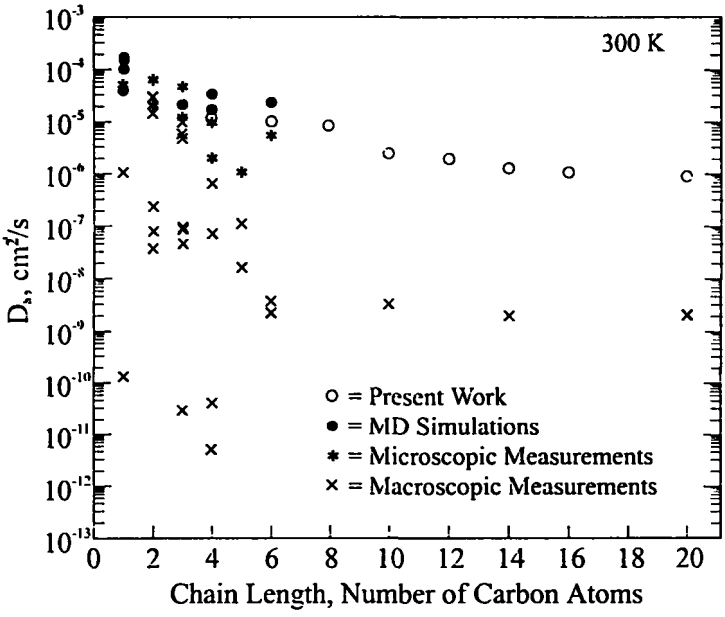

Fig. 46 Self-diffusivities as a function of chain length /265/.

experimental microscopic NMR and QENS values, however, so that this discrepancy may be due to the as yet unclear differences between some results obtained using these two experimental methods. Activation energies for short alkanes are constant and consistent with experiments, while there is a sudden jump between C_8 and C_{10}. This may be rationalized as

follows. Chains longer than C_8 always span at least an intersection region, so that a different diffusion mechanism with a conformational change having a higher activation energy is in operation. Diffusion anisotropy is also more significant for longer-chain alkanes, because of an increase in conformational memory, and decreases with temperature. At low temperatures, long chains prefer to stay in low energy conformations aligned along the straight channels, but at higher temperatures, they move out of these dips to probe all the available pore space. Finally, comparing the importance of Brownian motion and macrostate transition, it was observed that diffusion is almost always controlled by the transitions, especially at higher temperatures, because frictional resistance to motion within a macrostate is low. At lower temperatures (300 K in the simulations), there could be a critical chain length ~C_{40} above which friction dominates, which would imply that the diffusivity again decreases with chain length from this length on. Below the critical length, the transition rates control the total rate and are quite insensitive to chain length. The paper by Maginn et al. /265/ was discussed in some detail here, as it is illustrative for a general hierarchical methodology, employing a combination of different techniques (here BD, TST and short-time MD). Such hierarchical approaches are likely to become more important in the future for the simulation of complex diffusion and reaction problems in zeolites, as is apparent from this review.

Smit et al. /266/ studied diffusion of branched alkanes in silicalite and noticed a clear difference with the behavior of linear alkanes. A linear alkane can move relatively freely through all channels, with a preference for the straight channels for long alkanes, as we have just discussed. The head of a branched alkane, on the other hand, tends to prefer an intersection between a straight and a zig-zag channel. Its diffusion is an activated process, which can be described as hops between intersections. The case of 2-methyl hexane is discussed in more detail. Based on the techniques developed by Bennett /267/ and Chandler /254/, the transition rate is calculated as the product of the probability of finding a molecule at the top of a barrier, and the rate to move from this top to another valley or intersection in this case /42/. Like, e.g., in June et al. /252/ and Snurr et al. /255/, several free energy barriers per channel were found, although the dominating barrier is the one to move out of an intersection through a channel and into another intersection, so this was the one preserved to calculate the diffusivity at infinite dilution from TST. The free energy along the reaction coordinate was calculated using configuration-biased Monte-Carlo (CBMC). Dynamic corrections to account for barrier recrossings were not included and the lattice was assumed to be rigid, but both effects could in principle be included using the method discussed earlier.

As part of a series of papers by Auerbach and co-workers on the detailed study of benzene diffusion in Na-Y, several of which are reviewed in Section 3.2 on dynamic Monte-Carlo, Jousse and Auerbach /268, 269/ used dynamically corrected TST. The incentive for such a study was that the prefactors for the rates were kept constant at some reasonable value in the MC simulations, while recent experiments reveal that their role may be more important than previously anticipated. An unusually broad difference in values between the intra-cage S_{II}-S_{II} and the extra-cage S_{II}-W hops was found by NMR. The fact that benzene is a non-spherical molecule poses special problems to the application of TST, as was discussed by Snurr et al. /255/, who studied benzene diffusion in silicalite. The number of distinct types of sites and paths to consider in the case of Na-Y is much smaller, however, so that Jousse and Auerbach were able to perform both (approximate) TST and exact flux correlation function rate calculations. Because rapid thermalization of benzene is possible, dynamical recrossings and

multisite jumps are expected to only play a minor role. The TST result also depends on the choice of the dividing surface, however, and the dynamical factor is therefore expected to essentially correct for the error in locating this surface. Locating the dividing plane is especially difficult for *W-W* jumps, because its size is very much reduced by the *W-S*$_{II}$ dividing planes. This is confirmed by the results: the TST estimates are very close to the "exact" dynamically corrected results for *S*$_{II}$-*S*$_{II}$, *W-S*$_{II}$ and *S*$_{II}$-*W* jumps, but not for the *W-W* jumps, where TST was found to lead to qualitatively wrong results, because the corresponding minimum energy path is unstable and crosses the one for the *S*$_{II}$-*S*$_{II}$ jump (Fig. 47). Most

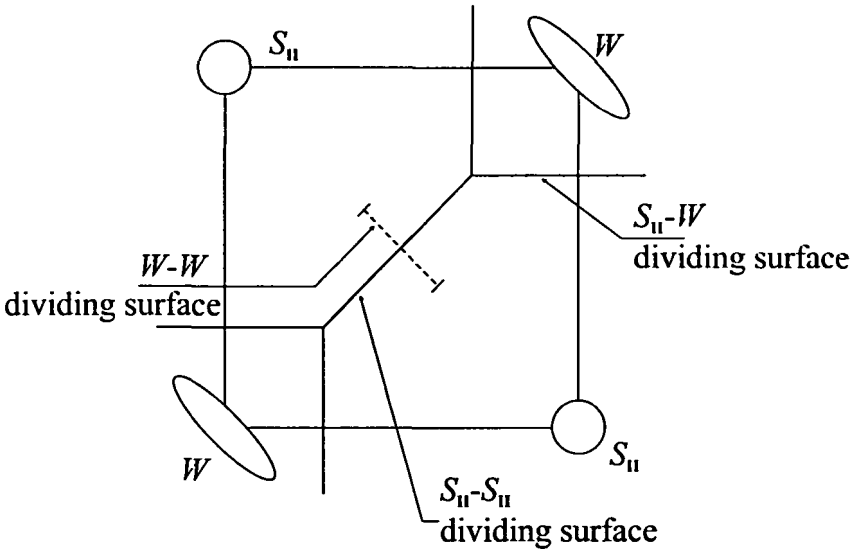

Fig. 47 Sketch of the projection on a plane containing two *S*$_{II}$ and two *W* sites of the dividing surfaces between the *S*$_{II}$ and *W* sites. The dividing surface used to calculate the *W*→*W* rate constant is indicated with dashed lines /268/.

moves out of the dividing surface end up in an *S*$_{II}$ site. Entropy effects disfavor *W-W* moves, so that the minimum energy path is very localized. At infinite dilution, but not at finite loading where *W-W* jumps become more likely due to *S*$_{II}$ blocking, the benzene cage-to-cage rate is dominated by the *S*$_{II}$-*W* jumps, the rate of which was calculated. This work shows that when a good initial guess of the dividing surface can be made, TST estimates the rate constants quite well, but corrections are needed otherwise. When trajectories can relax to several different product sites, TST cannot give an accurate site-to-site rate, only the total rate out of a site. The large difference in prefactors could not be fully accounted for, probably due to the negligence of the internal motions of benzene as well as the lattice vibrations, which are therefore expected to play a major role.

Tunca and Ford /270/ obtained fundamental rate constants for adsorbate motion at nonzero loadings using multidimensional TST. More specifically, the authors focussed on systems where the adsorption of a molecule is not highly localized in a single site, but rather distributed

throughout an uncorrugated cage. A theory was developed in which high-dimensional TST integrals are approximated using exact lower-dimensional information. The evaluation of the resulting integrals is performed with an importance sampling method involving the insertion of a single molecule, thus improving the statistical quality of the results. The theory was applied to the motion of CH_4 and Xe in ZK4. The results showed that hopping rates increase with loading in the cage, which is consisting with experimental trends.

4.3 Conclusions

To simulate diffusion in zeolites there are, as yet, fewer applications of transition-state theory than there are of dynamic Monte-Carlo and molecular dynamics. One reason is the need to accurately determine the potential energy surface, and, in particular, the saddle points corresponding to the transition states. Dynamical corrections to the TST rate constants are frequently necessary. The application of TST is especially difficult for zeolites with a complex unit cell and molecules with a large number of degrees of freedom, although hierarchical methods may help to simplify such problems.

While direct molecular dynamics simulations are now more frequently applied, they are too slow for complex systems. A combination of TST, MD and MC may be the solution to such problems. Also, new, promising theories have appeared in recent years to calculate the transition or hopping rates, such as the multidimensional TST of Tunca and Ford /270/ and the method by Dellago et al. /313/. Also the "hyper-MD" method of Voter /314/, already applied to diffusion on surfaces, can be cited in this context.

5 MAXWELL-STEFAN THEORY

5.1 Introduction

Besides the molecular simulation methods, the (macroscopic) Maxwell-Stefan approach could be extended to surface diffusion phenomena in porous media. Before developing a general theory for zeolite diffusion, a brief review of the Maxwell-Stefan theory for diffusion within a fluid phase will be presented, for which the diffusion theories are well developed (Krishna and Wesselingh /272/, Taylor and Krishna /312/).

As this section contains several frequently used symbols, a separate list of notations is included at the end.

5.2 Diffusion of a binary mixture

Consider diffusion within a binary fluid mixture made up of components 1 and 2. The molar diffusion flux of component 1, with respect to the molar average mixture velocity $\mathbf{u}$, $\mathbf{J}_1$, expressed as moles per square meter per second, can be related to the composition (mole fraction) gradient of component 1, ∇x_1, using Fick's law:

$$\mathbf{J}_1 \equiv c_1(\mathbf{u}_1 - \mathbf{u}) = -c_t D_{12} \nabla x_1 \tag{5.1}$$

In eq. (5.1) D_{12} represents the Fick diffusivity and c_t is the total molar concentration of the mixture. The corresponding relation for component 2 in the mixture is

$$\mathbf{J}_2 \equiv c_2(\mathbf{u}_2 - \mathbf{u}) = -c_t D_{12} \nabla x_2 . \tag{5.2}$$

Only one of the diffusion fluxes is independent because these diffusion fluxes sum to zero

$$\mathbf{J}_1 + \mathbf{J}_2 \equiv 0 \tag{5.3}$$

and there is only one independent composition gradient because the mole fractions sum to unity and the mole fraction gradients sum to zero:

$$x_1 + x_2 = 1; \quad \nabla x_1 + \nabla x_2 \equiv 0 . \tag{5.4}$$

The molar flux $\mathbf{N}_i$ with respect to a laboratory fixed co-ordinate reference frame is given by

$$\mathbf{N}_i \equiv c_i \mathbf{u}_i = c_i x_i \mathbf{u}_i = \mathbf{J}_i + x_i(\mathbf{N}_1 + \mathbf{N}_2) = -c_t D_{12} \nabla x_i + x_i(\mathbf{N}_1 + \mathbf{N}_2) \tag{5.5}$$

There is only one Fick diffusivity D_{12} characterising the binary mixture, which is equal for both components. For a binary mixture exhibiting strong thermodynamic non-ideality the Fick diffusivity D_{12} is a strong function of the composition. This behaviour is illustrated in Fig. 48a for diffusion in a mixture of methanol (1) and n-hexane (2) at a temperature $T = 313.15$ K /271/. We note that the Fick diffusivity D_{12} reduces sharply as the composition approaches a mole fraction of about 0.5. The reason for the "strange" behaviour of D_{12} with composition can be explained when we consider the non-ideal solution thermodynamics and adopt a more fundamental choice of the driving force for diffusion.

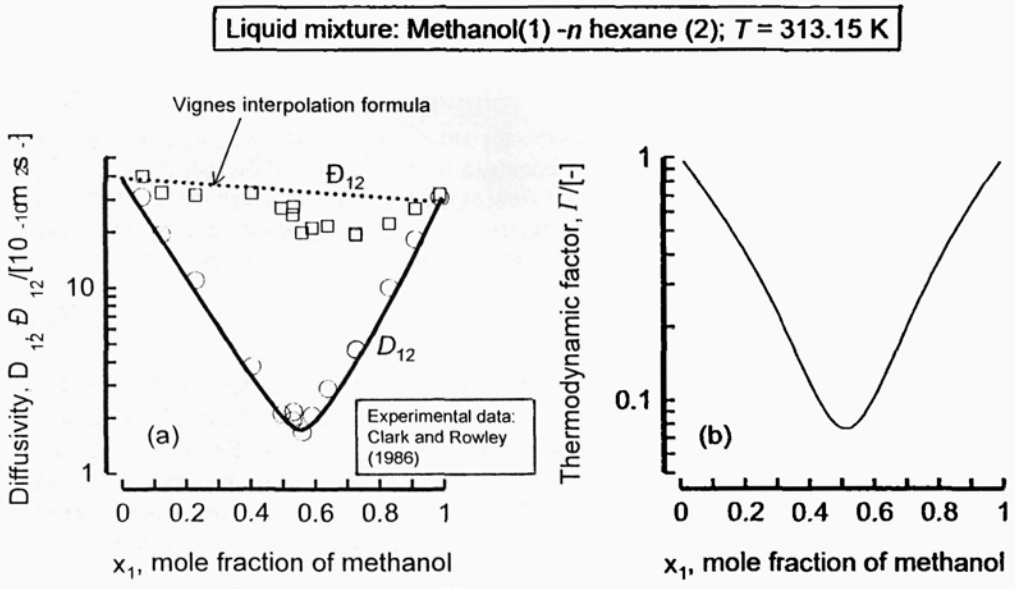

Fig. 48 (a) Experimental data for the Fick and Maxwell-Stefan diffusivity for the system methanol – *n*-hexane. Data from Clark and Rowley /271/. (b) The thermodynamic factor calculated for the methanol – *n*-hexane mixture using the NRTL model.

The proper driving force for diffusion is the gradient of the chemical potential and the more fundamental way to set up the constitutive relations for binary diffusion is to adopt the Maxwell-Stefan diffusion formulation /272/. In this theory we recognise that to affect relative motion between the species 1 and 2 in a fluid mixture we must exert a force on each species. This "driving" force is the chemical potential gradient, $\nabla_{T,p}\mu_1$, determined at constant temperature (T) and pressure (p) conditions. This force is balanced by friction between the diffusing species 1 and 2 in the binary mixture. The friction experienced by species 1 is proportional to the differences in the velocities of diffusion of species 1 and 2, $(\mathbf{u}_1 - \mathbf{u}_2)$, and to the concentration of species 2, which can be taken to be the mole fraction x_2. The force balance on the species 1 takes the form:

$$-\nabla_{T,p}\mu_1 = \frac{RT}{Đ_{12}} x_2(\mathbf{u}_1 - \mathbf{u}_2) \tag{5.6}$$

The term ($RT/Đ_{12}$) on the right hand side of eq. (5.6) may be interpreted to be the drag coefficient. With this definition, the Maxwell-Stefan diffusivity $Đ_{12}$ has the units [$m^2 s^{-1}$] and the physical significance of an *inverse* drag coefficient.

Multiplying both sides of eq. (5.6) by x_1 and introducing the molar fluxes N_i (cf. eq. (5.5)) we obtain

$$-\frac{x_1}{RT}\nabla_{T,p}\mu_1 = \frac{x_2\mathbf{N}_1 - x_1\mathbf{N}_2}{c_t Đ_{12}} \tag{5.7}$$

Equation (5.7) can be re-written in terms of the diffusion flux $\mathbf{J}_1$:

$$\mathbf{J}_1 \equiv \mathbf{N}_1 - x_1(\mathbf{N}_1 + \mathbf{N}_2) = c_1(\mathbf{u}_1 - \mathbf{u}) = -c_t Đ_{12}\left(\frac{x_1}{RT}\nabla_{T,p}\mu_1\right) \tag{5.8}$$

Comparing Fick's law, eq. (5.1), with eq. (5.8) shows that the basic difference between the Fick and Maxwell-Stefan formulations lies in the choice of the driving force for diffusion. For calculation purposes it is convenient to introduce the activity coefficient γ_1 and express this in the driving force on the right hand side of eq. (5.8) in terms of the composition gradient:

$$\frac{x_1}{RT}\nabla_{T,p}\mu_1 = \Gamma\nabla x_1; \quad \Gamma \equiv x_1\frac{\partial \ln(\gamma_1 x_1)}{\partial x_1} \tag{5.9}$$

where Γ is the thermodynamic correction factor portraying the non-ideal behaviour. For highly non-ideal mixtures the thermodynamic factor Γ is usually a strong function of the mixture composition. For the system methanol (1) – n-hexane (2), the calculation of the thermo-dynamic factor Γ is shown in Fig. 48 b. Comparison of the Figures 48 a and b shows that the strange behaviour of the Fick D_{12} is entirely to be ascribed to the strong composition dependence of Γ. Comparing eqs (5.1), (5.8) and (5.9) we can inter-relate the Fick and Maxwell-Stefan diffusivities as follows

$$D_{12} = Đ_{12}\Gamma \tag{5.10}$$

Calculation of the Maxwell-Stefan diffusivity $Đ_{12}$ for the system methanol – n-hexane using eq. (5.8) shows that $Đ_{12}$ is much less dependent on composition than the Fick D_{12}; compare the circles (D_{12}) and squares ($Đ_{12}$) in Fig. 48 a. The dotted line in Fig. 48 a represents a

logarithmic interpolation formula between the infinite dilution values of the diffusivities:

$$Đ_{12} = \left(Đ_{12}^{(x_1 \to 1)}\right)^{x_1} \left(Đ_{12}^{(x_1 \to 0)}\right)^{1-x_1} \tag{5.10a}$$

Eq. (5.10a) is due to Vignes /273/.

The example illustrated by methanol – n-hexane underlines the importance of using the proper driving forces to describe diffusion in non-ideal mixtures. The Fick diffusivity is a conglomerate of two separate concepts: drag effects and thermodynamic non-ideality effects. For gaseous mixtures at low to moderate pressures and for thermodynamically ideal liquid mixtures, the thermodynamic factor $\Gamma = 1$ and, therefore, the Fick and Maxwell-Stefan diffusivities are identical to each other. Furthermore, for thermodynamically ideal mixtures D_{12} ($\approx Đ_{12}$) is independent of composition x_1.

5.3 Generalisation to multicomponent mixtures

The Maxwell-Stefan relations (5.7) can be extended for a mixture containing n components by adding the various frictional contributions as follows

$$-\frac{x_i}{RT}\nabla_T \mu_i = \sum_{\substack{j=1 \\ j\neq i}}^{n} \frac{x_j \mathbf{N}_i - x_i \mathbf{N}_j}{c_t Đ_{ij}} = \sum_{\substack{j=1 \\ j\neq i}}^{n} \frac{x_j \mathbf{J}_i - x_i \mathbf{J}_j}{c_t Đ_{ij}}; \quad i = 1,2,\ldots n \tag{5.11}$$

The second equality holds irrespective of the reference velocity frame **u** chosen for the diffusion process. It is convenient to formulate eq. (5.11) in matrix notation by defining the matrices:
(i)(n-1) × (n-1) dimensional square matrix of thermodynamic factors $[\Gamma]$ defined by

$$\frac{x_i}{RT}\nabla_T \mu_i = \sum_{j=1}^{n-1} \Gamma_{ij} \nabla x_j; \quad \Gamma_{ij} = x_i \frac{\partial \ln\left(\gamma_i x_i\right)}{\partial x_j}; \quad i,j = 1,2\ldots n-1 \tag{5.12}$$

(ii) (n-1) ×(n-1) dimensional square matrix of drag coefficients B_{ij} (remember that the Maxwell-Stefan diffusivities have the significance of inverse drag coefficients)

$$B_{ii} = \frac{x_i}{Đ_{in}} + \sum_{\substack{k=1 \\ k\neq i}}^{n} \frac{x_k}{Đ_{ik}}; \quad B_{ij(i\neq j)} = -x_i\left(\frac{1}{Đ_{ij}} - \frac{1}{Đ_{in}}\right); \quad i,j = 1,2\ldots n-1 \tag{5.13}$$

(iii) (n-1) dimensional column matrix of diffusion fluxes:

$$\mathbf{J}_i \equiv c_t\left(\mathbf{u}_i - \mathbf{u}\right); \quad i = 1,2\ldots n-1 \tag{5.14}$$

With the above definitions, eq. (5.11) can be cast into a form that is the (n-1) dimensional matrix analogue of eq. (5.8)

$$(\mathbf{J}) = -c_t[B]^{-1}[\Gamma](\nabla x) \tag{5.15}$$

It is common to define a matrix of Fick diffusivities $[D]$ as (n-1) dimensional matrix analogue of eq. (5.1):

$$(\mathbf{J}) = -c_t[D](\nabla x) \tag{5.16}$$

and therefore we note the following matrix generalisation of eq. (10):

$$[D] = [B]^{-1}[\Gamma] \tag{5.17}$$

For the general multicomponent mixture it is difficult to ascribe simple physical interpretations to the elements of the Fick matrix $[D]$. While the diagonal elements of $[D]$ are positive definite, the off-diagonal elements can be of either sign.

5.4 The Maxwell-Stefan theory for diffusion in zeolites; points of departure from fluid phase diffusion

When applying the above set of equations for describing diffusion within a zeolite, there are several points where we depart from the conventional treatment of bulk fluid phase diffusion.
(i) Firstly, when we consider movement of species within a zeolite structure, it is important to realise that we are talking about movement of *sorbed* species. Diffusion and sorption processes within zeolites are closely inter-twined.
(ii) Secondly, when describing the diffusion of a mixture of n species within a zeolite, the "zeolite matrix" is treated as an additional (pseudo), $(n+1)$th component, in the mixture. So, when we speak, say, about diffusion of benzene (component 1) within silicalite we are in fact considering diffusion in a binary mixture made up of benzene (component 1) and silicalite (pseudo-component 2).
(iii) The third point concerns the concentration measures. Commonly used concentration measures for sorption are: (1) mol of sorbate (diffusant) per kg of zeolite, q_i, and (2) molecules of sorbate per unit cell of zeolite, Θ_i. Corresponding to these two concentration measures we could define the molar flux $\mathbf{N}_i$ in two different ways. The first alternative is in terms of moles of sorbate diffusing per square meter per second:

$$\mathbf{N}_i \equiv \rho q_i \mathbf{u}_i; \quad i = 1,2,...n-1, \tag{5.18}$$

where ρ is the zeolite matrix density expressed in kg per m^3. The zeolite matrix density serves as an analogue to the total mixture concentration used in eq. (5.1). The second alternative is to define $\mathbf{N}_i$ in terms of molecules transported per square meter per second

$$\mathbf{N}_i \equiv \rho \Theta_i \mathbf{u}_i; \quad i = 1,2,...n-1, \tag{5.19}$$

in which case ρ is the zeolite matrix density expressed as unit cells per m^3. Without loss of generality we proceed further with the choice of Θ_i as the concentration measure; relations in terms q_i can be written down in an analogous manner.
(iv) The fourth point of departure from bulk fluid phase diffusion concerns the choice of the reference frame for defining the diffusion fluxes $\mathbf{J}_i$. In almost all standard treatments of diffusion in zeolites /11, 274/, the reference velocity frame is *tacitly* chosen as one which moves with respect to the zeolite matrix, taken to be the $(n+1)$th component. The diffusion fluxes are therefore defined as

$$\mathbf{J}_i \equiv \rho \Theta_i (\mathbf{u}_i - \mathbf{u}_{n+1}); \quad i = 1,2,...n \tag{5.20}$$

In most applications of interest to chemical engineers the zeolite matrix can be considered to be stationary, i.e.

$$\mathbf{u}_{n+1} \equiv 0 \tag{5.21}$$

Equation (5.21) implies that molar flux $\mathbf{N}_i$ equals the diffusion flux $\mathbf{J}_i$:

$$\mathbf{J}_i \equiv \mathbf{N}_i \equiv \rho \Theta_i \mathbf{u}_i \tag{5.22}$$

(v) The fifth point concerns the choice of a composition measure analogous to the mole fraction for bulk fluid phases. The obvious choice is the fractional occupancy θ_i of the sorbate within the zeolite matrix, defined as

$$\theta_i \equiv \Theta_i / \Theta_{sat} = q_i / q_{sat}; \quad i = 1,2,...n \tag{5.23}$$

where Θ_{sat} and q_{sat} are the saturation loadings.

5.5 Diffusion of a single component in a zeolite

Let us first consider the simple case of diffusion of a single component (1) within a zeolite (considered to be pseudo-species 2). Fick's first law is usually written in the following form:

$$\mathbf{N}_1 = -\rho D_1 \nabla \Theta_1 \tag{5.24}$$

or in terms of the occupancy gradients

$$\mathbf{N}_1 = -\rho \Theta_{sat} D_1 \nabla \theta_1 \tag{5.25}$$

Equation (5.24), or (5.25) defines the Fick diffusivity D_1. Note that we use only one subscript (1) in order to distinguish the single component diffusivity within a zeolite from the bulk fluid phase diffusivity D_{12} in a binary mixture (cf. Eq. (5.1)). The Fick diffusivity D_1 is also called the *transport diffusivity* in the zeolite literature /11, 274/.

The Maxwell-Stefan formulation of single component diffusion, analogous to eq. (5.8), is

$$\mathbf{N}_1 = -\rho \Theta_{sat} Đ_1 \left(\frac{\theta_1}{RT} \nabla_{T,p} \mu_1 \right) \tag{5.26}$$

where μ_1 is the chemical potential of the sorbed species 1. Assuming equilibrium between the sorbed species and the bulk fluid phase we have the following relationship for the chemical potential μ_1

$$\mu_1 = \mu_1^0 + RT \ln(f_1) \tag{5.27}$$

where μ_1^0 is the chemical potential in the chosen standard state and f_1 is the fugacity. For not too high system pressures the component partial pressure, p_1, can be used in place of the component fugacity, f_1, *i.e.*, $f_1 \approx p_1$. The chemical potential gradients may be expressed in terms of the gradients of the occupancy, $\nabla\theta_1$, in a manner analogous to eq. (5.9):

$$\frac{1}{RT} \nabla \mu_1 = \frac{1}{\theta_1} \Gamma \nabla \theta_1; \quad \Gamma \equiv \theta_1 \frac{\partial \ln p_1}{\partial \theta_1} \tag{5.28}$$

where Γ is the thermodynamic correction factor. The Fick and Maxwell-Stefan diffusivities are therefore inter-related:

$$D_1 = Đ_1 \Gamma; \quad Đ_1 = \frac{D_1}{\Gamma} \tag{5.29}$$

In the zeolite diffusion literature the Maxwell-Stefan diffusivity $Đ_1$ is also called the "corrected" diffusivity and the thermodynamic correction factor Γ is called the Darken correction factor /275, 11, 274/, compare with eq. (1.3).

Consider the sorption data for benzene in silicalite-1 /276/ at a temperature $T = 343$ K; cf. Fig. 49 a. The experimental data are reasonably well represented by the Langmuir isotherm

$$\Theta_i = \frac{\Theta_{sat} b_i p_i}{1 + b_i p_i}; \quad \theta_i = \frac{b_i p_i}{1 + b_i p_i} \tag{5.30}$$

where the saturation capacity Θ_{sat} is four molecules per unit cell of silicalite and the Langmuir constant $b_1 = 6 \times 10^{-4}$ Pa^{-1}. The thermodynamic correction factor can be determined from eq. (5.28)

$$\Gamma = \frac{1}{1 - \Theta_i / \Theta_{sat}} = \frac{1}{1 - \theta_i} \tag{5.31}$$

Figure 49 b shows the variation of the thermodynamic factor with molecular loading. Notice the sharp increase in Γ as the Θ_i approaches the saturation capacity, Θ_{sat} (= 4). For bulk fluid phase diffusion (cf. Fig. 48) we had noted that the Fick diffusivity parallels the trend of Γ. The same situation holds for the Fick diffusivity data for benzene in silicalite-1 measured by Shah et al. /277/. As seen in Fig. 49 c D_i increases sharply as Θ_i approaches the saturation capacity, Θ_{sat} (= 4). The Maxwell-Stefan diffusivity $Đ_i$ displays a much smaller variation with sorbate loading; see the square symbols in Fig. 49 c.

For adsorption of benzene, *p*-xylene, *n*-hexane and *iso*-butane in silicalite several experimental studies have shown that the isotherm exhibits inflection behaviour /276–281/. The inflection in the isotherm is due to the preferential location of molecules at certain sites in the silicalite structure. There is some direct experimental evidence using FT-Raman spectroscopy to show the preferential siting of p-xylene at the channel intersections within the silicalite structure /282/. Broadly speaking, we can identify two distinct adsorption sites: (1) Site A, which represents the intersections between the straight channels and the zig-zag channels, and (2) Site B, which represents the channel interiors; see Fig. 50. The inflection behaviour is caused because these molecules prefer to occupy the intersections (Site A). However, at a loading, Θ_i of 4 molecules per unit cell (corresponding to 0.6935 mol/kg of silicalite) the intersections are all fully occupied. To obtain loadings higher than 4, these molecules must seek residence in the channel interiors, which is energetically more demanding. This leads to an inflection in the isotherm. Figure 51a shows the isotherm data for benzene in silicalite-1 at $T = 303$ K; the inflection at $\Theta = 4$ molecules per unit cell is evident.

The dual-site Langmuir (DSL) model:

$$\Theta_i = \frac{\Theta_{sat,A} b_{i,A} p_i}{1 + b_{i,A} p_i} + \frac{\Theta_{sat,B} b_{i,B} p_i}{1 + b_{i,B} p_i} = \frac{\left(\Theta_{sat,A} b_{i,A} + \Theta_{sat,B} b_{i,B}\right) p_i + \left(\Theta_{sat,A} + \Theta_{sat,B}\right) b_{i,A} b_{i,B} p_i^2}{1 + \left(b_{i,A} + b_{i,B}\right) p_i + b_{i,A} b_{i,B} p_i^2} \tag{5.32}$$

provides a good description for systems showing isotherm inflection /281, 283, 284/; see Fig. 51a. The thermodynamic factor can be determined by analytic differentiation of eq. (5.32); the result is

Fig. 49 (a) Pure component isotherms for sorption of benzene on silicalite-1 at a temperature of 343 K. Experimental data from Guo et al. /276/. The Langmuir model parameters are $\Theta_{sat} = 4$, $b_{1,A} = 6\times10^{-4}$ Pa^{-1}. (b) The thermodynamic correction factor calculated using the Langmuir model. (c) Fick and Maxwell-Stefan diffusivity data for benzene in silicalite-1 at 343 K. Data from Shah et al. /277/.

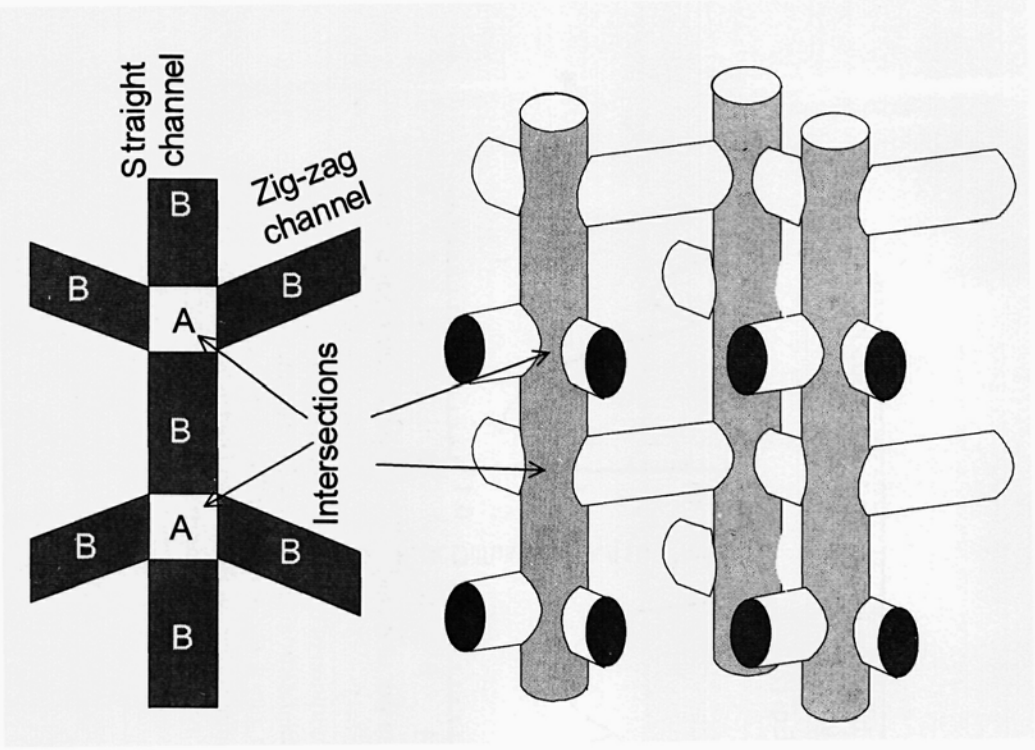

Fig. 50 Sorption sites within silicalite.

$$\Gamma = \left[\frac{\left[1+(b_{1,A}+b_{1,B})p_1+b_{1,A}b_{1,B}p_1^2\right]^2}{1+(b_{1,A}+b_{1,B})p_1+b_{1,A}b_{1,B}p_1^2\left[\left(\Theta_{sat,A}b_{1,A}+\Theta_{sat,B}b_{1,B}\right)+\left(\Theta_{sat,A}+\Theta_{sat,B}\right)2b_{1,A}b_{1,B}p_1\right]}\right.$$
$$\left.-\left[\left(\Theta_{sat,A}b_{1,A}+\Theta_{sat,B}b_{1,B}\right)p_1+\left(\Theta_{sat,A}+\Theta_{sat,B}\right)b_{1,A}b_{1,B}p_1^2\right]\left[\left(b_{1,A}+b_{1,B}\right)+2b_{1,A}b_{1,B}p_1\right]\right]\frac{\Theta_1}{p_1} \quad (5.33)$$

This correction factor shows two extrema: a maximum at the inflection point $\Theta_{sat,A} = 4$ and a minimum at a loading $\Theta_{sat,A} < \Theta_1 < \Theta_{sat}$ ($= \Theta_{sat,A} + \Theta_{sat,B}$). This behaviour is illustrated for adsorption of benzene on silicalite at temperatures of 303 K; see Fig. 51b. Since the Fick diffusivity is proportional to the thermodynamic factor, it can be expected to also exhibit two extrema. This is indeed verified by the experimental data of Shah et al. /277/; see Fig. 51c.

Vlugt et al. /285/ used Configurational-Bias Monte Carlo (CBMC) techniques to determine the sorption isotherms of linear and 2-methyl alkanes in silicalite-1 at 300 K; these isotherms are shown in Fig. 52. It is interesting to note that all branched alkanes exhibit an inflection at $\Theta_{sat,A} = 4$. Linear alkanes with six or more C atoms also show inflection behaviour. The thermodynamic correction factors, calculated from eq. (5.33), for the linear and branched alkanes are shown in Fig. 53. Since the Fick diffusivity D_1 is expected to follow the trend in Γ

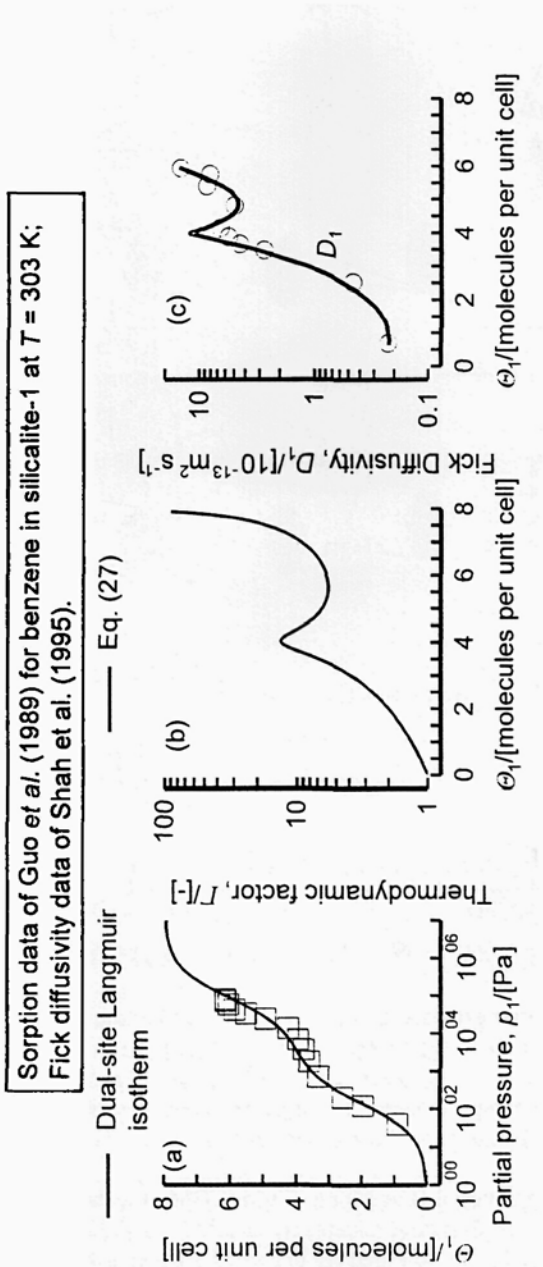

Fig. 51 (a) Pure component isotherms for sorption of benzene on silicalite-1 at a temperature of 303 K. Experimental data from Guo et al. /276/. The dual-site Langmuir model parameters are $\Theta_{sat,A} = 4$, $\Theta_{sat,B} = 4$, $b_{1,A} = 7\times10^{-5}$ Pa^{-1}, $b_{1,B} = 1.2\times10^{-5}$ Pa^{-1}. (b) The thermodynamic correction factor calculated using the Langmuir model. (c) Fick diffusivity data for benzene in silicalite-1 at 303 K. Data from Shah et al. /277/.

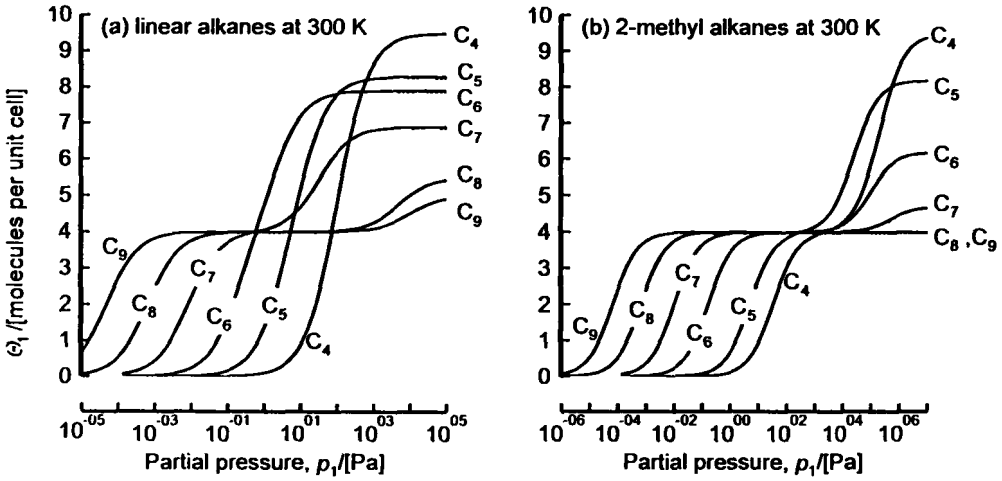

Fig. 52 (a) Pure component isotherms for linear alkanes in silicalite-1 at 300 K. The isotherms were calculated using Configurational-Bias Monte Carlo techniques by Vlugt et al. /285/. (b) Pure component isotherms for 2-methyl alkanes in silicalite-1 at 300 K. The isotherms were calculated using Configurational-Bias Monte Carlo techniques by Vlugt et al. /285/.

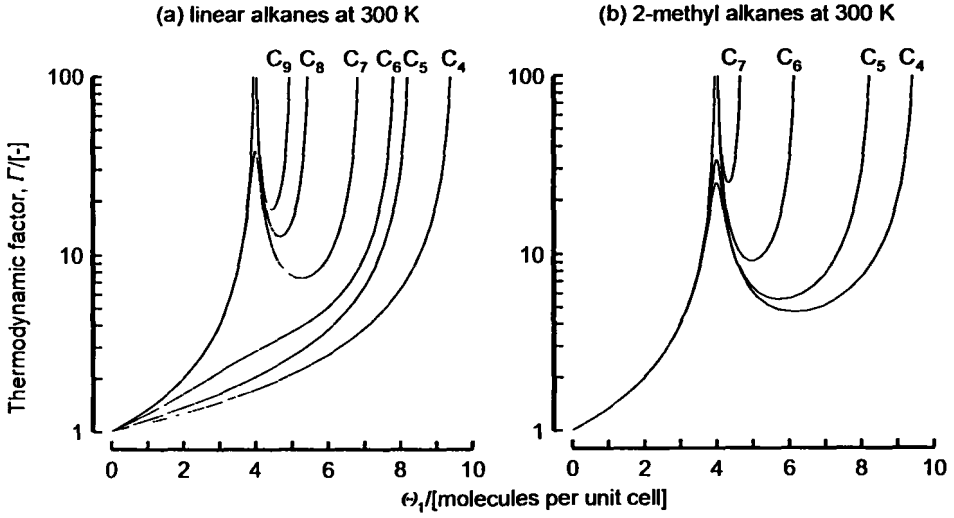

Fig. 53 (a) Thermodynamic factor for linear alkanes in silicalite-1 at 300 K calculated using the Dual-site Langmuir (DSL) model, eq. (5.32) from the isotherms shown in Fig. 52 (a). (b) Thermodynamic factor for 2-methyl alkanes in silicalite-1 at 300 K calculated using the Dual-site Langmuir (DSL) model, eq. (5.33) from the isotherms shown in Fig. 52(b).

we would expect to see striking differences between the occupancy dependency of the Fick diffusivities of say n-hexane and its isomer 2-methyl pentane as a function of the molecular loading. It would be most illuminating to obtain experimental confirmation of this prediction.

A three-site model for sorption of aromatics on ZSM-5 has been proposed by Rudzinski et al. /278/ in order to account for two inflection points observed under certain temperature conditions. The consequences for diffusion can be expected to be interesting but there is no experimental evidence in the literature.

5.6 The Maxwell-Stefan diffusivity

Mechanistically, the Maxwell-Stefan diffusivity $Đ_i$ may be related to the displacement of the adsorbed molecular species, λ, and the jump frequency, ν, which in general can be expected to be dependent on the total coverage /209, 198, 199, 202, 280/.

$$Đ_i = \frac{1}{z}\lambda^2 \nu \tag{5.34}$$

where z represent the number of nearest neighbour sites. The jump frequency ν can be expected to decrease with occupancy. If we assume that a molecule can migrate from one site to another only when the receiving site is vacant /275, 202/, the chance that this will occur will be a function of the fraction of unoccupied sites. A general form of the Maxwell-Stefan diffusion equation is therefore

$$Đ_i = Đ_i(0) f(1-\theta_i), \tag{5.35}$$

where $Đ_i$ (0) represents the Maxwell-Stefan diffusivity in the limit of zero loading and $f(1-\theta_i)$ is some function of the fraction of unoccupied sites.

The simplest model for the dependence of the Maxwell-Stefan diffusivity $Đ_i$ with occupancy is that it is independent of molecular loading within the zeolite.

$$Đ_i = Đ_i(0). \tag{5.36}$$

This is indeed found to be true in several cases /11/. As illustration of this behaviour see Fig. 54 a for diffusion of n-heptane in 5A (data from Ruthven and Doetsch /287/). However, in other cases $Đ_i$ decreases with increasing loading within the zeolite; see data in Fig. 54 b for diffusion of n-heptane in 13X (data from Ruthven and Doetsch /287/). It appears that increased occupancy leads to a hindering effect. The experimental data of Ruthven and Doetsch /287/ for n-heptane in 13X appears to follow a simple relationship

$$Đ_i = Đ_i(0)\left(1-\frac{\Theta_i}{\Theta_{sat}}\right)^8 = Đ_i(0)(1-\theta_i)^8, \tag{5.37}$$

where we have taken $\Theta_{sat} = 4$ molecules per unit cage. Figure 55 compares eq. (5.37) with the experimental data of Ruthven and Doetsch /287/. we see that the agreement is very good. The value of the exponent 8 can perhaps be interpreted as the number of nearest neighbour sites. The exponent in eq. (5.37) will therefore dependent on the particular molecule and the specified zeolite structure.

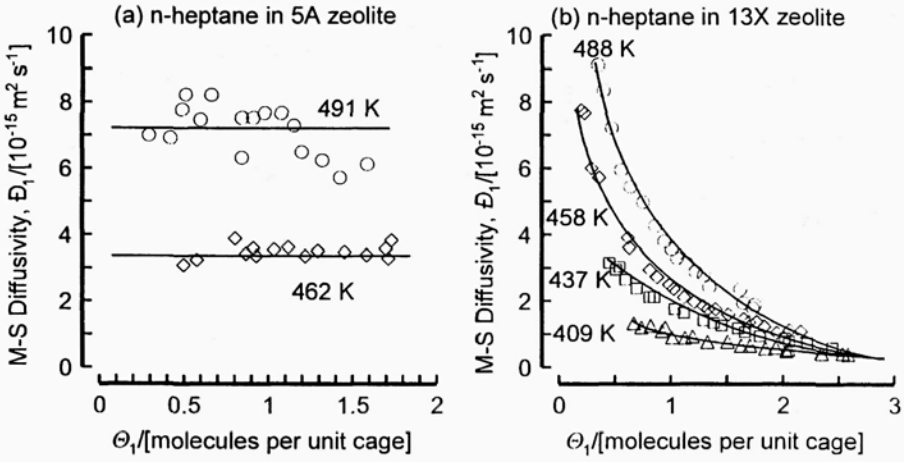

Fig. 54 (a) Maxwell-Stefan diffusivity data for n-heptane in 5A zeolite as a function of molecular loading. Data from Ruthven and Doetsch /287/. (a) Maxwell-Stefan diffusivity data for n-heptane in 13X zeolite as a function of molecular loading. Data from Ruthven and Doetsch /287/.

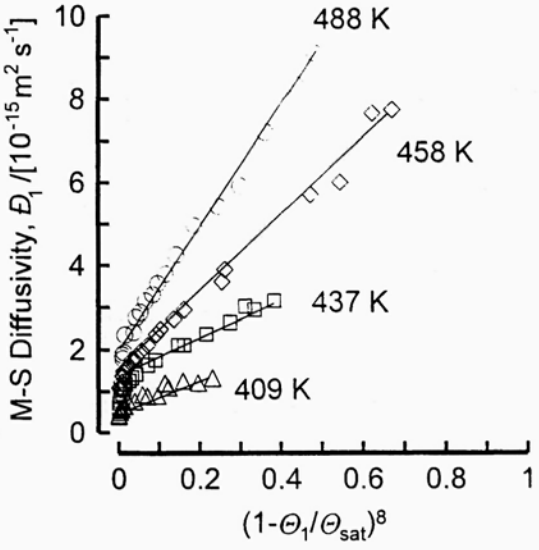

Fig. 55 Re-plotting of the data in Fig. 54 (b) for Maxwell-Stefan diffusivity for n-heptane in 13X zeolite in order to test the validity of the model proposed in eq. (5.37).

Diffusion within a zeolite structure is an activated process and this is evidenced by the fact that the Maxwell-Stefan diffusivity follows an Arrhenius temperature dependence. Figure 56 shows some experimental data to demonstrate the validity of the Arrhenius dependence.

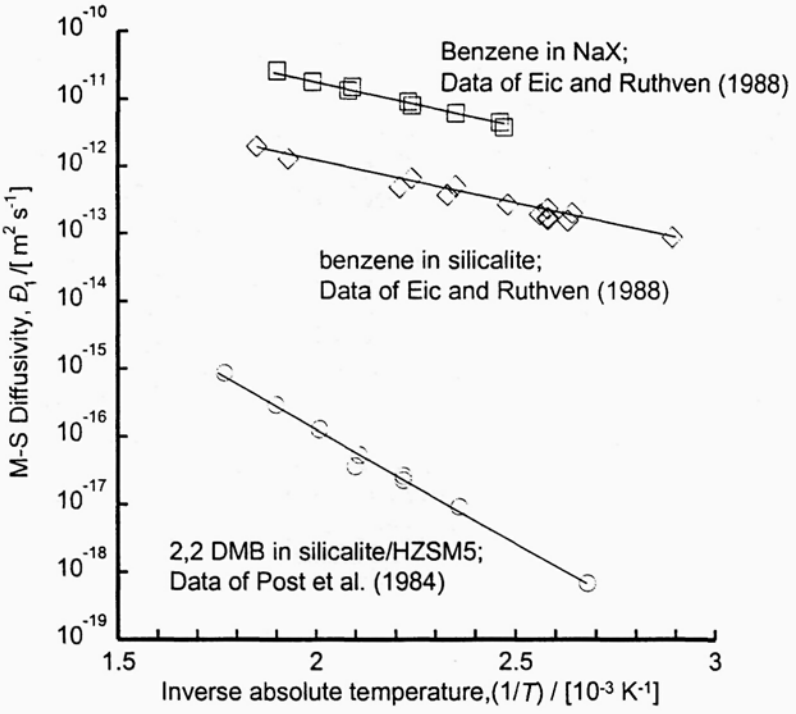

Fig. 56 **Arrhenius plot for the Maxwell-Stefan diffusivity. Various data sources cited in the review by Ruthven and Post /315/.**

5.7 Diffusion of multicomponent mixtures within a zeolite

In order to extend the analysis to two or more components diffusing within a zeolite, we draw inspiration from the Maxwell-Stefan equations (5.11), developed for bulk fluid mixtures. In writing the appropriate equations for diffusion of n components within a zeolite we treat the zeolite itself as species $(n+1)$ and consider the fractional occupancies to be the analogue of the mole fractions. So, eq. (5.11) modifies to

$$-\rho\frac{\theta_i}{RT}\nabla_T\mu_i=\sum_{\substack{j=1\\ j\neq i}}^{n}\frac{\theta_j\mathbf{N}_i-\theta_i\mathbf{N}_j}{\Theta_{sat}Đ_{ij}}+\frac{\theta_{n+1}\mathbf{N}_i}{\Theta_{sat}Đ_{i,n+1}};\quad i=1,2,\ldots n. \tag{5.38}$$

Since the occupancy of the zeolite structure is undefined, it is conventional to define Maxwell-Stefan diffusivities of species i in the zeolite, $Đ_i$ as /272/

$$Đ_i\equiv\frac{Đ_{i,n+1}}{\theta_{n+1}};\quad i=1,2..n \tag{5.39}$$

and with this definition eq. (5.38) is modified to

$$-\rho\frac{\theta_i}{RT}\nabla_T\mu_i=\sum_{\substack{j=1\\ j\neq i}}^{n}\frac{\theta_j\mathbf{N}_i-\theta_i\mathbf{N}_j}{\Theta_{sat}Đ_{ij}}+\frac{\mathbf{N}_i}{\Theta_{sat}Đ_i};\quad i=1,2,\ldots n\,. \tag{5.40}$$

In the Maxwell-Stefan formulation for zeolite diffusion, eq. (5.40), we have to reckon in general with two types of Maxwell-Stefan diffusivities: $Đ_{ij}$ and $Đ_i$. The $Đ_i$ are the same diffusivites as encountered earlier when we considered single component diffusion. Mixture diffusion introduces an additional complication due to sorbate-sorbate interactions. This interaction is embodied in the coefficients $Đ_{ij}$. We can consider this coefficient as representing the facility for counter-exchange, *i.e.* at a sorption site the sorbed species *j* is replaced by the species *i*. The net effect of this counter-exchange is a slowing down of a faster moving species due to interactions with a species of lower mobility. Also, a species of lower mobility is accelerated by interactions with another species of higher mobility. In the foregoing discussions we view the mobility as reflected in the coefficients $Đ_i$. The two types of Maxwell-Stefan diffusivities are portrayed in Fig. 57. In the inset to Fig. 57 we portray $Đ_{12}$ as representing the ease with which species 1 is replaced by species 2.

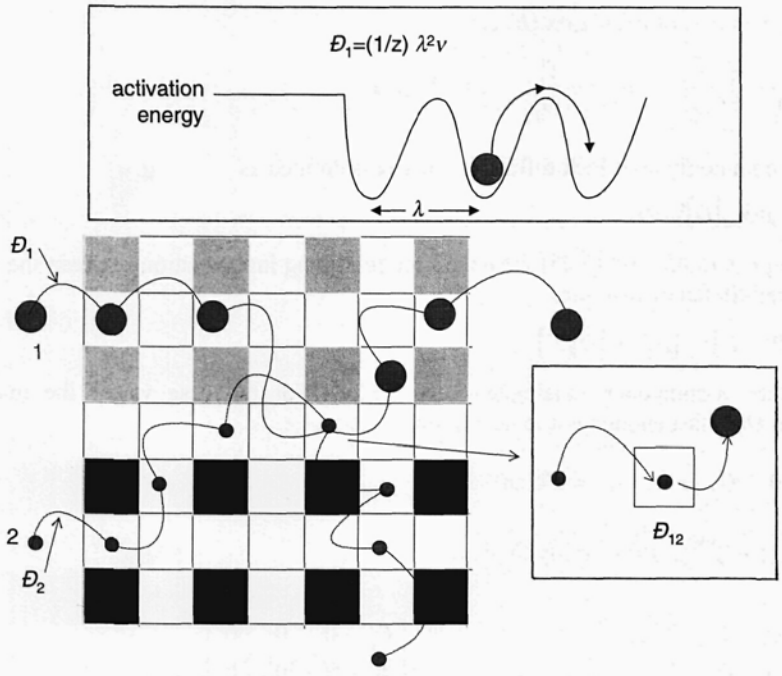

Fig. 57 Pictorial representation of the Maxwell-Stefan diffusivities.

There are no fundamental models as yet to predict the counter-exchange coefficient $Đ_{ij}$. A procedure for the estimation of the counter-sorption diffusivity has been suggested by Krishna /288/ based on the generalisation of Vignes /273/ relationship for diffusion in bulk liquid mixtures (cf. eq. (5.10a))

$$Đ_{ij} = \left[Đ_i\right]^{\theta_i/(\theta_i+\theta_j)}\left[Đ_j\right]^{\theta_j/(\theta_i+\theta_j)}, \tag{5.41}$$

which is essentially a logarithmic interpolation formula between the values of $Đ_i$ and $Đ_j$. We will seek validation of eq. (5.41) a little later in this review. It cannot be overstressed that the important advantage of the Maxwell-Stefan formulation is that the mixture diffusion behaviour can be estimated on the basis of information on the mobilities of the pure components, $Đ_i$ (i = 1,2,...n).

The chemical potential gradients in eq. (5.40) may be expressed in terms of the gradients of the occupancies by introduction of the matrix of thermodynamic factors $[\Gamma]$

$$\frac{1}{RT}\nabla\mu_i = \frac{1}{\theta_i}\sum_{j=1}^{n}\Gamma_{ij}\nabla\theta_j; \quad \Gamma_{ij} \equiv \theta_i\frac{\partial \ln p_i}{\partial\theta_j} \equiv \Theta_i\frac{\partial \ln p_i}{\partial\Theta_j}; \quad i,j = 1,2\ldots n. \tag{5.42}$$

Combining eqs (5.38) and (5.42) we can write down an explicit expression for the fluxes N_i using n-dimensional matrix notation

$$(\mathbf{N}) = -\rho\Theta_{sat}[B]^{-1}[\Gamma]\nabla(\theta) \tag{5.43}$$

where the elements of the matrix $[B]$ are

$$B_{ii} = \frac{1}{Đ_i} + \sum_{\substack{j=1\\ j\neq i}}^{n}\frac{\theta_j}{Đ_{ij}}; \quad B_{ij} = -\frac{\theta_i}{Đ_{ij}}; \quad i,j = 1,2....n. \tag{5.44}$$

The more commonly used Fick diffusivity matrix is defined as

$$(\mathbf{N}) = -\rho\Theta_{sat}[D]\nabla(\theta). \tag{5.45}$$

Comparing eqs (5.43) and (5.45) we obtain the following inter-relation between the Fick and the Maxwell-Stefan diffusivities

$$[D] = [B]^{-1}[\Gamma]; \quad [B]^{-1} = [D][\Gamma]^{-1}, \tag{5.46}$$

which is the n-component analogue of eq. (5.29). For the case where the interchange coefficient $Đ_{ij}$ is fast enough not to be a limiting factor, i.e.

$$\frac{1}{Đ_{ij}} \to 0; \quad Đ_{ij} \to \infty; \quad i,j = 1,2,...n \tag{5.47}$$

equations (5.43) – (5.46) simplify to yield

$$[D] = \begin{bmatrix} Đ_1 & 0 & 0 & 0 \\ 0 & Đ_2 & 0 & 0 \\ 0 & 0 & \ddots & 0 \\ 0 & 0 & 0 & Đ_n \end{bmatrix}[\Gamma]; \quad (\mathbf{N}) = -\rho\Theta_{sat}\begin{bmatrix} Đ_1 & 0 & 0 & 0 \\ 0 & Đ_2 & 0 & 0 \\ 0 & 0 & \ddots & 0 \\ 0 & 0 & 0 & Đ_n \end{bmatrix}[\Gamma]\nabla(\theta). \tag{5.48}$$

The thermodynamid correction factor matrix $[\Gamma]$ is generally non-diagonal and has a significant influence on the diffusion behaviour of mixtures. In the following, we shall illustrate several interesting features of this influence by considering a few special cases.

5.8 Diffusion of two components in a zeolite, following a Langmuir isotherm

For a binary mixture ($n = 2$) for which each component follows the Langmuir model, the mixture isotherm can be estimated from

$$\theta_i = \frac{\Theta_i}{\Theta_{sat}} = \frac{b_i p_i}{1 + b_1 p_1 + b_2 p_2}; \quad i = 1,2 \tag{5.49}$$

the matrix of thermodynamic correction factors can be obtained as

$$[\Gamma] = \begin{bmatrix} \Gamma_{11} & \Gamma_{12} \\ \Gamma_{21} & \Gamma_{22} \end{bmatrix} = \frac{\begin{bmatrix} 1-\theta_2 & \theta_1 \\ \theta_2 & 1-\theta_1 \end{bmatrix}}{1-\theta_1-\theta_2}. \tag{5.50}$$

The inverse of the drag coefficient matrix can be simplified to the form

$$[B]^{-1} = \frac{\begin{bmatrix} Đ_1 & 0 \\ 0 & Đ_2 \end{bmatrix}}{\left(1+\theta_1\frac{Đ_2}{Đ_{12}}+\theta_2\frac{Đ_1}{Đ_{12}}\right)} \begin{bmatrix} \left(1+\theta_1\frac{Đ_2}{Đ_{12}}\right) & \theta_1\frac{Đ_2}{Đ_{12}} \\ \theta_2\frac{Đ_1}{Đ_{12}} & \left(1+\theta_2\frac{Đ_1}{Đ_{12}}\right) \end{bmatrix} \tag{5.51}$$

and the elements of the Fick diffusivity matrix can be obtained after matrix manipulation as

$$\begin{bmatrix} D_{11} & D_{12} \\ D_{21} & D_{22} \end{bmatrix} = \frac{\begin{bmatrix} Đ_1 & 0 \\ 0 & Đ_2 \end{bmatrix}}{\left(1+\theta_1\frac{Đ_2}{Đ_{12}}+\theta_2\frac{Đ_1}{Đ_{12}}\right)(1-\theta_1-\theta_2)} \begin{bmatrix} \left(1-\theta_2+\theta_1\frac{Đ_2}{Đ_{12}}\right) & \left(1+\frac{Đ_2}{Đ_{12}}\right)\theta_1 \\ \left(1+\frac{Đ_1}{Đ_{12}}\right)\theta_2 & \left(1-\theta_1+\theta_2\frac{Đ_1}{Đ_{12}}\right) \end{bmatrix} \tag{5.52}$$

whereafter the fluxes can be calculated from eq. (5.45).

We could force-fit eq. (5.45) for the two fluxes N_i into the form of Fick's law for each species:

$$N_i = -\rho\Theta_{sat} D_{i,eff} \nabla\theta_i; \quad i = 1,2 \tag{5.53}$$

where the effective Fick diffusivities of components 1 and 2 are given by

$$D_{1,eff} = D_{11} + D_{12}\frac{\nabla\theta_2}{\nabla\theta_1}, \tag{5.54}$$

$$D_{2,eff} = D_{21}\frac{\nabla\theta_1}{\nabla\theta_2} + D_{22}. \tag{5.55}$$

For the case where the interchange coefficient $Đ_{12}$ is fast enough not to be a limiting factor (cf. Eq. (5.47)), the expressions (5.52), (5.54) and (5.55) for the effective Fick diffusivities simplify to give

$$D_{1,eff} = \frac{Đ_1}{(1-\theta_1-\theta_2)}\left((1-\theta_2)+\theta_1\frac{\nabla\theta_2}{\nabla\theta_1}\right), \tag{5.56}$$

$$D_{2,eff} = \frac{Đ_2}{(1-\theta_1-\theta_2)}\left((1-\theta_1)+\theta_2\frac{\nabla\theta_1}{\nabla\theta_2}\right), \tag{5.57}$$

which coincide with those given by Habgood /289/ and Round et al. /290/. While Habgood and Round derived the above expressions specifically for a two-component system our approach can be easily extended to the general multicomponent case starting with eq. (5.48). From eqs (5.56) and (5.57) we see that the effective Fick diffusivities are strong functions of both concentrations and concentration gradients. Furthermore, the effective diffusivity of component 1 is affected by the concentration gradient of component 2. This makes mixture diffusion in zeolites a highly coupled and non-linear process.

We shall illustrate the utility of the above formalisms by considering an example of permeation of a mixture of methane (1) and propane (2) through a silicalite membrane at a temperature of 303 K. This mixture is maintained at a total pressure ($p_{10} + p_{20}$) = 100 kPa in the upstream compartment (which is well-mixed) and allowed to diffuse through a thin layer (δ= 10 μm effective thickness) of silicalite-1 crystals grown on a porous stainless steel support. The apparatus is shown schematically in Fig. 58, and is described in detail by Kapteijn et al. /291/ and Van de Graaf et al. /292/. Other parameters of importance in the calculations presented below are: silicalite matrix density, $\rho = 1800$ kg/m^3; $q_{sat} = 1.58$ mol/kg of silicalite, which is equivalent to $\mathcal{O}_{sat} = 9.1$ molecules per unit cell; Langmuir parameters $b_1 = 4\times10^{-6}$ Pa^{-1}, $b_2 = 6.5\times10^{-4}$ Pa^{-1}; single component Maxwell-Stefan diffusivities, $Đ_1 = 1.04\times10^{-9}$ m^2 s^{-1}, $Đ_2 = 3.4\times10^{-11}$ m^2 s^{-1}. The downstream compartment is flushed with sweep gas and we assume in the calculations below that the partial pressures of the permeating components are negligibly small, i.e., $p_{1\delta} \approx p_{2\delta} \approx 0$.

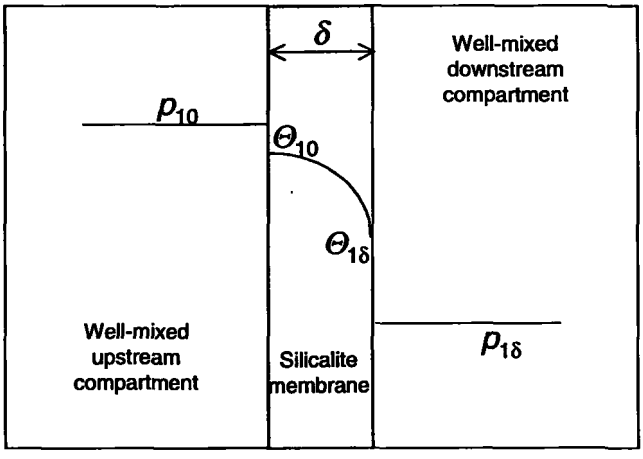

Fig. 58 Schematic of a silicalite membrane separation process for the separation of a hydrocarbon mixture.

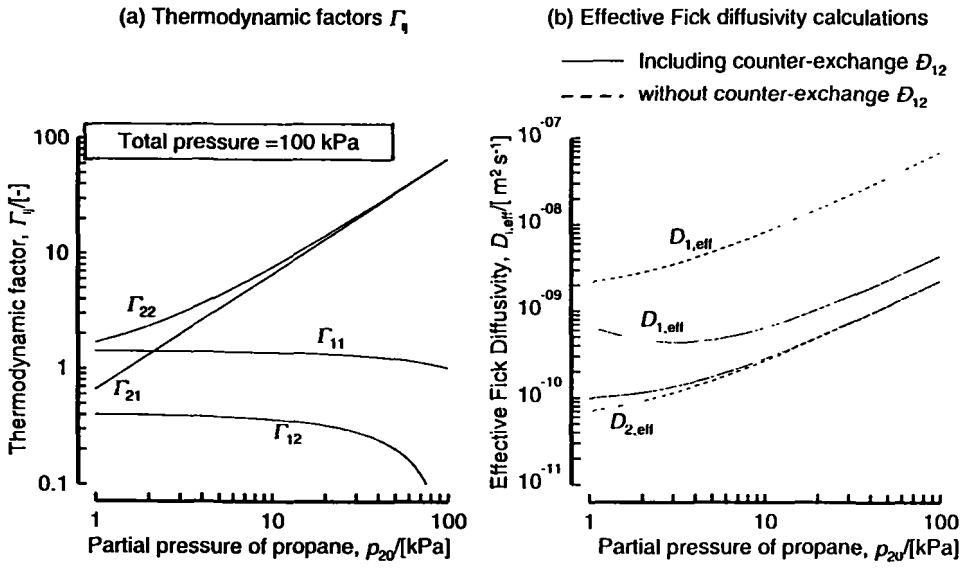

Fig. 59 (a) Thermodynamic factor matrix for the mixture of methane (1) and propane (2) in silicalite-1 at 303 K calculated from the multicomponent Langmuir model, eq. (5.50). The Langmuir parameters are: $b_1 = 4\times10^{-6}$ Pa^{-1}, $b_2 = 6.5\times10^{-4}$ Pa^{-1}, $q_{sat} = 1.58$ mol/kg of silicalite, which is equivalent to $\Theta_{sat} = 9.1$ molecules per unit cell.
(b) Effective Fick diffusivities as a function of the upstream mixture composition, calculated using eqs. (5.54)–(5.57) and taking the single component Maxwell-Stefan diffusivities, $Đ_1 = 1.04\times10^{-9}$ m^2 s^{-1}, $Đ_2 = 3.4\times10^{-11}$ m^2 s^{-1}.

Figure 59 a shows the elements of the matrix of thermodynamic factors $[\Gamma]$, calculated using eq. (5.50), to be strong functions of the upstream partial pressure of propane, p_{20}. The effective Fick diffusivities were calculated including interchange $Đ_{12}$ (eqs (5.52)–(5.55)) and also ignoring interchange (eqs (5.56), (5.57)). The interchange coefficient $Đ_{12}$ was determined using eq. (5.41). The occupancy gradients are calculated by assuming

$$\nabla\theta_i = \frac{\theta_{i0} - \theta_{i\delta}}{\delta} \approx \frac{\theta_{i0}}{\delta}. \tag{5.58}$$

The calculations, shown in Fig. 59 b demonstrate that diffusional interchange has a significant influence on the effective transport of methane (1) through the zeolite and has the effect of slowing down the intrinsically faster moving component. The intrinsically slow moving propane is not influenced by the presence of methane (the two curves for $D_{2,eff}$ virtually coincide).

With the upstream compartment maintained at constant composition, the concentration within the zeolite layer will build up to their steady-state values. The transient fluxes of methane and propane for a specific upstream condition: p_{10} = 95 kPa, p_{20} = 5 kPa can be calculated by solving the appropriate set of coupled partial differential equations (see Van de

Graaf et al. /292/ and Krishna et al. /283/ for details); the results are shown in Fig. 60 a. Ignoring interchange, $Đ_{12}$, we calculate much higher fluxes of methane as could have been anticipated from the effective diffusivity calculations seen in Fig. 59 b. A further point to note is the curious maximum in the flux of methane during the initial transience before the system evolves to a steady state. Propane (2), which has a higher sorption strength permeates preferentially through the membrane; this can be evidenced by calculating the permeation selectivity defined by

$$\text{Permeation selectivity} = \frac{N_2/N_1}{p_{20}/p_{10}} \tag{5.59}$$

The selectivity values are plotted in Fig. 60 b for various upstream partial pressures of propane. Ignoring interchange, $Đ_{12}$, leads to prediction of much lower selectivity values than measured experimentally by Van de Graaf et al. /292/. The agreement of the model with interchange with experimental data is significantly better. Their experiments can be taken as conclusive

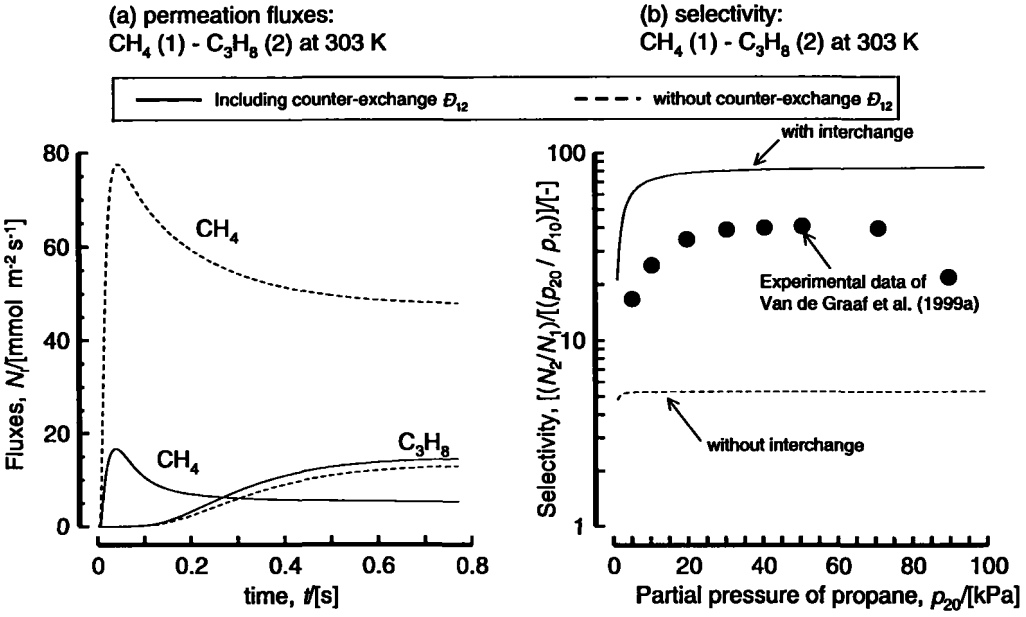

Fig. 60 (a) Transient permeation fluxes of methane (1) and propane (2) across a silicalite membrane at 303 K. The upstream partial pressures are maintained at $p_{10} = 95$ kPa, $p_{20} = 5$ kPa. (b) Permeation selectivity as a function of the upstream partial pressure of propane. Comparison of model calculations, with and without interchange, with experimental data of Van de Graaf et al. /292/. The parameters used in the calculations are: silicalite matrix density, $\rho = 1800$ kg/m^3; membrane thickness $\delta = 10$ μm; $q_{2,sat} = 1.58$ mol/kg of silicalite, which is equivalent to $\Theta_{2,sat} = 9.1$ molecules per unit cell; $\Theta_{1,sat} = \Theta_{2,sat}$; Langmuir: $b_1 = 4\times10^{-6}$ Pa^{-1}, $b_2 = 6.5\times10^{-4}$ Pa^{-1}; single component Maxwell-Stefan diffusivities, $Đ_1 = 1.04\times10^{-9}$ m^2 s^{-1}, $Đ_2 = 3.4\times10^{-11}$ m^{2}s^{-1}.

proof of the validity of the Maxwell-Stefan formulation and of the need to take the interchange mechanism into account.

The curious maximum observed for the transient flux of methane is a typical phenomenon observed during transient permeation of a mixture comprising of (1) a faster moving species with low sorption strength and (2) a slower moving species but with higher sorption strength. In this mixture, the faster moving species 1 will usually exhibit a maximum flux during transient permeation. To illustrate this, we present calculations for permeation of hydrogen (1) and n-butane (2) across a silicalite membrane at 295 K. For pure component permeations, with the upstream compartment maintained at 50 kPa, the transient fluxes are shown in Fig. 61 a. Hydrogen has a higher steady-state flux than n-butane. The situation changes dramatically when we consider permeation of a 50-50 mixture, with partial pressures $p_{10} = p_{20} = 50$ kPa; see Fig. 61 b. Under steady-state conditions, hydrogen has a much lower flux than n-butane because it is virtually excluded from the pores of silicalite by the more strongly sorbed n-butane. Again we note the curious sharp maximum in the flux of the faster-moving hydrogen during the initial transience. This maximum has been experimentally confirmed by experiments reported

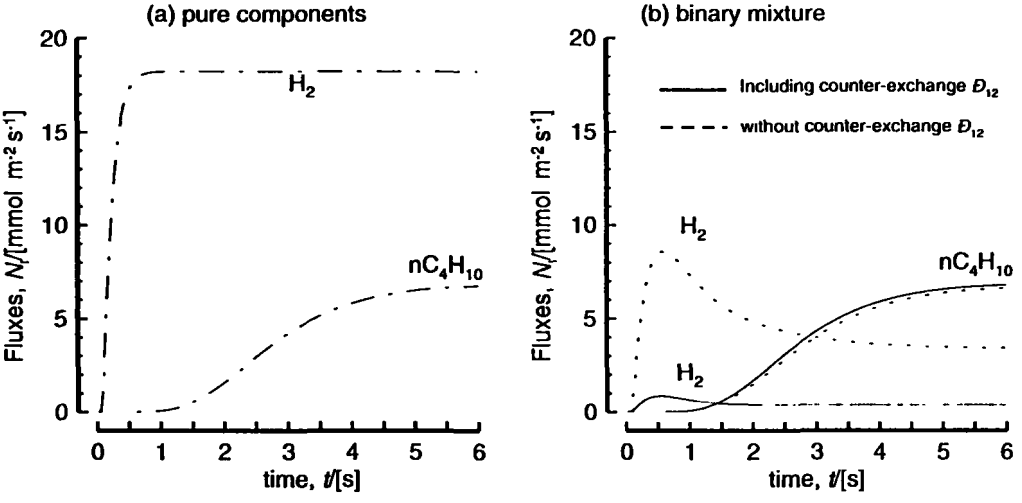

Fig. 61 (a) Transient permeation fluxes of pure components hydrogen and n-butane across a silicalite-1 membrane at 295 K. The upstream partial pressures are maintained at 50 kPa. (b) Transient permeation fluxes of a 50-50 mixture of hydrogen and n-butane across a silicalite-1 membrane at 295 K. The upstream partial pressures are maintained at p_{10} =50 kPa, p_{20} = 50 kPa. The parameters used in the calculations are: silicalite matrix density, $\rho = 1800$ kg/m^3; membrane thickness $\delta = 40$ μm; $q_{sat} = 1.0$ mol/kg of silicalite, which is equivalent to $\Theta_{sat} = 5.77$ molecules per unit cell; Langmuir parameters $b_1 = 1\times10^{-5}$ Pa^{-1}, $b_2 = 4\times10^{-4}$ Pa^{-1}; single component Maxwell-Stefan diffusivities, $Đ_1 = 1\times10^{-9}$ m^2 s^{-1}, $Đ_2 = 5\times10^{-11}$ m^2 s^{-1}. The downstream compartment is flushed with sweep gas and we assume in the calculations below that the partial pressures of the permeating components are negligibly small, i.e. $p_{1\delta} \approx p_{2\delta} \approx 0$.

by Kapteijn et al. /293/, and provides further support of the Maxwell-Stefan formulation. We note again in Fig. 61 b that inclusion of interchange $Đ_{12}$ has a significant impact on the magnitude of the fluxes of hydrogen, analogous to the results seen in Fig. 60 a.

The results seen in Fig. 61 provide the basis of a commercial process for separating hydrogen from a mixture of light hydrocarbons (methane, ethane, propane and butane) from refinery fuel gases by allowing the mixture to permeate through a carbon molecular sieve membrane (Rao and Sircar /294/); see Fig. 62. The hydrocarbons are much more strongly adsorbed than hydrogen and permeate selectively across the membrane. Propane and butanes are nearly completely removed in the permeate stream. Final purification of hydrogen by pressure swing adsorption is required before recycling back to the refinery. The advantage of this membrane separation process is that the hydrogen rich stream is recovered from the retentate (feed) side of the membrane and can be re-used in the refinery without the need for further recompression.

Krishna and Sie /295/ and Van de Graaf et al. /296/ discuss the benefits of incorporation of membrane separation concepts discussed in the foregoing within a catalytic reactor.

A further illustration of the coupled binary diffusion process is the uptake of a mixture of n-heptane (1) and benzene (2) by NaX zeolite. The zeolite crystals are exposed to a bulk vapour mixture maintaining a constant composition environment of benzene and n-heptane and the uptake of these components by the zeolite is monitored as a function of time. The experimentally measured transient uptake profiles by Kärger and Bülow /297/ are shown in Fig. 63. The profile for n-heptane exhibits a remarkable maximum at $t = 50$ min with a molecular loading that is significantly higher than the final (low) equilibrium loading. The results can be explained physically as follows. The Maxwell-Stefan mobility of n-heptane $Đ_1$ is about fifty times larger than the corresponding mobility of benzene $Đ_2$; this is because of differences in the molecular configurations. Initially, beginning with fresh zeolite crystals, n-heptane quickly penetrates the pores of the zeolite occupying the sorption sites. The sorption strength of n-heptane is however considerably lower than that of benzene due *inter alia* to differences in polarity. The adsorbed n-heptane eventually gets displaced from the sorption sites by benzene and the occupancy of n-heptane decreases from its maximum value to reach its final low saturation value. At equilibrium, achieved after about 5 hours, the pores of the zeolite are occupied predominantly by the more strongly adsorbed benzene.

The maximum in the transient flux or loading observed for the faster-moving, less strongly sorbed, species in Figures 60 a, 61 b and 63 must be seen as a direct consequence of the strong coupling between the diffusion of the two components. This coupling is a direct consequence of the non-diagonal elements in the matrix of thermodynamic factors $[\Gamma]$. If this matrix is forced to have zero non-diagonal elements, the transient profiles will show monotonic approaches to either a steady-state or equilibrium situation.

Kapteijn et al. /298/ have modified the treatment presented in this section to account for different saturation capacities $\Theta_{i,sat}$ of the two components in the mixture.

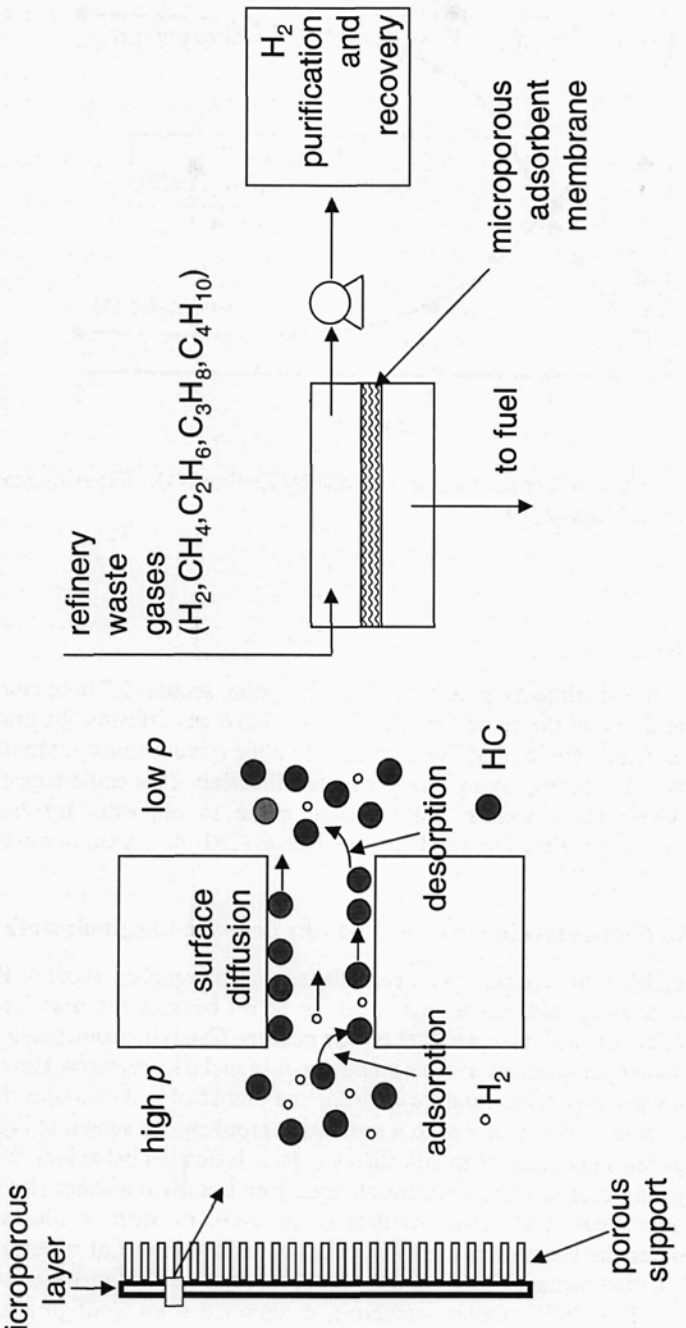

Fig. 62 A microporous carbon membrane can be used for separation of hydrocarbons from a gaseous mixture containing hydrogen. The hydrocarbons are more strongly adsorbed inside the micropores and are transported across the membrane much faster than hydrogen. Adapted from Rao and Sircar /294/.

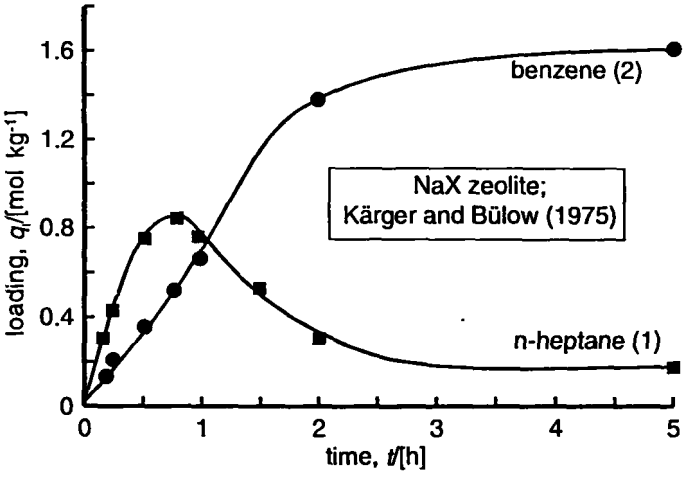

Fig. 63 Transient uptake of benzene and *n* -heptane by Zeolite NaX. Experimental results of Kärger and Bülow /297/.

5.9 Counter-diffusion

In the simulations and experiments, presented in the foregoing section 5.7 both components in the binary mixture move in the same direction, i.e. we have co-diffusion. In practice we also have situations in which the driving forces imposed on the system tends to move the two components in opposite directions, giving rise to counter-diffusion. This could happen within a zeolite catalyst where the reactants and products move in opposite directions. The experimental study of counter-diffusion by Moore and Katzer /299/ shows curious asymmetric behaviour.

5.10 Diffusion of two components in a zeolite, following dual-site Langmuir isotherms

We consider the problem of separation of linear alkanes from branched alkanes. Branched alkanes are preferred to linear alkanes as ingredients in petrol because the branched hydrocarbons burn more efficiently and have a higher octane number. Catalytic isomerisation is used to convert straight-chain hydrocarbons to their mono- or di-branched structures. However, the product of catalytic isomerisation is a mixture of linear and branched hydrocarbons that are in thermodynamic equilibrium; this gives rise to a separation problem. As shown in Fig. 52, the sorption isotherms of branched alkanes in silicalite-1 exhibit inflection behaviour and can be exploited to develop a process to separate linear alkanes from branched alkanes (Krishna and van den Broeke /300/; Vlugt et al. /301/; Krishna et al. /283/. In order to illustrate these concepts let us consider the specific example of diffusion of a mixture of n-hexane (*n*-C_6, component 1) and 3-methyl pentane (3MP, component 2) through a silicalite-1 membrane at a temperature of 362 K. The 50-50 mixture isotherms, determined from Configurational Bias Monte Carlo simulation techniques (Vlugt et al. /301/ are shown in Fig. 64 a. The mixture isotherms are well represented by the Dual-site Langmuir model for the mixture:

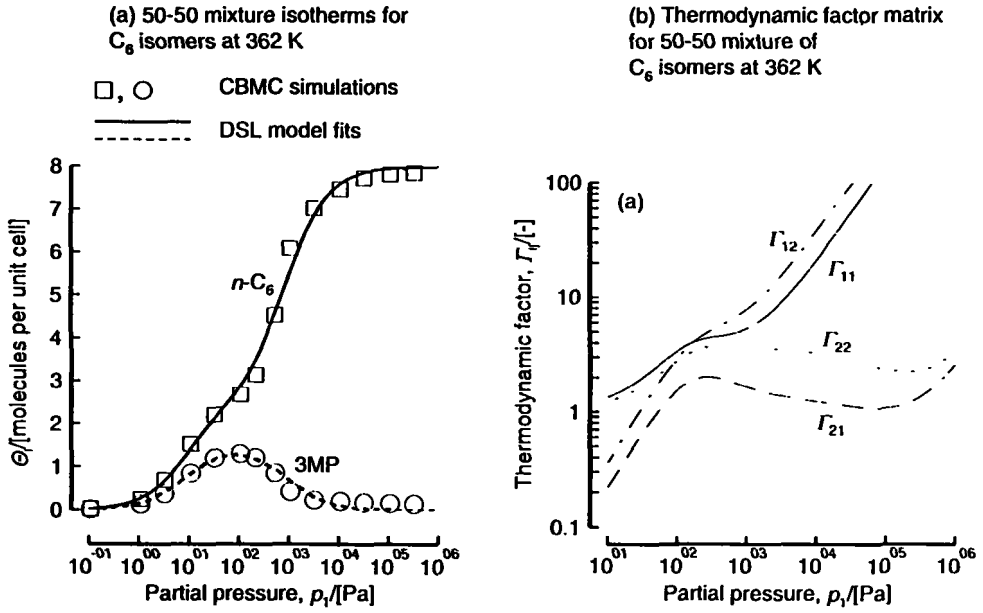

Fig. 64 (a) 50-50 mixture isotherms for (1) n-C_6 and (2) 3MP at 362 K in silicalite. The open square and circle symbols represent the CBMC simulations for (1) n-C_6 and (2) 3MP respectively. The continuous and dashed lines are the dual-site Langmuir (DSL) fits with the parameter values determined only from pure component CBMC simulation data. The dual-site Langmuir parameter values are for n-C_6: $\theta_{1A}=4$, $\theta_{1B}=4$, $k_{1A}=0.07\,\mathrm{Pa}^{-1}$, $k_{1B}=2\times10^{-3}\,\mathrm{Pa}^{-1}$ and for 3MP: $\theta_{2A}=4$, $\theta_{2B}=4$, $k_{2A}=0.045$, $k_{2B}=5\times10^{-6}$. (b) Matrix of thermodynamic factors for 50-50 mixture of n-C_6 and 3MP calculated using eqs (5.62) and (5.63).

$$\Theta_i = \frac{\left(\Theta_{sat,A}b_{i,A}+\Theta_{sat,B}b_{i,B}\right)p_i+\left(\Theta_{sat,A}+\Theta_{sat,B}\right)b_{i,A}b_{i,B}p_i^2}{1+\left(b_{1,A}+b_{1,B}\right)p_1+b_{1,A}b_{1,B}p_1^2+\left(b_{2,A}+b_{2,B}\right)p_2+b_{2,A}b_{2,B}p_2^2};\quad i=1,2 \tag{5.60}$$

For the 50-50 mixture, the branched alkane 3MP exhibits a curious maximum with respect to molecular loading within the silicalite structure. We see from Fig. 64 b that as the partial pressures increase to 100 Pa, the sorbate loading of both linear and branched alkanes increase till a maximum is reached in the loading of 3MP. This occurs at a total loading of 4 molecules per unit cell. Up to this point there is really no competition between n-C_6 and 3MP and both are almost equally easily adsorbed. Molecular simulations show that at 100 Pa shows all the 3MP molecules are located at the intersections between the straight channels and the zigzag channels whereas the n-C_6 molecules are located everywhere; see Fig. 65. The n-C_6 molecules fit nicely into both straight and zigzag channels (Smit and Maesen /302/); these molecules have a higher "packing efficiency" than 3MP. As the pressure is increased beyond 100 Pa, it is more efficient to obtain higher loading by "replacing" the 3MP with n-C_6; this entropic effect

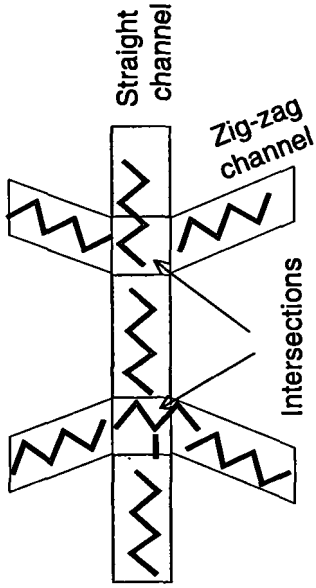

Fig. 65 Preferential siting of 3 MP alkanes at the intersections between the straight and zig-zag channels. The linear alkane can be located at any position within the silicalite structure.

is the reason behind the curious maximum in the 3MP isotherm. The same phenomena has been observed for hydrocarbon mixtures of linear and 2-methyl alkanes with 4–7 carbon atoms (Krishna et al. /303/; Vlugt et al. /301/.

In eqs (5.60), both components are assumed to have the same saturation capacities, $\Theta_{sat,A}$ and $\Theta_{sat,B}$, for the two sites A and B; this is valid for the C_6 isomers being considered here. The fractional occupancies are

$$\theta_i = \frac{\Theta_i}{\Theta_{sat,A} + \Theta_{sat,B}}. \tag{5.61}$$

The matrix of thermodynamic factors $[\Gamma]$ can be derived using eq. (5.42); the result is:

$$[\Gamma] \equiv \frac{\begin{bmatrix} A_3(B_2 - \Theta_2 B_4)/p_1 & A_3\Theta_1 B_4/p_1 \\ B_3\Theta_2 A_4/p_2 & B_3(A_2 - \Theta_1 A_4)/p_2 \end{bmatrix}}{A_2 B_2 - \Theta_1 A_4 B_2 - \Theta_2 A_2 B_4}, \tag{5.62}$$

where

$$
\begin{aligned}
A_2 &= \left(\Theta_{sat,A} b_{1,A} + \Theta_{sat,B} b_{1,B}\right) + \left(\Theta_{sat,A} + \Theta_{sat,B}\right) b_{1,A} b_{1,B} (2p_1) \\
A_3 &= \left(\Theta_{sat,A} b_{1,A} + \Theta_{sat,B} b_{1,B}\right) p_1 + \left(\Theta_{sat,A} + \Theta_{sat,B}\right) k_{1A} k_{1B} p_1^2 \\
A_4 &= \left(b_{1,A} + b_{1,B}\right) + b_{1,A} b_{1,B} (2p_1) \\
B_2 &= \left(\Theta_{sat,A} b_{2,A} + \Theta_{sat,B} b_{2,B}\right) + \left(\Theta_{sat,A} + \Theta_{sat,B}\right) k_{2A} k_{2B} (2p_2) \\
B_3 &= \left(\Theta_{sat,A} b_{2,A} + \Theta_{sat,B} b_{2,B}\right) p_2 + \left(\Theta_{sat,A} + \Theta_{sat,B}\right) k_{2A} k_{2B} p_2^2 \\
B_4 &= \left(b_{2,A} + b_{2,B}\right) + b_{2,A} b_{2,B} (2p_2)
\end{aligned}
\qquad (5.63)
$$

The calculations of $[\Gamma]$ for various values of the partial pressure of component 1, p_1 ($=p_2$), are shown in Fig. 64 b. It is interesting to note that Γ_{21} and Γ_{22} decrease when the partial pressure increases beyond 100 kPa; beyond this point 3MP experiences strong inflection (see Fig. 64 a). Since the thermodynamic factor strongly influences diffusion behaviour, we should expect a corresponding influence on the permeation characteristics across a silicalite membrane. Figures 66 a and 66 b shows the transient permeation fluxes of a 50-50 mixture of *n*-C_6 and

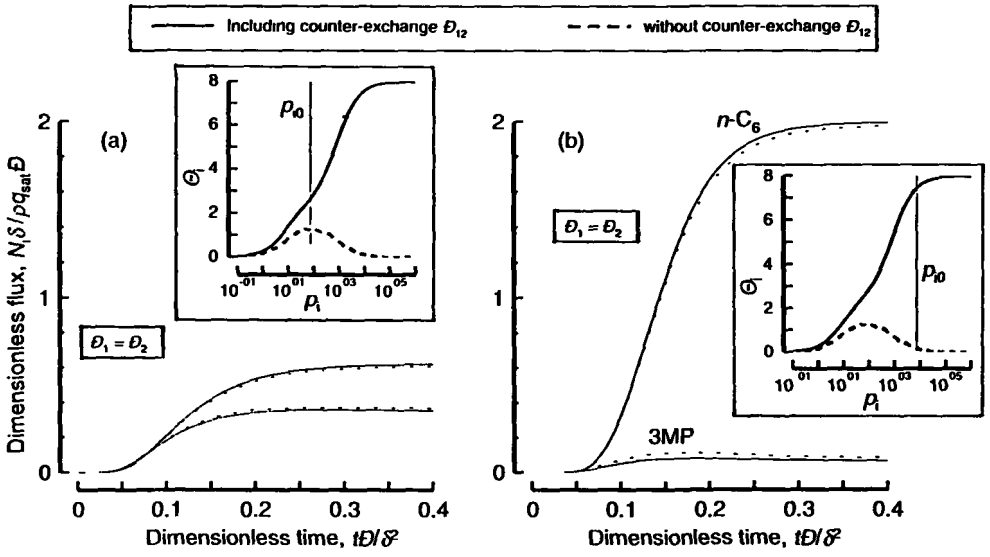

Fig. 66 Transient diffusion fluxes for permeation of a 50-50 mixture of n-C_6 and 3MP across a silicalite membrane. The upstream and downstream compartments are maintained at a total pressure of 84 kPa (atmospheric pressure at Boulder). In the upstream compartment the hydrocarbons account for (a) 0.18 mole % and (b) 18 mole %, the remainder being inert gas helium. An excess of sweep gas in the downstream compartment ensures that the partial pressures of the hydrocarbons are virtually zero. The insets to the figure indicate the partial pressures used in simulations (a) and (b). (a) In this case the partial pressures of n-C_6 and 3MP in the upstream compartment are 75.60 Pa. (b) In this case the partial pressures of n-C_6 and 3MP in the upstream compartment are 7560 Pa. The conditions used in the simulation (b) are identical to those used in the experiments of Funke et al. /304/ at the University of Colorado, Boulder, USA.

3MP at 362 K for two different choices of upstream partial pressures, indicated in the insets to the Figure 66. In the simulations we assume that the pure component Maxwell-Stefan diffusivities are identical for the isomers, i.e. $Đ_1 = Đ_2$; this assumption is a conservative one from the viewpoint of separation of the isomers as we expect the branched isomer to have a lower mobility within the silicalite structure. Since the interchange coefficient $Đ_{12}$ has a value intermediate between $Đ_1$ and $Đ_2$ (cf. Eq. (5.41)) we must also have $Đ_1 = Đ_2 = Đ_{12}$.

There are several interesting aspect of the permeation results presented in Fig. 66. Firstly, we note that with or without interchange, the results are virtually identical. This leads us to conclude that diffusional interchange between sorbed species is important only when the species have significantly different mobilities $Đ_1$ and $Đ_2$. When the mobilities are close to each other, the phenomenon of interchange does not influence the results, as in the example of diffusion of C_6 isomers. Secondly, we note from Fig. 66 a that when the upstream partial pressures correspond to conditions near the maximum in the mixture isotherm for 3MP, the steady-state selectivity for separation of *n*-C_6 with respect to 3MP, defined by eq. (5.59), is only 1.75. If the upstream partial pressures are chosen to be sufficiently high, corresponding to a situation where the branched alkane 3MP is virtually excluded from the zeolite (cf. inset to Fig. 66 b), the permeation selectivity for separation of n-C_6 with respect to 3MP increases to value of about 30. For high selectivity we should ensure that we operate at upstream partial pressures where the branched alkane exhibits inflection; under such conditions "packing efficiency", or entropy effects ensures that the branched alkanes are virtually excluded from the zeolite.

Funke et al. /304/ have presented experimental evidence to suggest that the high selectivities seen in Fig. 66 b can be realised in practice. The same separation principle, relying on differences in packing efficiencies between linear and branched alkanes can be used for separation of n-butane from isobutane (Kapteijn et al. /291/) and n-hexane from 2,2 dimethyl butane (Gump et al. /305/).

5.11 Tracer diffusion and self-diffusivity

Let us apply the above set of equations for tracer diffusion. This system consists of two species 1 and 2 where 1 and 2 are the same molecular species but 1 is labelled or tagged (e.g. by radioactive means). Such experiments are usually carried out to determine the self-diffusivity of a molecular species in a zeolite. The situation can be treated as a special case of binary diffusion, discussed in the foregoing. The conditions of experiment are such that the gradients for diffusion of the tagged and untagged species are equal in magnitude and opposite in sign:

$$\nabla\theta_1 + \nabla\theta_2 = 0 \tag{5.64}$$

and consequently the fluxes of tagged and untagged species sum to zero:

$$\mathbf{N}_1 + \mathbf{N}_2 = 0. \tag{5.65}$$

Applying the restriction (5.64) to eq. (5.45) for binary diffusion we obtain, after imposing $Đ_1 = Đ_2$ for the tagged and untagged species, and performing some matrix manipulations:

$$N_1 = -\rho\Theta_{sat} D^* \nabla\theta_1 = -\rho\Theta_{sat} \frac{1}{\left(\frac{1}{Đ_1} + \frac{\theta_1 + \theta_2}{Đ_{12}}\right)} \nabla\theta_1, \tag{5.66}$$

which shows that the tracer diffusivity D^* is

$$D^* = \frac{1}{\left(\frac{1}{Đ_1} + \frac{\theta_1 + \theta_2}{Đ_{12}}\right)}. \tag{5.67}$$

Equation (5.67) shows that the tracer diffusivity reduces to the Maxwell-Stefan diffusivity only when the interchange coefficient is exceedingly high (cf. eq. (5.47)):

$$D^* \to Đ_1 \quad \text{when } Đ_{12} \to \infty \tag{5.68}$$

There is considerable experimental evidence to support this conclusion; see for example the data in Fig. 67 (Kärger and Ruthven /11/). Self-diffusivity or tracer diffusivity experiments can therefore be used in practice to provide information on the Maxwell-Stefan or "corrected" diffusivity $Đ_1$. In view of the discussions following eq. (5.34) we expect, in general, the self-diffusivity to be dependent on the molecular loading. This expectation is fulfilled in good measure by experimental results. In Fig. 68, the oft-cited NMR self-diffusivity data of Kärger and Pfeifer /306/, has been re-plotted so that the five sets of data are drawn to the same scales. This figure shows a variety of observed dependencies on molecular loading. The self-diffusivity D^* for n-hexane and xylene isomers in NaX decreases with sorbate loading; see Figs 68 a and b.

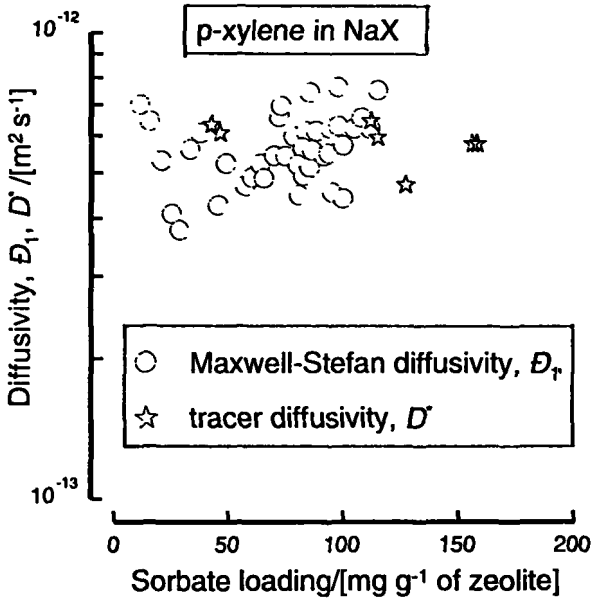

Fig. 67 Comparison between the Maxwell-Stefan diffusivity and self-diffusivity. Data for p-xylene in NaX taken from Kärger and Ruthven /11/.

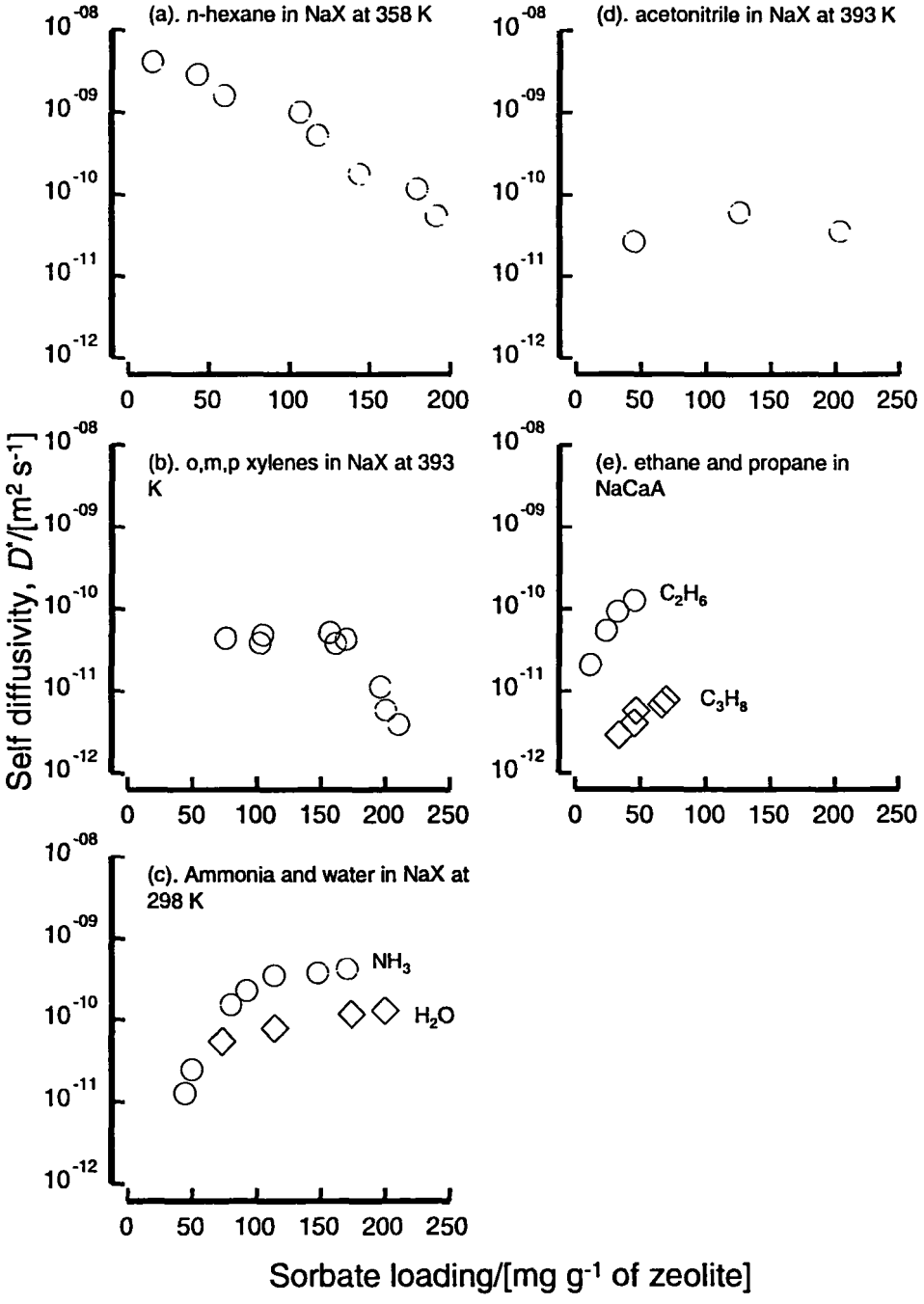

Fig. 68 Dependence of the self-diffusivity on molecular loading in the zeolite. Data for various molecules in NaX and NaCaA taken from Kärger and Pfeifer /306/.

The self-diffusivity D^* for NH_3, H_2O in NaX increases with increased sorbate loading (cf. Fig. 68 c); the same is found for C_2H_6 and C_3H_8 in NaCaA (cf. Fig. 68 e). The diffusivity D^* of acetonitrile in NaX appears to be practically independent of sorbate loading; see Fig 68 d. The fundamental understanding of such dependencies is essential and one clue would be to resort to Monte-Carlo simulations and molecular dynamics (Aust et al. /209/; Bhide and Yashonath /217/; Van den Broeke et al. /213/; Coppens et al. /174, 175/; Dahlke and Emig /210/; Palekar and Rajadhyaksha /204, 206/; Saravanan and Auerbach /224, 225/; Keil /311/) (see sections 2, 3).

5.12 The Onsager, or Irreversible Thermodynamics, formulation for zeolite diffusion

We have modelled zeolite diffusion using the Maxwell-Stefan approach which has been developed only in the last decade, starting with the papers of Krishna /288, 307, 308/. Prior to the development of this approach, an alternative formalism for zeolite diffusion based on the thermodynamics of irreversible processes was in vogue. This approach stems from the classic works of Onsager, Prigogine and De Groot and Mazur and has been used by several researchers (Kärger /309/; Yang et al. /310/). We compare below the Onsager formulation with the Maxwell-Stefan approach with the objective of pointing out the differences and limitations, if any, of either approach.

In the Onsager formulation, a linear relation is postulated between the fluxes and the chemical potential gradients:

$$(\mathbf{N}) = -\rho\Theta_{sat}[L]\frac{1}{RT}\nabla(\mu) \tag{5.69}$$

where L_{ij} are the elements of the matrix of Onsager coefficients having the units of [$m^2\ s^{-1}$]. From eq. (5.42) the chemical potential gradients can related to the occupancy gradients and so eq. (5.69) may be re-written in the form

$$(\mathbf{N}) = -\rho\Theta_{sat}[L]\begin{bmatrix} 1/\theta_1 & 0 & 0 \\ 0 & \ddots & 0 \\ 0 & 0 & 1/\theta_n \end{bmatrix}[\Gamma](\nabla\theta). \tag{5.70}$$

Comparison with the Fick and Maxwell-Stefan formulations gives the following inter-relationship

$$[L] = [B]^{-1}\begin{bmatrix} \theta_1 & 0 & 0 \\ 0 & \ddots & 0 \\ 0 & 0 & \theta_n \end{bmatrix} = [D][\Gamma]^{-1}\begin{bmatrix} \theta_1 & 0 & 0 \\ 0 & \ddots & 0 \\ 0 & 0 & \theta_n \end{bmatrix}. \tag{5.71}$$

Specifically for single component diffusion above system of eqs (5.69)–(5.71) reduce to

$$\mathbf{N}_1 = -\rho\Theta_{sat}L_1\frac{1}{RT}\nabla\mu_1 = -\rho\Theta_{sat}L_1\frac{1}{\theta_1}\Gamma\nabla\theta_1 \tag{5.72}$$

with

$$L_1 = Đ_1\theta_1 = \frac{D_1}{\Gamma}\theta_1, \tag{5.73}$$

which shows that if the Maxwell-Stefan diffusivity $Đ_1$ is independent of occupancy, the

Onsager single component coefficient L_1 is directly proportional to the occupancy. In the event $Đ_1$ is inversely proportional to the occupancy, L_1 is indendent of occupancy.

For a two-component system, eq. (5.71) simplifies to

$$[L]=\begin{bmatrix} \frac{1}{Đ_1}+\frac{\theta_2}{Đ_{12}} & -\frac{\theta_1}{Đ_{12}} \\ -\frac{\theta_2}{Đ_{12}} & \frac{1}{Đ_2}+\frac{\theta_1}{Đ_{12}} \end{bmatrix}^{-1}\begin{bmatrix} \theta_1 & 0 \\ 0 & \theta_2 \end{bmatrix}, \tag{5.74}$$

which can be rearranged using matrix algebra to give

$$\begin{bmatrix} L_{11} & L_{12} \\ L_{21} & L_{22} \end{bmatrix}=\frac{\begin{bmatrix} \left(\frac{1}{Đ_2}+\frac{\theta_1}{Đ_{12}}\right)\theta_1 & \frac{\theta_1\theta_2}{Đ_{12}} \\ \frac{\theta_2\theta_1}{Đ_{12}} & \left(\frac{1}{Đ_1}+\frac{\theta_2}{Đ_{12}}\right)\theta_2 \end{bmatrix}}{\frac{1}{Đ_1}\frac{1}{Đ_2}+\frac{\theta_2}{Đ_{12}}\frac{1}{Đ_2}+\frac{1}{Đ_1}\frac{\theta_1}{Đ_{12}}} \tag{5.75}$$

confirming the validity of the Onsager reciprocal relations:

$$L_{12}=L_{21}. \tag{5.76}$$

Further, it is interesting to note that the interchange coefficient $Đ_{12}$ contributes not only to the off-diagonal coefficients L_{12} and L_{21} but also to the main coefficients L_{11} and L_{22}. As a consequence, the main coefficients L_{11} and L_{22} cannot be identified, respectively, with the pure component Onsager coefficients L_1 and L_2 (Yang et al. /310/). Figure 69 presents a comparison of the Fick, Maxwell-Stefan and Onsager coefficients for the system methane (1) – propane (2). It is interesting to note the strong composition (occupancy) dependence of L_{11}, making the use of the Onsager formulation inconvenient for solution of practical problems.

When the interchange coefficient is large, $Đ_{12}\to\infty$, the Onsager matrix reduces to

$$\begin{bmatrix} L_{11} & L_{12} \\ L_{21} & L_{22} \end{bmatrix}=\begin{bmatrix} \theta_1 Đ_1 & 0 \\ 0 & \theta_2 Đ_2 \end{bmatrix} \tag{5.77}$$

and only for this case can the main coefficients be identified with the pure component Onsager coefficients, i.e. $L_{11}=L_1$ and $L_{22}=L_2$.

For tracer diffusion, imposition of the constraint (5.64), and $Đ_1 = Đ_2$ for the tagged and untagged species we obtain

$$\mathbf{N}_1=-\rho\Theta_{sat}L^*\nabla\theta_1=-\rho\Theta_{sat}\left(\frac{L_{11}}{\theta_1}-\frac{L_{12}}{\theta_2}\right)\nabla\theta_1 \tag{5.78}$$

showing that the Onsager tracer coefficient L^* equals the pure component Onsager coefficient L_1 only for the case where the cross-coefficient L_{12} vanishes.

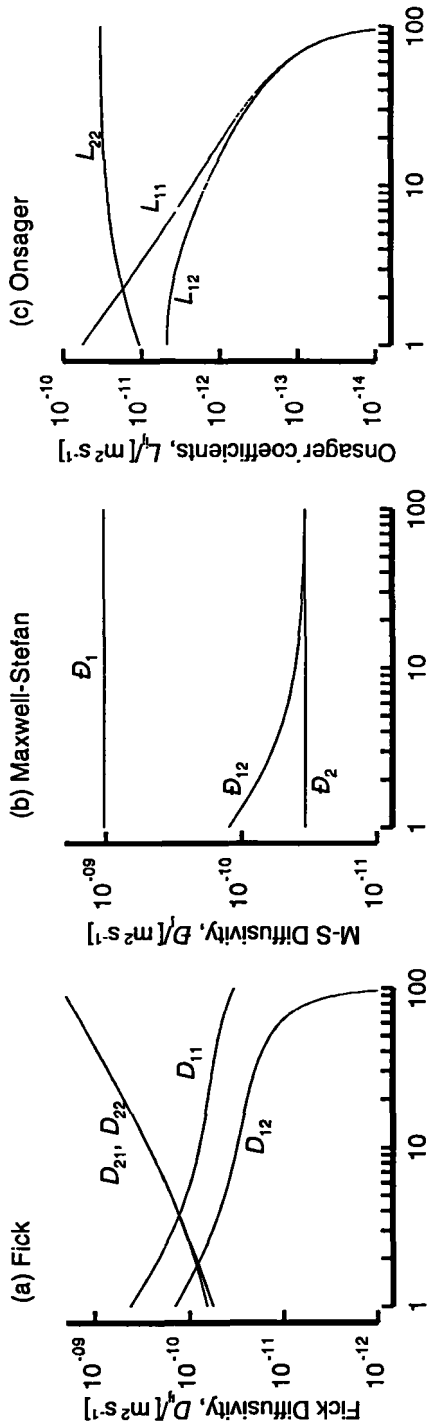

Fig. 69 (a) Fick, (b) Maxwell-Stefan and (c) Onsager coefficients for diffusion in a mixture of methane (1) and propane (2) in silicalite-1 at 303 K. The mixture isotherms and thermo-dynamic correction factors are calculated from the multi-component Langmuir model, eq. (5.50). The Langmuir parameters are: $b_1 = 4\times10^{-6}$ Pa^{-1}, $b_2 = 6.5\times10^{-4}$ Pa^{-1}. The single component Maxwell-Stefan diffusivities, $Đ_1 = 1.04\times10^{-9}$ m^2 s^{-1}, $Đ_2 = 3.4\times10^{-11}$ m^2 s^{-1}.

5.12 Concluding remarks

The Maxwell-Stefan formulation provides the most convenient and general description of mixture diffusion in zeolitic structures. There is, as yet, no adequate theory for *a priori* prediction of the Maxwell-Stefan diffusivities $Đ_i$ and $Đ_{ij}$ for a given molecular species in a specified zeolite structure. For some molecule – zeolite combination the $Đ_i$ vary with the loading, and there is a need to develop models to predict this from first principles, using the methods discussed in Sections 2-4.

Notation for Section 5

A_2, A_3, A_4	parameters defined in eq. (5.63)
b_i	parameter in the Langmuir adsorption isotherm, Pa^{-1}
B_2, B_3, B_4	parameters defined in eq. (5.63)
$[B]$	square matrix of drag coefficients, m^{-2} s
c_i	molar concentration of species i, mol m^{-3}
c_t	total molar concentration of the fluid mixture, mol m^{-3}
D_i	Fick diffusivity of component 1 in zeolite, m^2 s^{-1}
D_{12}	Fick diffusivity of 1-2 binary in fluid mixture, m^2 s^{-1}
$[D]$	matrix of Fick diffusivities, m^2/s
$Đ_i$	Maxwell-Stefan diffusivity of species i in zeolite, m^2/s
$Đ_{12}$	Maxwell-Stefan of 1-2 binary in fluid mixture, m^2/s
$Đ_{ij}$	Maxwell-Stefan diffusivity describing interchange between i and j, m^2/s
$D_{i,eff}$	Effective Fick diffusivity for component i diffusing in a zeolite, m^2/s
$Đ^*$	tracer or self-diffusivity, m^2/s
f_i	fugacity of species i; $f_i = p_i$ for ideal gases, Pa
(J)	$(n-1)$ dimensional column vector of diffusion fluxes, mol m^{-2} s^{-1} or molecules m^{-2} s^{-1}
$\mathbf{J}_i$	molar or molecular diffusion flux of species i relative to the molar average reference velocity **u**, mol m^{-2} s^{-1} or molecules m^{-2} s^{-1}
$[L]$	matrix of Onsgager coefficients, m^2 s^{-1}
n	number of diffusing species, dimensionless
$\mathbf{N}_i$	molar or molecular flux of species i, mol m^{-2} s^{-1} or molecules m^{-2} s^{-1}
$\mathbf{N}_t$	mixture molar or molecular flux, mol m^{-2} s^{-1} or molecules m^{-2} s^{-1}
p	system pressure, Pa
p_i	partial pressure of species i, Pa
q_i	adsorbed species concentration or loading, mol kg^{-1}
q_{sat}	total saturation concentration or loading, mol kg^{-1}
R	gas constant, 8.314 J mol^{-1} K^{-1}
t	time, s
T	absolute temperature, K
$\mathbf{u}_i$	velocity of the diffusing species i, m s^{-1}
u	molar average mixture velocity, m s^{-1}
x_i	mole fraction of species i, dimensionless
z	number of nearest neighbour sites, dimensionless
Greek letters	
δ	length of diffusion path or thickness of membrane, m
γ_i	activity coefficient of species i, dimensionless

Γ	thermodynamic correction factor, dimensionless
$[\Gamma]$	matrix of thermodynamic factors, dimensionless
θ_i	fractional surface occupancy of component *i*
Θ_i	molecular loading, molecules per unit cell or per cage
$\Theta_{i,sat}$	saturation loading, molecules per unit cell or per cage
$\Theta_{sat,A}$	maximum loading of site A, molecules per unit cell
$\Theta_{sat,B}$	maximum loading of site B, molecules per unit cell
Θ_{max}	maximum loading in the zeolite, $\Theta_{max}=(\Theta_{sat,A}+\Theta_{sat,B})$
λ	lateral displacement, m
μ_i	molar chemical potential, $J\ mol^{-1}$
ν	jump frequency, s^{-1}
ρ	density of membrane, number of unit cells per m^3 or $kg\ m^{-3}$
Subscripts	
A	referring to site A, intersections
B	referring to site B, channel interiors
1	component 1 in binary mixture
2	component 2 in binary mixture
max	referring to maximum loading
sat	referring to saturation conditions
i,j	components in mixture
eff	effective parameter
p	derivative at constant pressure
T,p	derivative at constant temperature and pressure
$n+1$	pseudo species
Superscripts	
*	tracer coefficient
Vector and Matrix Notation	
( )	component vector
[ ]	square matrix
Operators	
∇	gradient or nabla

6 OUTLOOK

Ever more powerful computers enable the determination of reliable diffusion coefficients for atoms and molecules in zeolites. Highly elaborated methods lead to a coincidence of calculated and measured values. Various comparisons of measurements by PFG NMR and QUENS with calculations demonstrated the reliability of the results. The reason for some deviations between uptake measurements and PFG NMR methods seems to be clarified /339/. Nijhuis et al. /339/ developed an ultrahigh vacuum system, called the Multitrack (a variant of the TAP-system) to measure the transport diffusion at low accupancy of n-butane in silicalite-1. This method is much quicker than conventional macroscopic techniques. External transport limitations, which seem to be responsible for the deviations between uptake and PFG NMR measurements, can easily be avoided. The obtained macroscopic or transport diffusivities were in good agreement with earlier reported microscopic values. Further clarification of the deviations can also be expected from the recently developed tracer exchange experiments with positron emission

profiling (TEX-PEP) /340/ to measure *in situ* self-diffusivities on a macroscopic time scale and at elevated temperature. When applied to 2-methylpentane and n-hexane diffusion in silicalite, TEX-PEP showed fair agreement with most macroscopic measurements of the transport diffusion, and considerable disagreement with microscopic techniques measuring self-diffusion /340/.

Many simulations reported in the literature examine the behaviour for guest molecules in zeolites using the approximation of a rigid lattice, others compare results obtained from a rigid and a flexible lattice. The results for both cases often agreed quite well, but often differ considerably. The assumption of a rigid lattice is an approximation which cannot be adequate in all cases. Fritzsche et al. /341/ investigated the influence of lattice vibrations on the diffusion of methane in a cation-free zeolite of structure type LTA. Over a wide range of temperatures and for different interaction parameters it was shown that the self-diffusion coefficients obtained with flexible and with rigid lattices are practically the same. The lack of effect of the lattice vibrations on the diffusion of guest molecules leads to the conclusion that the mutual thermalization of the guest molecules is sufficient for the passage of the potential barrier. The authors argue the reason why the steric effect of the "breathing" window has a small influence is perhaps the symmetrical nature of this steric effect. It leads not only to instantaneous lower but, also with the same probability, to instantaneous higher potential barriers. For fast processes taking place inside the cavity, e.g. relaxations or chemical reactions, the influence of lattice vibrations cannot be neglected.

The problem of single-file diffusion and expecially the transition from single-file to normal diffusion needs further clarification. A single particle in the tube not in contact with other particles is assumed to undergo normal diffusion with a mean square displacement of

$$\left\langle Z^2 \right\rangle = 2D_1 t \tag{6.1}$$

where D_1 denotes a single-file diffusion coefficient. Single-file diffusion is a movement of particles in a narrow tube, where due to steric restrictions passing of the particles is forbidden. Therefore, the relative order of the particles is conserved. In the case of hard particles, this happens if the particle diameter, d_p, is greater than half the tube diameter d_T. For the case where a single particle undergoes normal diffusion, the time behavior in a single-file system of infinite length is given by

$$\left\langle Z^2 \right\rangle = 2F\sqrt{t} \tag{6.2}$$

where F denotes the single-file mobility:

$$F = \frac{1-\theta}{\theta} d_p \sqrt{\frac{D_1}{\pi}} = l\sqrt{\frac{D_1}{\pi}} \tag{6.3}$$

where

$$l = a - d_p = \frac{1-\theta}{\theta} d_p \tag{6.4}$$

denotes the mean free path between two adjacent particles, and a is the mean distance between the centers of adjacent particles. In a system where the particle diameter is about half the tube diameter $d_p \approx 0.5\, d_T$, occasional passages between the particles occur so that the order

of the particles is no longer conserved. Hahn and Kärger /130/ showed that in this case, for sufficiently long times, the process of particle passage will dominate and the mean square displacement in the system eventually increases linearly with observation time, while at short times the influence of particle passages is still small and the time behavior is dominated by the single-file process. The transition time between single-file behavior and normal diffusion due to particle passages is given by /130/

$$t_c = \frac{4F^2\tau^2}{a^4} \tag{6.5}$$

where a denotes the length of independent elementary displacements and τ the time interval between them. As soon as boundary conditions became relevant, substantial deviations from the previous equations may occur. In single-file systems with closed ends, and under the assumption that the particles are pointlike and that, except for the preserved particle sequence, there is no correlation between the positions of the diffusants at the beginning and at the end of the experiment, the mean square displacement is

$$\left\langle Z^2 \right\rangle = \frac{1}{3}\frac{(1-\theta)^2}{\theta} L d_p \tag{6.6}$$

where L is the file length. Eq. 6.6 gives much smaller values for the mean square displacement than the corresponding value for restricted normal diffusion in one direction. The risk that the observed molecular mean square displacement is reduced by blockage of the crystallite surface is therefore much larger in single-file systems than in case of normal diffusion. This behavior has to be taken into consideration if one compares the results of measurements by different methods. PFG NMR covers the range of observation times between 10^{-1} and 1s, QUENS between 10^{-13} and 10^{-9} s, and ZLC between seconds and larger. It is quite possible, therefore, that the techniques trace completely different diffusional regimes /130/.

In the future calculations of diffusivities of zeolites with defects, charges, etc. will be done. A further field of investigations will be reactions in zeolites.

REFERENCES

1. Weigel, O. and Steinhoff, E. *Z. Kristallogr., Kristallgeometrie, Kristallphys., Kristallchem.* **1924**, *61*, 125
2. Barrer, R.M. *J. Soc. Chem. Ind. London* **1945**, *64*, 130
3. Barrer, R.M. *J. Chem. Soc.* **1948**, pp 127, 2158
4. Weisz, P.B. and Frilette, V.J. *J. Phys. Chem.* **1960**, *64*, 382
5. Weisz, P.B., Frilette, V.J., Maatman, R.W. and Mower, E.B. *J. Catal.* **1962**, *1*, 307
6. Szostak, R. *Handbook of Molecular Sieves*, Van Nostrand Reinhold, New York (1992)
7. Meier, W.M., Olson, D.H. and Baerlocker, Ch. *Atlas of Zeolites Structure Types*, Elsevier, Amsterdam (1996) (4th Ed.)
8. Szostak, R. *Molecular Sieves, Principles of Synthesis and Identification*, Van Nostrand Reinhold, New York (1989)
9. Weitkamp, J. and Puppe, L. (Eds.) *Catalysis and Zeolites - Fundamentals and Applications*, Springer, Berlin (1999)

10. Weisz, P.B. *Chemtech* **1973**, *3*, 498
11. Kärger, J. and Ruthven, D.M. *Diffusion in Zeolites and Other Microporous Solids*, John Wiley, New York (1992)
12. Rees, L.V.C. *Stud. Surf. Sci. Catal.* **1994**, *84*, 1133
13. Post, M.F.M. *Stud. Surf. Sci. Catal.* **1991**, *58*, 391
14. Chen, N.Y., Degnan, T.F. and Smith, C.M. *Molecular Transport and Reaction in Zeolites*, VCH, New York (1994)
15. Keil, F. *Diffusion and Chemical Reactions in Gas/Solid Catalysis*, Springer, Berlin (1999); (in German)
16. Karge, H.G.; Hunger, M., and Beyer, H.K. in /9/, pp. 198
17. Brandani, S.; Jama, M.; Ruthven, D. *Microporous Mesoporous Mat.* (in press)
18. Darken, L.S. *Trans. AIME* **1948**, *175*, 184
19. Barrer, R.M.; Jost, W. *Trans. Faraday Soc.* **1949**, *45*, 928
20. Barrer, R.M. *Trans. Faraday Soc.* **1941**, *37*, 590
21. Theodorou, C.N.; Snurr, R.Q., and Bell, A.T. in: Alberti, G. and Bein, T. (Eds.) *Comprehensive Supramolecular Chemistry,* Vol. 7, Pergamon Press, New York (1996), pp. 507
22. El Amrani, S.; Kolb, M. *J. Chem. Phys.* **1993**, *98*, 1509
23. Gelten, R.J. *Monte Carlo Simulations of Catalytic Surface Reactions,* Ph.D. Thesis, TU Eindhoven (1999)
24. Binder, K. (Ed.) *Monte Carlo Methods in Statistical Physics*, Topics in curr. Phys., Vol. 7, Springer, Berlin (1986) (2nd Ed.)
25. Binder, K. in: Domb, C.; Green, M.S. (Eds.) *Phase Transition and Critical Phenomena*, Vol. 5b, Academic Press, New York (1976), pp. 1
26. Eyring, H. *J. Chem. Phys.* **1935**, *3*, 107
27. Gelten, R.J.; van Santen, R.A.; Jansen, A.P.J. in: Balbuena, P.B.; Seminario, J.M. (Eds.) *Molecular Dynamics: From Classical to Quantum Methods (Theoretical and Computational Chemistry 7)*, Elsevier, Amsterdam (1999)
28. Van Kampen, N.G. *Stochastic Processes in Physics and Chemistry*, North-Holland, Amsterdam (1992)
29. Wayne, R.P. in: Bamford, C.H.; Tipper, C.F.H. (Eds.) *Chemical Kinetics*, Vol. 2 (The Theory of Kinetics) Elsevier, Amsterdam (1969), pp. 214
30. Goodman, R.H.; Graff, D.S.; Sander, L.M.; Leroux-Hugon, P. and Clément, E. *Phys. Rev. E.* **1995**, *52*, 5904
31. Sales, J.L.; Uñac, R.O.; Gargiulo, M.V.; Bustos, V. and Zgrablich, G. *Langmuir* **1995**, *12*, 95
32. Meng, B. and Weinberg, W.H. *Surf. Sci.* **1997**, *374*, 443
33. Silverberg, M. and Ben-Shaul, A. *Surf. Sci.* **1989**, *214*, 17
34. Tammaro, M.; Sabella, M. and Evans, J.W. *J. Chem. Phys.* **1995**, *103*, 10277
35. Catlow, C.R.A. (Ed.) *Modelling of Structure and Reactivity in Zeolites*, Academic Press, New York (1992)
36. Bell, A.T.; Maginn, E.J.; Theodorou, D.N. in: Ertl, G.; Knözinger, H.; Weitkamp, J. (Eds.) *Handbook of Heterogeneous Catalysis*, VCH, Weinheim, Vol. 3, pp. 1165
37. Demontis, P.; Suffritti, G.B. *Chem. Rev.* **1997**, *97*, 2845
38. Bates, S.P. and van Santen, R.A. *Adv. Cat.* **1998**, *42*, 1
39. Evans, D.J. and Morriss, G.P. *Statistical Mechanics of Nonequilibrium Liquids*, Academic Press, New York (1990)

40. Leach, A.R. *Molecular Modeling - Principles and Applications*, Longman, Singapore (1996)
41. Allen, M.P. and Tildesley, D.J. *Computer Simulation of Liquids*, Clarendon Press, Oxford (1987)
42. Frenkel, D. and Smit, B. *Understanding Molecular Simulation*, Academic Press, New York (1996)
43. Sadus, R.J. *Molecular Simulation of Fluids - Theory, Algorithms and Object-Orientation*, Elsevier (1999)
44. Rowley, R.L. *Statistical Mechanics for Thermophysical Property Calculations*, Prentice Hall, Englewood Cliffs (1994)
45. Field, M.J. *A Practical Introduction to the Simulation of Molecular Systems*, Cambridge University Press, Cambridge (1999)
46. Haile, J.M. *Molecular Dynamics Simulation*, John Wiley, New York (1992)
47. Rapaport, D.C. *The Art of Molecular Dynamics Simulation*, Cambridge University Press, Cambridge (1995)
48. Haberlandt, R.; Fritzsche, S.; Peinel, G. and Heinzinger, K. *Molecular Dynamics*, Vieweg, Braunschweig (1995) (in German)
49. Stallmach, R. and Kärger, J. *Adsorption* **1999**, *5*, 117
50. Ruthven, D.M. and Derrah, M.I. *J. Chem. Soc. Faraday Trans. I* **1972**, *68*, 2332
51. Bezus, A.G.; Kiselev, A.V.; Lopatkin, A.A. and Du, P.Q. *J. Chem. Soc. Faraday Trans. II* **1978**, *74*, 367
52. Demontis, P.; Fois, E.S.; Suffritti, G. and Quartieri, S. *J. Phys. Chem.* **1990**, *94*, 4329
53. Demontis, P.; Fois, E.S.; Suffritti, G. *J. Phys. Chem.* **1992**, *96*, 1482
54. Demontis, P.; Suffritti, G.; Mura, P. *Chem. Phys. Lett.* **1992**, *191*, 553
55. Kiselev, A.V. and Du, P.Q. *J. Chem. Soc. Faraday Trans. II* **1981**, *77*, 1
56. Goodbody, S.J.; Watanabe, K.; MacGowan, D.; Walton, J.P.R.B. and Quirke, N. *J. Chem. Faraday Trans.* **1991**, *87*, 1951
57. Fritzsche, S.; Haberlandt, R.; Kärger, J.; Pfeifer, H. and Heinzinger, K. *Chem. Phys. Lett.* **1992**, *198*, 283
58. Fritzsche, S.; Haberlandt, R.; Kärger, J.; Pfeifer, H. and Wolfsberg, M. *Chem. Phys. Lett.* **1990**, *171*, 109
59. Schrimpf, G.; Schlenkrich, M.; Brickmann, J. and Bopp, P. *J. Phys. Chem.* **1992**, *96*, 7404
60. Jaramillo, E. and Auerbach, S.M. *J. Phys. Chem. B* **1999**, *103*, 9589
61. Henson, N.J., Cheetham, A.K.; Stöckenhuber, M.; Lercher, J.A. *J. Chem. Soc. Faraday Trans.* **1998**, *94*, 3759
62. Nicholson, D.; Boutin, A. and Pellenq, R.J.-M. *Mol. Sim.* **1996**, *17*, 217
63. June, R.L.; Bell, A.T. and Theodorou, D.N. *J. Phys. Chem.* **1990**, *94*, 1508
64. June, R.L.; Bell, A.T. and Theodorou, D.N. *J. Phys. Chem.* **1990**, *94*, 8232
65. Pickett, S.D.; Nowak, A.K.; Thomas, J.M.; Peterson, B.K.; Swift, J.F.P.; Cheetham, A.K.; den Ouden, C.J.J.; Smit, B. and Post, M.F.M. *J. Phys. Chem.* **1990**, *94*, 1233
66. Kiselev, A.V.; Lopatkin, A.A. and Shulga, A.A. *Zeolites* **1985**, *5*, 261
67. Yashonath, S. *J. Phys. Chem.* **1991**, *95*, 5877
68. Yashonath, S. *Chem. Phys. Lett.* **1991**, *177*, 54
69. Santikary, P.; Yashonath, S. and Ananthakrishna, G. *J. Phys. Chem.* **1992**, *96*, 10469
70. Yashonath, S. and Santikary, P. *Phys. Rev. B* **1992**, *45*, 10095
71. Yashonath, S. and Santikary, P. *J. Phys. Chem.* **1993**, *97*, 3849

72. Santikary, P. and Yashonath, S. *J. Solid State Chem.* **1993**, *106*, 184
73. Yashonath, S. and Santikary, P. *J. Phys. Chem.* **1994**, *98*, 6368
74. Bandyopadhyay, S. and Yashonath, S. *J. Solid State Chem.* **1994**, *111*, 151
75. Jost, S.; Bär, N.-K.; Fritzsche, S.; Haberlandt, R. and Kärger, J. *J. Phys. Chem. B* **1998**, *102*, 6375
76. Hirschfelder, J.O.; Curtiss, C.F. and Bird, R.B. *Molecular Theory of Gases and Liquids*, John Wiley, New York (1954), p. 964
77. Heink, W.; Kärger, J.; Pfeifer, H.; Datema, K.P. and Nowak, A.K. *J. Chem. Soc. Faraday Trans.* **1992**, *88*, 3505
78. Hufton, J.R. *J. Phys. Chem.* **1991**, *95*, 8836
79. Hall, L.H. *Group theory and symmetry in chemistry*, McGraw Hill, New York (1969)
80. Slater, J.C. and Kirkwood, J.G. *Phys. Rev.* **1931**, *37*, 682
81. Yashonath, S.; Bandyopadhyay, S. *Chem. Phys. Lett.* **1994**, *228*, 284
82. Demontis, P.; Suffritt, G.B.; Quartieri, S.; Fois, E.S. and Gamba, A. *J. Phys. Chem.* **1988**, *92*, 867
83. Bandyopadhyay, S. and Yashonath, S. *J. Chem. Phys.* **1995**, *99*, 4286
84. van Koningsveld, H. in: van Bekkum, H.; Flanigen, E.M. and Jansen, J.C. (Eds.) *Introduction to zeolite science and practice*, Elsevier, Amsterdam (1991), p. 35, *Stud. Surf. Sci. Catal.* Vol. 58
85. Yashonath, S. and Santikary, P. *J. Phys. Chem.* **1993**, *97*, 13778
86. Demontis, P.; Suffritti, G.B.; Quartieri, S.; Gamba, A. and Fois, E.S. *J. Chem. Soc. Faraday Trans.* **1991**, *87*, 1657
87. Demontis, P.; Suffritti, G.B.; Quartieri, S.; Fois, E.S. and Gamba, A. *Zeolites* **1987**, *7*, 522
88. Demontis, P.; Suffritti, G.B.; Quartieri, S.; Fois, E.S. and Gamba, A. *J. Phys. Chem.* **1988**, *92*, 867
89. Matthews, G.P.; Smith, E.B. *Mol. Phys.* **1976**, *32*, 1719
90. Caro, J.; Hocvar, S.; Kärger, J.; Rieckert, L. *Zeolites*, **1986**, *6*, 213
91. Demontis, P.; Suffritti, G.B. and Mura, P. *Chem. Phys. Lett.* **1992**, *191*, 553
92. Caro, J.; Bülow, M.; Schirmer, W.; Kärger, J.; Heink, W.; Pfeifer, H. and Zdanov, S. *J. Chem. Soc. Faraday Trans.* **1985**, *81*, 2541
93. Bandyopadhyay, S. and Yashonath, S. *Chem. Phys. Lett.* **1994**, *223* 363
94. Fritzsche, S.; Haberlandt, R.; Kärger, J.; Pfeifer, H. and Heinzinger, K. *Chem. Phys.* **1993**, *174*, 229
95. Fritzsche, S.; Haberlandt, R.; Kärger, J.; Pfeifer, H. and Heinzinger, K. *Chem. Phys. Lett.* **1995**, *242*, 361
96. Jost, S.; Fritzsche, S.; Haberlandt, R. *Chem. Phys. Lett.* **1997**, *279*, 385
97. Fritzsche, S.; Haberlandt, R.; Hofmann, G.; Kärger, J.; Heinzinger, K. and Wolfsberg, M. *Chem. Phys. Lett.* **1997**, *265*, 253
98. Haberlandt, R. *Thin Solid Films* **1998**, *330*, 34
99. Cohen de Lara, E.; Kahn, R.; Goulay, A.M. *J. Chem. Phys.* **1989**, *90*, 7482
100. Heink, W.; Kärger, J.; Ernst, S. and Weitkamp, J. *Zeolites* **1994**, *14*, 320
101. Demontis, P.; and Suffritti, G.B. *Chem. Phys. Lett.* **1994**, *223*, 355
102. Fritzsche, S.; Gaub, M.; Haberlandt, R. and Hofmann, C. *Mol. Model.* **1996**, *2*, 286
103. Catlow, C.R.A.; Freeman, C.M., Vessal, B.; Tomlinson, S.M. and Leslie, M. J. *Chem. Soc. Faraday Trans.* **1991**, *87*, 1947
104. Kawano, M.; Vessal, B. and Catlow, C.R.A. *J. Chem. Soc., Chem. Commun.* **1992**, *12*, 879

105. Vessal, B.; Leslie, M. and Catlow, C.R.A. *Mol. Simul.* **1989**, *3*, 123
106. Nicholas, J.B.; Trouw, F.R.; Mertz, J.E.; Iton, L.E.; Hopfinger, A. *J. Phys. Chem.* **1993**, *97*, 4149
107. Nowak, A.K.; den Ouden, C.J.J.; Pickett, S.D.; Smit, B.; Cheetham, A.K.; Post, M.F.M. and Thomas, J.M. *J. Phys. Chem.* **1991**, *95*, 848
108. Ermoshin, V.A. and Engel, V. *J. Phys. Chem. B* **1999**, *103*, 5116
109. Jackson, J.D. *Classical Elecrodynamics*, John Wiley, New York (1962), p. 101
110. Buckingham, A.D.; Fowler, P.W.; Hutchinson, J.M. *Chem. Rev.* **1988**, *88*, 963
111. Ermoshin, V.A.; Smirnov, K.S. and Bougeard, D. *Chem. Phys.* **1996**, *202*, 53
112. Berendsen, H.J.C.; Postma, J.P.M.; van Gunsteren, W.F.; DiNola, A.; Haak, J.R. *J. Chem. Phys.* **1984**, *81*, 3684
113. Chiang, A.S.; Dixon, A.G. and Ma, Y.H. *Chem. Eng. Sci.* **1984**, *39*, 1461
114. Fritzsche, S.; Haberlandt, R.; Kärger, J.; Pfeifer, H. and Waldherr-Teschner, M. *Stud. Surf. Sci. Catal.* **1994**, *84*, 2139
115. Fritzsche, S.; Haberlandt, R. and Kärger, J. *Z. Phys. Chemie* **1995**, *189*, 211
116. Maginn, E.J.; Bell, A.T. and Theodorou, D.N. *J. Phys. Chem.* **1993**, *97*, 4173
117. Cummings, P.T. and Evans, D.J. *Ind. Eng. Chem. Res.* **1992**, *31*, 1237
118. Fritzsche, S.; Haberlandt, R.; Kärger, J.; Pfeifer, H. and Heinzinger, K. *Chem. Phys.* **1993**, *174*, 229
119. Tepper, H.L.; Hoogenboom, J.P.; van der Vegt, N.F.A. and Briels, W.J. *J. Chem. Phys.* **1999**, *110*, 11511
120. Sholl, D. *Chem. Phys. Lett.* **1999**, *305*, 269
121. Gaub, M.; Fritzsche, S.; Haberlandt, R. and Theodorou, D.N. *J. Phys. Chem. B* **1999**, *103*, 4721
122. Kukla, V.; Kornatowski, J.; Demuth, D.; Girnus, I.; Pfeiffer, H.; Rees, L.V.C.; Schunk, S.; Unger, K.K. and Kärger, J. *Science* **1996**, *272*, 702
123. Nivarthi, S.S.; McCormick, A.V. and Davis, H.T. *Chem. Phys. Lett.* **1994**, *229*, 298
124. Jobic, H.; Hahn, K.; Kärger, J.; Bee, M.; Tuel, A.; Noack, M.; Girnus, I. and Kearley, G. *J. Phys. Chem.* **1997**, *110*, 5834
125. Sholl, D.S. and Fichthorn, K. *Phys. Rev. Lett.* **1997**, *79*, 3569
126. Sholl, D.S. and Fichthorn, K. *J. Chem. Phys.* **1997**, *107*, 4384
127. Keffer, D.; McCormick, A.V. and Davis, H.T. *Mol. Phys.* **1996**, *87*, 367
128. Hahn, K. and Kärger, J. *J. Chem. Phys.* **1998**, *109*, 5691
129. Sholl, D.S. and Fichthorn, K.A. *J. Chem. Phys.* **1998**, *109*, 5693
130. Hahn, K. and Kärger, J. *J. Phys. Chem. B.* **1998**, *102*, 5766
131. Webster, C.E.; Drago, R.S. and Zerner, M.C. *J. Phys. Chem. B* **1999**, *103*, 1242
132. Dumont, D. and Bougeard, D. *Zeolites* **1995**, *15*, 650
133. Nicholas, J.B.; Trouw, F.R.; Mertz, J.E.; Iton, L.E.; Hopfinger, A.J. *J. Phys. Chem.* **1993**, *97*, 4149
134. June, R.L.; Bell, A.T. and Theodorou, D.N. *J. Phys. Chem.* **1992**, *96*, 1051
135. Maginn, E.J.; Bell, A.T. and Theodorou, D.N. *J. Phys. Chem.* **1996**, *100*, 7155
136. Runnebaum, R.C. and Maginn, E.J. *J. Phys. Chem. B* **1997**, *101*, 6394
137. Webb III, E.B., Grest, G.S. and Mondello, M. *J. Phys. Chem. B* **1999**, 103, 4949
138. Stepanov, A.G.; Shubin, A.A.; Luzgin, M.V.; Jobic, H. and Thiel, A. *J. Phys. Chem. B* **1998**, *102*, 10860
139. Siepman, J.I.; Karaborni, S. and Smit, B. *Nature* **1993**, *365*, 330
140. Jorgensen,W.L.; Madura, J.D. and Swenson, C.J. *J. Am. Chem. Soc.* **1984**, *106*, 6638

141. Corma, A.; Catlow, C.R.A. and Sastre, G. *J. Phys. Chem. B* **1998**, *102*, 7085
142. Smith, W.; Forester, T.R.; *J. Mol. Graphics* **1996**, *14*, 136
143. Catlow, C.R.A.; Freeman, C.M.; Vessal, B.; Tomlinson, S.M. and Leslie, M. *J. Chem. Soc. Faraday Trans.* **1991**, *87*, 1947
144. Oie, T.; Maggiora, T.M.; Christoffersen, R.E. and Duchamp, D.J. *Int. J. Quantum Chem., Quantum Biol. Symp.* **1981**, *8*, 1
145. Hernández, E. and Catlow, C.R.A. *Proc. Roy. Soc. London A* **1995**, *448*, 143
146. Sastre, G.; Corma, A. and Catlow, C.R.A. *Mat. Res. Soc. Symp. Proc.* **1998**, *527*, 481
147. Sastre, G.; Catlow, C.R.A. and Corma, A. *J. Phys. Chem. B* **1999**, *103*, 5187
148. Jost, S.; Bär, N.-K.; Fritzsche, S.; Haberlandt, R. and Kärger, J. *J. Phys. Chem. B.* **1998**, *102*, 6375
149. Gergidis, L.N. and Theodorou, D.N. *J. Phys. Chem. B* **1999**, *103*, 3380
150. Grillo, M.E. and de Agudelo, M.M.R. *J. Mol. Catal. A* **1997**, *119*, 105
151. Demontis, P.; Suffritti, G.B. and Tilocca, A. *J. Phys. Chem. B* **1999**, *103*, 8141
152. Cavalcante, C.L.; Eic, M.; Ruthven, D.M. and Occelli, M.L. *Zeolites* **1995**, *15*, 293
153. Gorring, R.L. *J. Catal.* **1973**, *31*, 13
154. Rijckaert, J.P. and Bellmans, A. *Faraday Discuss. Chem. Soc.* **1978**, *66*, 95
155. Nakazaki, Y.; Goto, N. and Inui, T. *J. Catal.* **1992**, *136*, 141
156. Nowak, A.K.; Cheetham, A.K.; Pickett, S. D. and Ramdas, S. *Mol. Simul.* **1987**, *1*, 67
157. Demontis, P.; Yashonath, S. and Klein, M.L. *J. Phys. Chem.* **1989**, *93*, 5016
158. Bull, L.M.; Henson, N.J.; Cheetham, A.K.; Newsam, J.M. and Heyes, S.J. *J. Phys. Chem.* **1993**, *97*, 11776
159. Chitra, R. and Yashonath, S. *Chem. Phys. Lett.* **1995**, *234*, 16
160. Snurr, R.Q. and Kärger, J. *J. Phys. Chem. B* **1997**, *101*, 6469
161. Edgar, T.F. and Himmelblau, D.M. *Optimization of Chemical Processes*, McGraw Hill (1988), p. 222
162. Schlecht, M.F. *Molecular Modeling on the PC*, Wiley-VCH (1998), p. 200 ff.
163. Wigner, E. *Trans. Faraday Soc.* 1938, *34*, 29
164. Von Neumann, J.; Ulam, S. *Bull. Am. Chem. Soc.* **1945**, *51*, 660
165. Metropolis, N.; Ulam, S. *J. Am. Stat. Ass.* **1949**, *44*, 335
166. Metropolis, N.; Rosenbluth, A.W.; Rosenbluth, M.N.; Teller, A.H.; Teller, E. *J. Chem. Phys.* **1953**, *21*, 1087
167. McQuarrie, D.A. *Statistical Mechanics*; Harper & Row, New York, 1976
168. Chandler, D. *Introduction to Modern Statistical Mechanics*; Oxford University Press, New York, 1987
169. Smit, B.; Siepmann, J.I. *Science* **1994**, *264*, 1118
170. Smit, B. *Molecular Physics* **1995**, *85*, 153
171. Scogin, J.H, Ph.D. thesis, Tulane University, 1988, Ch. 2
172. Nelson, P.H.; Kaiser, A.B.; Bibby, D.M. *J. Catal.* **1991**, *127*, 101
173. Fichthorn, K.A.; Weinberg, W.H. *J. Chem. Phys.* **1991**, *95*, 1090
174. Coppens, M.-O.; Bell, A.T.; Chakraborty, A.K. *Chem. Eng. Sci.* **1998**, *53*, 2053
175. Coppens, M.-O.; Bell, A.T.; Chakraborty, A.K., *Chem. Eng. Sci.* **1999**, *54*, 3455
176. Coppens, M.-O.; Bell, A.T.; Chakraborty, A.K., 1999. In: *Scientific Computing in Chemical Engineering* (F. Keil, W. Mackens, H. Voss and J. Werther, Eds.) Springer Verlag, Berlin, 1999, p. 200
177. Jansen, A.P.J. *Comput. Phys. Commun.* **1995**, *86*, 1
178. Nieminen, R.M.; Jansen, A.P.J. *Appl. Cat. A* **1997**, *160*, 99

179. Lukkien, J.J.; Segers, J.P.L.; Hilbers, P.A.J.; Gelten, R.J.; Jansen, A.P.J. *Phys. Rev. E* **1998**, *58*, 2598
180. Gelten, R.J.; van Santen, R.A.; Jansen, A.P.J. In: *Molecular Dynamics: From Classical to Quantum Methods (Theoretical and Computational Chemistry 7)* (P.B. Balbuena, J.M. Seminario, Eds.), Elsevier, Amsterdam, 1999
181. Gillespie, D.T. *J. Comput Phys.* **1976**, *22*, 403
182. Lombardo, S.J.; Bell, A.T. *Surf. Sci. Rep.* **1991**, *13*, 1
183. Huitema, H.E.A.; Van der Eerden, J.P. *J Chem. Phys.* **1999**, *110*, 3267
184. Montroll, E.W.; Weiss, G.H. *J. Math. Phys.* **1965**, *6*, 167
185. Barber, M.N.; Ninham, B.W. *Random and Restricted Walks*; Gordon and Breach, New York, 1970
186. Shlesinger, M.F.; Weiss, G.H. *The Wonderful World of Stochastics. A Tribute to Elliott W. Montroll*; North-Holland, Amsterdam, 1985
187. Haus, J.W.; Kehr, K.W. *Phys. Rep.* **1987**, *150*, 263
188. Weiss, G.H. *Aspects and Applications of the Random Walk*; North-Holland, Amsterdam, 1994
189. Hughes, B.D. *Random Walks and Random Environments*; Oxford University Press, New York, 1995
190. Bardeen, J.; Herring, C. In: *Imperfections in Nearly Perfect Crystals* (W. Shockley, Ed.), Wiley, New York, 1952, p. 261-288.
191. Manning, J.R. *Diffusion Kinetics for Atoms in Crystals*; Van Nostrand Reinhold, Princeton, 1968
192. Le Claire, A.D. In: *Physical Chemistry - An Advanced Treatise* Vol. 10 (H. Eyring; D. Henderson; W. Jost, Ed.), Academic Press, New York, 1970, 261
193. Murch, G.E. *Atomic Diffusion Theory in Highly Defective Solids*; Trans. Tech. SA Publications, Rockport, MA, 1980
194. Fedders, P.A.; Sankey, O.F. *Phys. Rev. B* **1977**, *15*, 3580
195. Sankey, O.F.; Fedders, P.A. *Phys. Rev. B* **1977**, *15*, 3586
196. Fedders, P.A.; Sankey, O.F. *Phys. Rev. B* **1978**, *18*, 5938
197. Murch, G.E.; Thorn, R.J. *J. Phys. Chem. Solids* **1977**, *38*, 789
198. Reed, D.A.; Ehrlich, G. *Surface Sci.* **1981**, *102*, 588
199. Reed, D.A.; Ehrlich, G. *Surface Sci.* **1981**, *105*, 603
200. Kehr, K.W.; Kutner, R.; Binder, K. *Phys. Rev. B* **1981**, *23*, 4931
201. Kehr, K.; Binder, K. In: *Applications of the Monte Carlo Methods in Statistical Physics* (K. Binder, Ed.), Springer, Berlin, 1984, p. 181-221
202. Riekert, L.H. *A.I.Ch.E. J.* **1971**, *17*, 446
203. Palekar, M.G.; Rajadhyaksha, R.A. *Indian J. Techn.* **1983**, *21*, 373
204. Palekar, M.G.; Rajadhyaksha, R.A. *Chem. Eng. Sci.* **1985**, *40*, 1085
205. Patwardhan, V.S. *Chem. Eng. Sci.* **1989**, *44*, 2619
206. Palekar, M.G.; Rajadhyaksha, R.A. *Chem. Eng. Sci.* **1986**, *41*, 463
207. Pitale, K.K.; Rajadhyaksha, R.A. *Cur. Sci.* **1988**, *57*, 172
208. Theodorou, D.N.; Wei, J. *J. Catal.* **1983**, *83*, 205
209. Aust, E.K.; Dahlke, K.; Emig, G. *J. Catal.* **1989**, *115*, 86
210. Dahlke, K.; Emig, G. *Catal. Today* **1991**, *8*, 439
211. Frank, B; Dahlke, K.; Emig, G.; Aust, E.; Broucek, R.; Nywit, M. *Microporous Mat.* **1993**, *1*, 43
212. Nelson, P.H.; Wei, J. *J. Catal.* **1991**, *131*, 369

213. Van den Broeke, L.P.J.; Nijhuis, S.A.; Krishna, R. *J. Catal.* **1992**, *136*, 463
214. Faux, D.A.; Hall, C.K.; Sundaresan, S. *Chem. Eng. Sci.* **1991**, *46*, 2359
215. Rajadhyaksha, R.A.; Pitale, K.K.; Tambe, S.S. *Chem. Eng. Sci.* **1990**, *45*, 1935
216. Van Tassel, P.R.; Somers, S.A.; Davis, H.T.; McCormick, A.V. *Chem. Eng. Sci.* **1994**, *49*, 2979
217. Bhide, S.Y.; Yashonath, S. *J. Chem. Phys.* **1999**, *111*, 1658
218. Gladden, L.F.; Hargreaves, M.; Alexander, P. *Chem. Eng. J.* **1999**, *74*, 57
219. Auerbach, S.M.; Henson, N.J.; Cheetham, A.K.; Metiu, H.I. *J. Phys. Chem.* **1995**, *99*, 10600
220. Auerbach, S.M.; Bull, L.M.; Henson, N.J.; Metiu, H.I.; Cheetham, A.K. *J. Phys. Chem.* **1996**, *100*, 5923
221. Auerbach, S.M.; Metiu, H.I. *J. Chem. Phys.* **1996**, *105*, 3753
222. Auerbach, S.M.; Metiu, H.I. *J. Chem. Phys.* **1997**, *106*, 2893
223. Auerbach, S.M. *J. Chem. Phys.* **1997**, *106*, 7810
224. Saravanan, C.; Auerbach, S.M. *J. Chem. Phys.* **1997**, *107*, 8120
225. Saravanan, C.; Auerbach, S.M. *J. Chem. Phys.* **1997**, *107*, 8132
226. Saravanan, C.; Jousse, F.; Auerbach, S.M. *J. Chem. Phys.* **1998**, *108*, 2162
227. Saravanan, C.; Jousse, F.; Auerbach, S.M. *Phys. Rev. Lett.* **1998**, *80*, 5754
228. Saravanan, C.; Auerbach, S.M. *J. Chem. Phys.* **1999**, *110*, 11000
229. Snurr, R.Q.; Bell, A.T.; Theodorou, D.N. *J. Phys. Chem.* **1994**, *98*, 11948
230. Jousse, F.; Leherte, L.; Vercauteren, D.P. *J. Phys. Chem. B* **1997**, *101*, 4717
231. Jousse, F.; Auerbach, S.M.; Vercauteren, D.P. *J. Phys. Chem. B* **1998**, *102*, 6507
232. Zhang, L.; Seaton, N.A. *Chem. Eng. Sci.* **1994**, *49*, 41
233. Sahimi, M.; Gavalas, G.R.; Tsotsis, T.T. *Chem. Eng. Sci.* **1990**, *45*, 1443
234. Mo, W.T.; Wei, J. *Chem. Eng. Sci.* **1986**, *41*, 703
235. Sundaresan, S.; Hall, C.K. *Chem. Eng. Sci.* **1986**, *41*, 1631
236. Ruthven, D.M. *Canad. J. Chem.* **1974**, *52*, 3523
237. Tsikoyiannis, J.G.; Wei, J. *Chem. Eng. Sci.* **1991**, *46*, 233
238. Frank, B; Dahlke, K.; Emig, G. *Chem. Ing. Techn.* **1992**, *64*, 1104.
239. Wang, J.G.; Li, Y.W.; Chen, S.Y.; Peng, S.Y. *Catal. Lett.* **1994**, *26*, 189
240. Wang, J.G.; Li, Y.W.; Chen, S.Y.; Peng, S.Y. *Zeolites* **1995**, *15*, 288
241. Klemm, E.; Wang, J.-G.; Emig, G. *Chem. Eng. Sci.* **1997**, *52*, 3173
242. Trout, B.L.; Chakraborty, A.K.; Bell, A.T. *Chem. Eng. Sci.* **1997**, *52*, 2265
243. Hinderer, J.; Keil, F.J. *Chem. Eng. Sci.* **1996**, *51*, 2667
244. Keil, F.J.; Hinderer, J.; Garayhi, A.R. *Catal. Today* **1999**, *50*, 637
245. Neurock, M.; Hansen, E.W. *Comput. Chem. Eng.* **1998**, *22*, S1045
246. Jensen, K.F.; Rodgers, S.T.; Venkataramani, R. *Curr. Op. Sol. St. & Mat. Sci.* **1998**, *6*, 562
247. Tahir-Kheli, R.A.; Elliott, R.J. *Phys. Rev. B* **1983**, *27*, 844
248. Sargent., R.W.H.; Whitford, C.J., in *Molecular Sieve Zeolites II* (Ed.: R.I. Gould), Advances in Chemistry Series 102, American Chemical Society, Washington D.C., **1971**
249. Bétemps, M.; Jutard, A. *J. Phys. D: Appl. Phys.* **1980**, *13*, 423
250. Ruthven, D.M.; Derrah, I.H. *J. Chem. Soc. Faraday Trans. I* **1972**, *68*, 2332
251. Kärger, J.; Pfeifer, H.; Haberlandt, R. *J. Chem. Soc. Faraday Trans. I* **1980**, *76*, 1569
252. June, R.L.; Bell, A.T.; Theodorou, D.N. *J. Phys. Chem.* **1991**, *95*, 8866
253. Voter, A.; Doll, J. *J. Chem. Phys.* **1985**, *82*, 80
254. Chandler, D. *J. Chem. Phys.* **1978**, *68*, 2959
255. Snurr, R.Q.; Bell, A.T.; Theodorou, D.N. *J. Chem. Phys.* **1994**, *98*, 11948

256. Nowak, A.K.; Cheetham, A.K.; Picket, S.D.; Ramdas, S. *Mol. Simul.* **1987**, *1*, 67
257. Schröder, K.-P.; Sauer, J. *Z. Phys. Chem. (Leipzig)* **1990**, *271*, 289
258. Fukui, K.; Kato, S.; Fujimoto, H. *J. Am. Chem. Soc.* **1975**, *97*, 1
259. Vineyard, G. *J. Phys. Chem. Solids* **1957**, *3*, 121
260. Gusev, A.A.; Suter, U.W. *J. Chem. Phys.* **1993**, *99*, 2228
261. Schrimpf, G.; Brickmann, J. *J. Comput.-Aided Mater. Design* **1995**, *2*, 49
262. Mosell, T.;Schrimpf, G.; Hahn, C; Brickmann, J. *J. Phys. Chem.* **1996**, *100*, 4571
263. Mosell, T.;Schrimpf, G.; Brickmann, J. *J. Phys. Chem.* **1996**, *100*, 4582
264. Maginn, E.J.; Bell, A.T.; Theodorou, D.N. *J. Phys. Chem.* **1995**, *99*, 2057
265. Maginn, E.J.; Bell, A.T.; Theodorou, D.N. *J. Phys. Chem.* **1996**, *100*, 7155
266. Smit, B.; Loyens, L.D.J.C.; Verbist, G.L.M.M. *Faraday Discuss.* **1997**, *106*, 93
267. Bennett, C.H. In: *Diffusion in Solids: Recent Developments* (A.S. Nowick and J.J. Burton, Eds.), Academic Press, New-York, 1975; pp. 73-113
268. Jousse, F.; Auerbach, S.M. *J. Chem. Phys.* **1997**, *107*, 9629
269. Jousse, F.; Leherte, L.; Vercauteren, D.P. *J. Phys. Chem. B* **1997**, *101*, 4717
270. Tunca, C.; Ford, D.M. *J. Chem. Phys.* **1999**, *111*, 2751
271. Clark, W.M. and Rowley, R.L. *AIChE J.*, **1986**, *32*, 1125
272. Krishna, R. and Wesselingh, J.A. *Chem. Eng. Sci.* **1997**, *52*, 861
273. Vignes, A. *Ind. Eng. Chem. Fundam.* **1966**, *5*, 189
274. Ruthven, D.M. *Principles of Adsorption and Adsorption Processes* John Wiley, New York (1984)
275. Barrer, R.M. *Zeolites and Clay minerals as Sorbents and Molecular sieves.* Academic Press, London (1978)
276. Guo, C.J.; Talu, O. and Hayhurst, D.T. *AIChE J.* **1989**, *35*, 573
277. Shah, D.B., Guo, C.J. and Hayhurst, D.T. *J. Chem. Soc. Farad. Trans.* **1995**, *91*, 1143
278. Rudzinski, W.; Narkiewicz-Michalek, J.; Szabelski, P. and Chiang, A.S.T. *Langmuir* **1997**, *13*, 1095
279. Sun, M.S.; Talu, O. and Shah, D.B. *J. Phys. Chem.* **1996**, *100*, 17276
280. Takaishi, T.; Tsutsumi, K.; Chubachi, K. and Matsumoto *J. Chem. Soc. Farad. Trans.* **1998**, *94*, 601
281. Song, L. and Rees, L.V.C. *J. Chem. Soc. Farad. Trans.* **1997**, *93*, 649
282. Ashtekar, S.; Hastings, J.J. and Gladden, L.F. *J. Chem. Soc. Farad. Trans.* **1998**, *94* (8), 1157
283. Krishna, R.; Smit, B. and Vlugt, T.J.H. *Chem. Eng. Sci.* **1999**, *54*, 1751
284. Micke, A.; Bülow, M.; Kocirik, M. and Struve, P. *J. Phys. Chem.* **1994**, *98*, 12337
285. Vlugt, T.J.H., Krishna, R. and Smit, B. *J. Phys. Chem. B* **1999**, *103*, 1102
286. Zhdanov, V.P. *Surface Sci.* **1985**, *194*, L13
287. Ruthven, D.M. and Doetsch, I.H. *AIChE J.* **1976**, *22*, 882
288. Krishna, R. *Chem. Eng. Sci.* **1990**, *45*, 1779
289. Habgood, H.W. *Canad. J. Chem.* **1958**, *36*, 1384
290. Round, G.F.; Habgood, H.W. and Newton, R. *Separation Science* **1966**, *1*, 219
291. Kapteijn, F.; van de Graaf, J.; Moulijn, J.A. *J. Mol. Catal. A-Chem.* **1998**, *134*, 201
292. Van de Graaf, J.; Kapteijn, F. and Moulijn, J.A. *AIChE J.* **1999**, *45*, 497
293. Kapteijn, F.; Bakker, W.J.W.; van de Graaf, J.; Zheng, G.; Poppe, J. and Moulijn, J.A. *Catalysis Today* **1995**, *25*, 213
294. Rao, M.B. and Sircar, S. *Gas Separation and Purification* **1993**, *7*, 279
295. Krishna, R. and Sie, S.T. *Chem. Eng. Sci.* **1994**, *49*, 4029

296. Van de Graaf, J.M.; Zwiep, M.; Kapteijn, F. and Moulijn, J.A. *Chem. Eng. Sci.* **1999b**, *54*, 1441
297. Kärger, J. and Bülow, M. *Chem. Eng. Sci.* **1975**, *30*, 893
298. Kapteijn, F.; Moulijn, J.A. and Krishna, R. *Chem. Eng. Sci.*, **2000**, submitted for publication
299. Moore, R.M. and Katzer, J.R. *AIChE J.* **1972**, *18*, 816
300. Krishna, R. and van den Broeke, L.J.P. *Chem. Eng. J.* **1995**, *57*, 155
301. Vlugt, T.J.H.; Zhu, W.; Kapteijn, F.; Moulijn, J.A.; Smit B. and Krishna, R. *J. Am. Chem. Soc.* **1998**, *120*, 5599
302. Smit, B. and Maesen, T.L.M. *Nature* **1995**, *374*, 42
303. Krishna, R.; Smit, B. and Vlugt, T.J.H. *J. Phys. Chem. A* **1998**, *102*, 7727
304. Funke, H.H.; Argo, A.M.; Falconer, J.L. and Noble, R.M. *Ind. Eng. Chem. Res.* **1997**, *36*, 137
305. Gump, C.J.; Noble, R.D. and Falconer, J.L. *Ind. Eng. Chem. Res.* **1999**, *38*, 2775
306. Kärger, J. and Pfeifer, H. *Zeolites* **1987**, *7*, 90
307. Krishna, R. *Chem. Eng. Sci.* **1993**, *48*, 845
308. Krishna, R. *Gas Separation and Purification* **1993**, *7*, 91
309. Kärger, J. *Surface Science* **1973**, *36*, 797
310. Yang, R.T.; Chen, Y.D. and Yeh, Y.T. *Chem. Eng. Sci.* **1991**, *46*, 3089
311. Keil, F.J. *Chem. Eng. Sci.* **1996**, *51*, 1543
312. Taylor, R. and Krishna, R. *Multicomponent Mass Transfer*, Wiley, New York (1993)
313. Dellago, C.; Bolhuis, P.G.; Csajka, F.S.; Chandler, D. *J. Chem. Phys.* **1998**, *108*, 1964
314. Voter, A.F. *Phys. Rev. Lett.* **1997**, *78*, 3908
315. Ruthven, D.M. and Post, M.F.M. **2000**, *Diffusion in zeolite molecular sieves*, Chapter in *Introduction to zeolite science and technology*, in press
316. Riekert, L. *Adv. Catal.* **1970**, *21*, 281.
317. Richards, P.M. *Phys. Rev. B* **1977**, *16*, 1393.
318. Van Beijeren, H.; Kehr, K.W.; Kutner, R. *Phys. Rev. B* **1983**, *28*, 5711.
319. Kärger, J. *Phys. Rev. A* **1992**, *45*, 4173.
320. Kärger, J.; Petzold, M.; Pfeifer, H.; Ernst, S.; Weitkamp, J. *J. Catal.* **1992**, *136*, 283.
321. Hahn, K.; Kärger, J. *J. Phys. A* **1995**, *28*, 3061
322. Kehr, K.W.; Kutner, R.; Binder, K. *Phys. Rev. B* **1977**, *16*, 1393.
323. Mandelbrot, B.B. *The Fractal Geometry of Nature* Freeman: San Francisco, 1982
324. Havlin, S.; Ben-Avraham, D. *Adv. Phys.* **1987**, *36*, 695.
325. Kärger, J.; Pfeifer, H.; Vojta, G. *Phys. Rev. A* **1988**, *37*, 4514.
326. Bouchaud, J.-P.; Georges, A. *Phys. Rep.* **1990**, *195*, 127.
327. Hahn, K.; Kärger, J.; Kukla, V. *Phys. Rev. Lett.* **1996**, *76*, 2762
328. Kärger, J.; Keller, W.; Pfeifer, H.; Ernst, S.; Weitkamp, J. *Micropor. Mat.* **1995**, *3*, 401.
329. Kärger, J. In: *Access in Nanoporous Materials* (T.J. Pinnavaia; M.F. Thorpe, Eds.), Plenum: New York, 1995.
330. Czarnecki, G.; Dudek, M.R.; Pekalski, A.; Cislo, J. *J. Phys. A* **1996**, *29*, 3367.
331. Rödenbeck, C.; Kärger, J.; Hahn, K. *J. Chem. Phys.* **1999**, *110*, 3970.
332. Rödenbeck, C.; Kärger, J.; Hahn, K. *J. Catal.* **1995**, *157*, 656.
333. Schuring, D.; Jansen, A.P.J.; van Santen, R.A. *J. Phys. Chem.* **2000**, in press
334. Sholl, D.S.; Fichthorn, K.A. *Phys. Rev. E* **1997**, *55*, 7753
335. Sholl, D.S. *Chem. Eng. J.* **1999**, *74*, 25
336. Sholl, D.S.; Lee, C.K. *J. Chem. Phys.* **2000**, *112*, in press

337. Okino, M.S.; Snurr, R.Q.; Kung, H.H.; Ochs, J.E.; Mavrovouniotis, M.L. *J. Chem. Phys.* **1999**, *111*, in press
338. Rödenbeck, C.; Kärger, J.; Hahn, K. *Phys. Rev. E* **1997**, *55*, 5697
339. Nijhuis, T.A.; van den Broeke, L.J.P.; van de Graaf, J.M.; Kapteijn, F.; Makkee, M.; Moulijn, J.A. *Chem. Eng. Sci.* **1997**, *52*, 3401
340. Schumacher, R.R.; Anderson, B.G.; Noordhoek, N.J.; de Gauw, F.J.M.M.; de Jong, A.M.; de Voigt, M.J.A.; van Santen, R.A. *Microp. Mesoporous Mat.* **2000**; in press
341. Fritzsche, S.; Wolfsberg, M.; Haberlandt, R.; Demontis, P.; Suffritti, G.B.; Tilocca, A. *Chem. Phys. Lett.* **1998**, *296*, 253